PHOTOCATALYTIC OXIDATION OF GAS PHASE VOLATILE ORGANIC COMPOUNDS (VOCS) USING NANOSTRUCTURE TITANIUM DIOXIDE BASED MATERIALS

(PENGOKSIDAAN PEMANGKINAN FOTO BAGI SEBATIAN ORGANIK MERUAP BERFASA GAS (VOCs) MENGGUNAKAN TITANIUM DIOKSIDA BERSTRUKTUR NANO)

MOHD YUSUF OTHMAN
WAN AZELEE WAN ABU BAKAR
KHAIDAWATI SAIYUDI

RESEARCH VOTE NO:
74248

Jabatan Kimia
Fakulti Sains
Universiti Teknologi Malaysia

2007

PHOTOCATALYTIC OXIDATION OF GAS PHASE VOLATILE ORGANIC COMPOUNDS (VOCS) USING NANOSTRUCTURE TITANIUM DIOXIDE BASED MATERIALS

(Keywords: Photocatalyic, degradation, photoactivity, catalyst)

Various atomic ratios of metal doped TiO_2 were prepared using Mn^{2+}, Fe^{2+}, Fe^{3+}, Cu^{2+}, Zn^{2+}, Cu^{2+} co-doped with Fe^{3+} and Zn^{2+} co-doped with Fe^{3+}. Photocatalytic degradation of CH_2Cl_2, $CHCl_3$ and CCl_4 using various atomic ratios of metal doped TiO_2 showed the existence of optimum dopant ratio, which indicates the dependency of photoactivity of doped TiO_2 on dopant concentration. Besides, dopants can affect the photoactivity of doped TiO_2 by acting as hole/electron traps or as recombination centres. Using doped catalysts such as Fe^{2+}/TiO_2, Fe^{3+}/TiO_2, Cu^{2+}/TiO_2, Zn^{2+}/TiO_2, $Cu^{2+}/Fe^{3+}/TiO_2$ and $Zn^{2+}/Fe^{3+}/TiO_2$ gave higher degradation of VOCs than pure TiO_2. However, adding of Mn^{2+} was detrimental to the process. The rate of degradation of the studied chlorinated hydrocarbons follows the order: $CHCl_3$ > CH_2Cl_2 > CCl_4. This indicates different VOCs will have different levels of degradation although same catalyst was used in the photocatalytic degradation experiment. In photocatalytic degaradation of $CHCl_3$ and CCl_4 mixtures, low concentration of $CHCl_3$ and CCl_4 mixtures shows higher degradation than CCl_4. The Cl· radicals do not attack C-Cl bond s in CCl_4, therefore, Cl· radicals formed during the illumination of UV lamp may contribute to the degradation of $CHCl_3$. Consequently, more $CHCl_3$ was degraded. Possible model for photocatalytic degradation of VOCs were proposed, utilizing data from fragments analysis using GC-MS. SEM/EDX, UV-Vis and ellipsometer were used to characterize the structural and optical properties of thin films. Addition of dopants shifted the absorption edge of TiO_2 and this indicated the changes of band gap energy. The film thickness for all catalyst samples is between 227-251 nm and within the acceptable range of thin films (< 1000 nm).

PENGOKSIDAAN PEMANGKINAN FOTO BAGI SEBATIAN ORGANIK MERUAP BERFASA GAS (VOCs) MENGGUNAKAN TITANIUM DIOKSIDA BERSTRUKTUR NANO

(Kata kunci: Pemangkinan foto, pengdegradasian, aktiviti foto, mangkin)

TiO_2 dop dengan pelbagai nisbah logam ion telah disediakan dengan menggunakan Mn^{2+}, Fe^{2+}, Fe^{3+}, Cu^{2+}, Zn^{2+}, Cu^{2+} ko-dop Fe^{3+} dan Zn^{2+} ko-dop Fe^{3+}. Mangkin foto degradasi CH_2Cl_2, $CHCl_3$ dan CCl_4 dengan menggunkan TiO_2 dop dengan pelbagai nisbah logam ion menunjukkan kewujudan satu nilai optimum bahan pendop terhadap TiO_2. nilai ini menunjukkan bahawa aktiviti mangkin foto TiO_2 bergantung kepada kepekatan bahan pendop. Bahan pendop mempengaruhi aktiviti pemangkin foto TiO_2 dengan bertindak sebagai perangkap e^-/h^+ atau sebagai pusat pengabungan. Penggunaan TiO_2 dop dengan logam seperti Fe^{2+}/TiO_2, Fe^{3+}/TiO_2, Cu^{2+}/TiO_2, Zn^{2+}/TiO_2, $Cu^{2+}/Fe^{3+}/TiO_2$ dan $Zn^{2+}/Fe^{3+}/TiO_2$ memberikan degradasi VOCs yang lebih tinggi daripada TiO_2 tanpa bahan pendop. Manakala penambahan Mn^{2+} memberikan kesan yang negatif. Pendegradasina VOCs mengikut kadar: $CHCl_3 > CH_2Cl_2 > CCl_4$. Ini menunjukkan VOCs yang berbeza akan memberikan degradasi yang berbeza walaupun mangkin yang sama digunakan. Dalam mangkin foto degradasi campuran $CHCl_3$ dan CCl_4, campuran berkepkatan rendah menunjukkan degradasi yang lebih tinggi daripada degradasi CCl_4. Ini disebabkan oleh radikal Cl· tidak menyerang ikatn C-Cl dalam CCl_4, dengan itu, radikal Cl· yang terbentuk dalam penyinaran UV akan meyerang $CHCl_3$. Akibatnya, lebih banyak $CHCl_3$ didegradasikan. Dengan menggunakn maklumat yang diperolehi daripada GC-MS, model bagi pendegradasian VOCs boleh dicadangkan. SEM/EDX, Spektrofotometer UV-Vis dan ellipsometer telah digunakan untuk mencirikan saput tipis. Penambahan bahan pendop mengubah penyerapan TiO_2 ke kawasan nampak dan ini menunjukkan perubahan tenaga lubang jalur. Ketebalan saput tipis adalah di antara 227-251 nm dan ini adalah dalam lingkungan ketebalan saput tipis (< 1000 nm).

Benefits Report Guidelines

A. Purpose

The purpose of the Benefits Report is to allow the IRPA Panels and their supporting experts to assess the benefits derived from IRPA-funded research projects.

B. Information Required

The Project Leader is required to provide information on the results of the research project, specifically in the following areas:

- Direct outputs of the project;
- Organisational outcomes of the project; and
- Sectoral/national impacts of the project.

C. Responsibility

The Benefits Report should be completed by the Project Leader of the IRPA-funded project.

D. Timing

The Benefits Report is to be completed within three months of notification by the IRPA Secretariat. Only IRPA-funded projects identified by MPKSN are subject to this review. Generally, the Secretariat will notify Project Leaders of selected projects within 18 months of project completion.

E. Submission Procedure

One copy of this report is to be mailed to :

IRPA Secretariat
Ministry of Science, Technology and the Environment
14th, Floor, Wisma Sime Darby
Jalan Raja Laut
55662 Kuala Lumpur

Benefit Report

1. Description of the Project

A. Project identification

1. Project number : 03-02-06-0127 EA001 (vot 74248)

Project title : Photocatalytic Oxidation of Gas Phase Volatile Organic Compounds

2. (VOCs) Using Nanostructure Titanium Dioxide Based Materials

3. Project leader : P.M. Dr. Mohd Yusuf Othman

B. Type of research

Indicate the type of research of the project (Please see definitions in the Guidelines for completing the Application Form)

[ ] Scientific research (fundamental research)

[√] Technology development (applied research)

[ ] Product/process development (design and engineering)

[ ] Social/policy research

C. Objectives of the project

1. Socio-economic objectives

Which socio-economic objectives are adressed by the project? (Please indentify the sector, SEO Category and SEO Group under which the project falls. Refer to the Malaysian R&D Classification System brochure for the SEO Group code)

Sector : Manufacturing and Construction

SEO Category : Manufacturing (S20600)

SEO Group and Code : Industrial Chemicals and Related Products (S20607)

2. Fields of research

Which are the two main FOR Categories, FOR Groups, and FOR Areas of your project? (Please refer to the Malaysia R&D Classification System brochure for the FOR Group Code)

a. Primary field of research

FOR Category : Applied Sciences and Technologies

FOR Group and Code : Manufacturing and Process Technologies and Engineering (F10602)

FOR Area : Material Processing Technology

b. Secondary field of research

FOR Category : Engineering Science

FOR Group and Code : Chemical Engineering (F10702)

FOR Area : Catalyst Chemicals

D. Project duration

What was the duration of the project?

36 Months

E. Project manpower

How many man-months did the project involve?

72 Man-months

F. Project costs

What were the total project expenses of the project?

RM 196,500.00

G. Project funding

Which were the funding sources for the project?

Funding sources	Total Allocation (RM)
IRPA	RM 196,500.00

II. Direct Outputs of the Project

A. Technical contribution of the project

1. **What was the achieved direct output of the project :**

For scientific (fundamental) research projects?

- [ ] Algorithm
- [ ] Structure
- [√] Data
- [ ] Other, please specify : _____

For technology development (applied research) projects :

- [√] Method/technique
- [ ] Demonstrator/prototype
- [ ] Other, please specify : _____

For product/process development (design and engineering) projects:

- [√] Product/component
- [ ] Process
- [ ] Software
- [ ] Other, please specify : _____

2. How would you characterise the quality of this output?

- [ ] Significant breakthrough
- [ ] Major improvement
- [√] Minor improvement

B. Contribution of the project to knowledge

1. How has the output of the project been documented?

- [√] Detailed project report
- [ ] Product/process specification documents
- [ ] Other, please specify : _____

2. Did the project create an intellectual property stock?

- [ ] Patent obtained
- [ ] Patent pending
- [ ] Patent application will be filed
- [ ] Copyright

3. What publications are available?

- [√] Articles (s) in scientific publications — How Many: 1
- [√] Papers(s) delivered at conferences/seminars — How Many: 5
- [ ] Book
- [ ] Other, please specify : _____

4. How significant are citations of the results?

- [ ] Citations in national publications — How Many: _____
- [ ] Citations in international publications — How Many: _____
- [√] None yet
- [ ] Not known

lll. Organisational Outcomes of the Project

A. Contribution of the project to expertise development

1. How did the project contribute to expertise?

[ ]	PhD degrees	How Many: _____
[√]	MSc degrees	How Many: 5 students
[ ]	Research staff with new specialty	How Many: _____
[ ]	Other, please specify: _____	

2. How significant is this expertise?

- [ ] One of the key areas of priority for Malaysia
- [√] An important area, but not a priority one

B. Economic contribution of the project?

1. How has the economic contribution of the project materialised?

- [ ] Sales of manufactured product/equipment
- [ ] Royalties from licensing
- [√] Cost savings
- [ ] Time savings
- [ ] Other, please specify : _____

2. How important is this economic contribution ?

[ ]	High economic contribution	Value:	RM_____
[√]	Medium economic contribution	Value:	RM 100,000.00
[ ]	Low economic contribution	Value:	RM_____

3. When has this economic contribution materialised?

- [ ] Already materialised
- [ ] Within months of project completion
- [ ] Within three years of project completion
- [ ] Expected in three years or more
- [√] Unknown

C Infrastructural contribution of the project

1. What infrastructural contribution has the project had?

- [√] New equipment Value: RM _____
- [ ] New/improved facility Investment : RM _____
- [ ] New information networks
- [ ] Other, please specify: _____

2. How significant is this infrastructural contribution for the organisation?

- [ ] Not significant/does not leverage other projects
- [√] Moderately significant
- [ ] Very significant/significantly leverages other projects

D. Contribution of the project to the organisation's reputation

1. How has the project contributed to increasing the reputation of the organisation

- [ ] Recognition as a Centre of Excellence
- [ ] National award
- [ ] International award
- [ ] Demand for advisory services
- [√] Invitations to give speeches on conferences
- [ ] Visits from other organisations
- [ ] Other, please specify: _____

2. How important is the project's contribution to the organisation's reputation ?

☐	Not significant
☑	Moderately significant
☐	Very significant

1V. National Impacts of the Project

A. Contribution of the project to organisational linkages

1. Which kinds of linkages did the project create?

- [ ] Domestic industry linkages
- [ ] International industry linkages
- [√] Linkages with domestic research institutions, universities
- [ ] Linkages with international research institutions, universities

2. What is the nature of the linkages?

- [ ] Staff exchanges
- [√] Inter-organisational project team
- [ ] Research contract with a commercial client
- [ ] Informal consultation
- [ ] Other, please specify: _____

B. Social-economic contribution of the project

1. Who are the direct customer/beneficiaries of the project output?

Customers/beneficiaries:	Number:
_____	_____
_____	_____
_____	_____

2. How has/will the socio-economic contribution of the project materialised ?

- [ ] Improvements in health
- [ ] Improvements in safety
- [√] Improvements in the environment
- [ ] Improvements in energy consumption/supply
- [ ] Improvements in international relations
- [ ] Other, please specify: _____

3. How important is this socio-economic contribution?

	High social contribution
√	Medium social contribution
	Low social contribution

4. When has/will this social contribution materialised?

	Already materialised
	Within three years of project completion
	Expected in three years or more
√	Unknown

Date: 4 July 2007 **Signature:**

UNIVERSITI TEKNOLOGI MALAYSIA

BORANG PENGESAHAN
LAPORAN AKHIR PENYELIDIKAN

TAJUK PROJEK: **PHOTOCATALYTIC OXIDATION OF GAS PHASE VOLATILE ORGANIC COMPOUNDS (VOCS) USING NANOSTRUCTURE TITANIUM DIOXIDE BASED MATERIALS**

Saya **MOHD YUSUF OTHMAN**
(HURUF BESAR)

Mengaku membenarkan **Laporan Akhir Penyelidikan** ini disimpan di Perpustakaan Universiti Teknologi Malaysia dengan syarat-syarat kegunaan seperti berikut :

1. Laporan Akhir Penyelidikan ini adalah hakmilik Universiti Teknologi Malaysia.
2. Perpustakaan Universiti Teknologi Malaysia dibenarkan membuat salinan untuk tujuan rujukan sahaja.
3. Perpustakaan dibenarkan membuat penjualan salinan Laporan Akhir Penyelidikan ini bagi kategori TIDAK TERHAD.
4. * Sila tandakan (/)

☐	SULIT	(Mengandungi maklumat yang berdarjah keselamatan atau Kepentingan Malaysia seperti yang termaktub di dalam AKTA RAHSIA RASMI 1972).
☐	TERHAD	(Mengandungi maklumat TERHAD yang telah ditentukan oleh Organisasi/badan di mana penyelidikan dijalankan).
☑	TIDAK TERHAD	

_____
TANDATANGAN KETUA PENYELIDIK

_____
Nama & Cop Ketua Penyelidik

Tarikh : _____

CATATAN : ***** *Jika Laporan Akhir Penyelidikan ini SULIT atau TERHAD, sila lampirkan surat daripada pihak berkuasa/organisasi berkenaan dengan menyatakan sekali sebab dan tempoh laporan ini perlu dikelaskan sebagai SULIT dan TERHAD.*

End of Project Report Guidelines

A. Purpose

The purpose of the End of Project is to allow the IRPA Panels and their supporting group of experts to assess the results of research projects and the technology transfer actions to be taken.

B. Information Required

The following Information is required in the End of Project Report :

- Project summary for the Annual MPKSN Report;
- Extent of achievement of the original project objectives;
- Technology transfer and commercialisation approach;
- Benefits of the project, particularly project outputs and organisational outcomes; and
- Assessment of the project team, research approach, project schedule and project costs.

C. Responsibility

The End of Project Report should be completed by the Project Leader of the IRPA-funded project.

D. Timing

The End of Project Report should be submitted within three months of the completion of the research project.

E. Submission Procedure

One copy of the End of Project is to be mailed to :

IRPA Secretariat
Ministry of Science, Technology and the Environment
14th Floor, Wisma Sime Darby
Jalan Raja Laut
55662 Kuala Lumpur

End of Project Report

A. Project number : 03-02-06-0127 EA001 (vot 74248)

Project title: Photocatalytic Oxidation of Gas Phase Volatile Organic Compounds (VOCs) Using Nanostructure Titanium Dioxide Based Materials

Project leader: P.M. Dr. Mohd Yusuf Othman

Tel: 07-5534126 **Fax: 07-5566162**

B. Summary for the MPKSN Report (for publication in the Annual MPKSN Report, please summarise the project objectives, significant results achieved, research approach and team structure)

The main objectives of this project can be summarized as follows;

1. To develop an environmental catalyst with excellent photocatalytic activity for the destruction of gas phase VOCs.
2. To identify the optimum conditions for catalyst preparations and photocatalytic reactions.
3. To investigate the chemical, optical and electrical properties of the catalyst.

In order to achieve the above targeted objectives firstly we have carried out synthesize of various photocatalysts based on TiO_2, We also prepared doped photocatalysts using selected first transistion metals. All prepared photocatalysts were tested towards degradation of various volatile organic compounds using home-built photomicroreactor.

Mechanistic study was also conducted using the best photocatalyst identified from the screening test done earlier. Characterization of the best photocatalyst was done using various analytical techniques such as XRD, SEM-EDX, XPS, FTIR, TGA/DTG and nitrogen adsorption technique.

The result obtained so far still need some improvements especially on the property of photocatalysts. As such further experimental modifications will be adopted integrating metal oxides which could alter the excitation energy of the photocatalysts.

This project involves three researcher, and five research students

C. Objectives achievement

- **Original project objectives** (Please state the specific project objectives as described in Section ll of the Application Form)

1. To develop an environmental catalyst with excellent photocatalytic activity for the destruction of gas phase VOCs.
2. To identify the optimum conditions for catalyst preparations and photocatalytic reactions.
3. To investigate the chemical, optical and electrical properties of the catalyst.

- **Objectives Achieved** (Please state the extent to which the project objectives were achieved)

1. To develop an environmental catalyst with excellent photocatalytic activity for the destruction of gas phase VOCs.
2. To identify the optimum conditions for catalyst preparations and photocatalytic reactions.
3. To investigate the chemical, optical and electrical properties of the catalyst.

- **Objectives not achieved** (Please identify the objectives that were not achieved and give reasons)

D. Technology Transfer/Commercialisation Approach (Please describe the approach planned to transfer/commercialise the results of the project)

The findings of this research will help in solving air pollution problem caused by VOCs emitted from industries and household materials or furniture. The best catalyst can be coated on glass or tiles, which are the major building materials.

E. Benefits of the Project (Please identify the actual benefits arising from the project as defined in Section lll of the Application Form. For examples of outputs, organisational outcomes and sectoral/national impacts, please refer to Section lll of the Guidelines for the Application of R&D Funding under IRPA)

- **Outputs of the project and potential beneficiaries** (Please describe as specifically as possible the outputs achieved and provide an assessment of their significance to users)

- A supported titanium dioxide base catalyst with improved technology, knowledge and skills relevant to catalysis

- An understanding of the chemical, physical, optical and electrical properties of nanostructure

- Papers in scientific and engineering journals covering environmental catalysis, air pollution control and surface science

- **Organisational Outcomes** (Please describe as specifically as possible the organisational benefits arising from the project and provide an assessment of their significance)

1. Expertise development: 5 MSc students
2. Economic contribution: Royalties from licensing
3. Infrastructural contribution: Demand for advisory services
4. Industrial problems solving

- **National Impacts** (If known at this point in time, please describes specifically as possible the potential sectoral/national benefits arising from the project and provide an assessment of their significance)

1. Organisation linkages – domestic industry linkage and linkages with other universities or research institution.
2. Socio-economic contribution – improvement in health, safety and environment.

F. Assessment of project structure

- **Project Team** (Please provide an assessment of how the project team performed and highlight any significant departures from plan in either structure or actual man-days utilised)

- This project was conducted within given time frame.
- This project also involved 3 researchers and 5 master students.

- **Collaborations** (Please describe the nature of collaborations with other research organisations and/or industry)

G. Assessment of Research Approach (Please highlight the main steps actually performed and indicate any major departure from the planned approach or any major difficulty encountered)

This research approached undertaken in this project was according to original research methodology.

H. Assessment of the Project Schedule (Please make any relevant comment regarding the actual duration of the project and highlight any significant variation from plan)

The project conducted according to initial project schedule.

I. Assessment of Project Costs (Please comment on the appropriateness of the original budget and highlight any major departure from the planned budget)

The overall costs of the project actually spend was 137,840.21. This is 70.15 % the original approved budget.

J. Additional Project Funding Obtained (In case of involvement of other funding sources, please indicate the source and total funding provided)

—

K. Other Remarks (Please include any other comment which you feel is relevant for the evaluation of this project)

—

Date : 4 July 2007 **Signature :**

UNIVERSITI TEKNOLOGI MALAYSIA
Research Management Centre

PRELIMINARY IP SCREENING & TECHNOLOGY ASSESSMENT FORM

(To be completed by Project Leader submission of Final Report to RMC or whenever IP protection arrangement is required)

1. **PROJECT TITLE IDENTIFICATION** :

Photocatalytic Oxidation of Gas Phase Volatile Organic Compounds (VOCs) Using Nanostructure Titanium Dioxide Based Materials

Vote No: 74248

2. **PROJECT LEADER** :

Name : MOHD YUSUF OTHMAN

Address : Department of Chemistry, Faculty of Science, Universiti Teknologi Malaysia, 81310 Skudai, Johor Darul Takzim.

Tel : 07-5534126 Fax : 07-5566162 e-mail : myusuf@kimia.fs.utm.my

3. **DIRECT OUTPUT OF PROJECT** *(Please tick where applicable)*

Secientific Research	Applied Research	Product/Process Development
☐ Algorithm	☑ Method/Technique	☑ Product / Component
☐ Structure	☐ Demonstration / Prototype	☐ Process
☑ Data		☐ Software
☐ Other, please specify	☐ Other, please specify	☐ Other, please specify
_____	_____	_____
_____	_____	_____
_____	_____	_____

4. INTELLECTUAL PROPERTY *(Please tick where applicable)*

☑ Not patentable	☐ Technology protected by patents
☐ Patent search required	☐ Patent pending
☐ Patent search completed and clean	☐ Monograph available
☐ Invention remains confidential	☐ Inventor technology champion
☐ No publications pending	☐ Inventor team player
☐ No prior claims to the technology	☐ Industrial partner identified

5. LIST OF EQUIPMENT BOUGHT USING THIS VOT

1. Note book and printer

2. High vacuum glass piping system

3. Digital Mass Flowmeter

4. Gas Regulator

6. STATEMENT OF ACCOUNT

a)	APPROVED FUNDING	RM : 149,254.71
b)	TOTAL SPENDING	RM : 196,500.00
c)	BALANCE	RM : 47,245.29

7. TECHNICAL DESCRIPTION AND PERSPECTIVE

Please tick an executive summary of the new technology product, process, etc., describing how it works. Include brief analysis that compares it with competitive technology and signals the one that it may replace. Identify potential technology user group and the strategic means for exploitation.

a) Technology Description

Some modification of photocatalytic techniques werw carried out. More investigations might to be done for the betterment of products.

b) Market Potential

Not yet. The obtained products still need improvement before they could be commercialized.

Signature of Projet Leader :- Date : 4 July 2008

c) Commercialisation Strategies

Improvement of products still need to be done

8. RESEARCH PERFORMANCE EVALUATION

a) FACULTY RESEARCH COORDINATOR

Research Status	( )	( )	( )	( )	( )	( )
Spending	( )	( )	( )	( )	( )	( )
Overall Status	( )	( )	( )	( )	( )	( )
	Excellent	Very Good	Good	Satisfactory	Fair	Weak

Comment/Recommendations :

_____

_____

_____

_____

_____

_____

…… Name : ……

Signature and stamp of JKPP Chairman

Date : ……

b) RMC EVALUATION

Research Status	( )	( )	( )	( )	( )	( )
Spending	( )	( )	( )	( )	( )	( )
Overall Status	( )	( )	( )	( )	( )	( )
	Excellent	Very Good	Good	Satisfactory	Fair	Weak

Comments :-

_____

_____

_____

_____

_____

_____

Recommendations :

☐ Needs further research

☐ Patent application recommended

☐ Market without patent

☐ No tangible product. Report to be filed as reference

…….. Name : …….

Signature and Stamp of Dean / Deputy Dean
Research Management Centre

Date : …….

CHAPTER 1

INTRODUCTION

1.1 Heterogeneous Photocatalytic Oxidation

Photocatlytic oxidation (PCO) is an attractive technology for the remediation of organic pollutants. It is economical, simple and can be easily implemented. The process harnesses radiant energy from natural or artificial light sources with heterogeneous catalyst to degrade the organic pollutants into their mineral components (Hoffmann, 1995; Mills, 1993; Fox, 1993). PCO has a promising application for the degradation of VOCs in process air stream (Hester, 1995). PCO can readily mineralize simple organic molecules into CO_2 and H_2O at ambient conditions using molecular oxygen as the primary oxidant, but complex pollutants are often more difficult to degrade with undesirable intermediates and by-products formed. In addition, the rate of decomposition is usually slow (Djeghri, 1980).

1.2 Titanium Dioxide as Photocatalyst

Heterogeneous photocatalysis using TiO_2 has several attractions: (a) TiO_2 is relatively inexpensive, (b) it dispenses with the use of other coadjutant reagents, (c) it shows efficient destruction of toxic contaminants, (d) it operates at ambient temperature and pressure and (e) the reaction products are usually CO_2 and H_2O, or HCl, in the case of chlorinated organic compounds (Alberici, 1997) (f) able to utilize visible and / or near-UV light (g) biologically and chemically inert (h) photostable (i.e not liable to photoanodic corrosion for example) (Mills, 1997).

Most of the current wide interest in using TiO_2 in catalytic studies stems from the highly reactive radicals (•OH and $•O_2^-$) formed when irradiated together with handling facilities (Monneyron, 2003). It can be seen that TiO_2 exists in two main crystallographic forms, anatase and rutile. For anatase, the bandgap energy is 3.23 eV

while the bandgap energy for rutile is 3.02 eV (Litter, 1999, Mills, 1997). It is no surprise that different samples of TiO_2 exhibit different photocatalytic activities towards the same organic substrate under otherwise identical reaction conditions. Such differences can be qualitatively attributed to differences in morphology, crystal phase, specific surface area, particle aggregate size and surface density of OH groups in the TiO_2 samples (Mills, 1997). For the degradation of organic compounds, the pure TiO_2 anatase exhibited the best catalytic efficiency, while pure rutile was the poorer catalyst. The recombination rate of e^- and h^+ in rutile is very highdue to its relatively low dielectric constants compare to anatase. The conduction band level of anatase is sufficiently negative for the reduction of oxygen, whereas for rutile is close to the oxygen reduction potential thus retarded the reduction of oxygen (Braun, 1993).

1.4 Effect of Metal Ions (M^{n+})

Knowledge of the effects of impurities on the pigment properties is essential in order to be able to improve the photocatalytic properties by doping transition metal elements (Karvinen, 2003). On the other hand, doping of TiO_2 produces crystal defects and surface modifications, which alter the photocatalytical properties of TiO_2 (Malati, 1984). Cr^{3+}/TiO_2 co-deposited with RuO_2 and Pt had been used as photocatalyst for water decomposition (Bogarello, 1982). The facts indicate that introducing two or more proper metals onto nanocrystalline TiO_2 particles will improve the photocatalytic effect of TiO_2. Co-doping rare earth metal and transition metal ions onto the nanocrystalline TiO_2 may achieve the same effect as the noble and transition metal ions were codeposited onto TiO_2 (Yang, 2002).

Degradation of a certain organic molecule will depend not only on its chemical properties, such as its capacity for chemisorption and reacting with photogenerated radicals, but on the catalyst properties and affinity for the molecule and its degradation intermediates. For instance, catalysts showing a very high degradation activity for certain species may be inactive for others or its intermediates (Arana, 2001). The effect of metal ion doping is strongly depends on the factors such as the dopant concentration, the particle size of the nanocrystalline TiO_2, the distribution of the dopants and so on

(Yang, 2002). The high degree of recombination between photogenerated electrons and holes is a major limiting factor controlling the photocatalytic efficiency (He, 2003). In this case, the deposited metal on the surface of TiO_2 can act as a sink for photoinduced charge carrier, promoting interfacial charge-transfer process. This migration of generated electrons to metal particle, on the one hand, can increase the lifetime of the holes and suppress the electron-hole recombination, beneficial to the photocatalytic oxidation of organic pollutants (Dionysiou, 2000; Hirano, 1997). The addition of metal ions M^{n+} can also trap electrons (or holes) at the semiconductor surface (Eq. 1.1 and 1.2).

$$M^{n+} + e^- \longrightarrow M^{(n-1)+} \quad (1.1)$$

$$M^{n+} + h^+ \longrightarrow M^{(n+1)+} \quad (1.2)$$

and the energy level for $M_{n+}/M_{(n+1)+}$ lies above the valence band (E_{vb}). The uses of partially field *d* orbital of first row transition metal ions as dopants or co-catalyst resulted in an increased rate of formation of •OH (Eq. 1.4, Eq. 1.5). This is due to the electrons in valence band of TiO_2 can be transferred to the energy level of metal ions. Consequently, the lifetime of h^+ can be prolonged and more •OH will be formed.

$$TiO_2 \xrightarrow{h\nu} TiO_2\,(e^-_{cb}, h^+_{vb}) \quad (1.3)$$

$$h^+ + OH^- \longrightarrow \bullet OH \quad (1.4)$$

$$h^+ + H_2O \longrightarrow \bullet OH + H^+ \quad (1.5)$$

When dopants are added into TiO_2, the bulk and surface properties and the photoactivity are strongly dependent on the method used for photocatalyst preparation. The dominant parameters include the character and concentration of the dopant and the thermal treatment (Palmisano, 1994). In highest concentrations the dissolved metal ions have detrimental effect on the rate of organic substrate removal, which was attributed to hν oxidation of reduced metals by •OH or photogenerated holes, proceeding in competition with Eq. 1.4 and 1.5 (Butler, 1993).

1.5 Kinetics Study

Owing to the complex mechanism of reactions, it is difficult to develop a model for the dependence of the photocatalytic degradation rate on the experimental parameters for the whole treatment time. Thus, kinetic modelling of the photocatalytic process is usually restricted to the analysis of the initial rate of potocatalytic degradation. This can be obtained from the initial slope and the initial VOCs' concentration in an experiment in which the variation of the VOCs concentration is measured as a function of time. The extrapolation of the photocatalytic degradation rate to time = 0 avoids the possible interference from by-products. The initial photocatalytic degradation rate (r_0) is observed to be a function of the initial VOCs' concentration (C_0). A linear plot of reciprocal initial rate (r_0^{-1}) versus reciprocal initial concentration (C_0^{-1}) is often obtained, that gives k as the L-H rate constant and K as the Langmuir adsorption constant of the VOCs in the photocatalytic degradation reaction (Kim, 2002).

The inherent uncertain nature (due to the presence of chain reactions and chain termination) of photochemical processes makes the evaluation of reaction kinetics rather complicated, thus requiring extensive and methodical studies in this area (Feiyen, 2002). In this study, kinetics and possible pathways for the photocatalytic degradation of chloroform, carbon tetrachloride and dichloromethane were being studied.

1.6 Photocatalytic Degradation Mechanism

In the last decade, the mechanism of heterogeneous photocatalysis has been investigated by many researchers. According to Fu, Zeltner and Anderson, a photocatalytic reaction proceeds on the surface of semiconductors via several steps: (1) production of electron-hole pairs by irradiating the semiconductor by light whose energy is higher than the band gap energy of the semiconductor (E.q 1.3); (2) separation of the photogenerated electrons and holes due to trapping by species that are adsorbed on the semiconductor; (3) redox reaction between the trapped electrons and holes and the adsorbates present on the surface; (4) desorption of the products and reconstruction of surface (Fu, 1996).

Oxidative pathway can be performed by direct hole attack or mediated by •OH radicals, in their free or adsorbed form. The oxidative pathway leads, in many cases, to

complete mineralization of an organic substrate to CO_2 and H_2O (Litter, 1999). In this study, the gas-phase photocatalytic degradation of dichloromethane, chloroform and carbon tetrachloride was investigated in detailed.

$$Ti^{4+} + e^- \longrightarrow Ti^{3+} \quad (1.11)$$

$$Ti^{3+} + O_{2ads} \longrightarrow O^-_{2ads} + Ti^{4+} \quad (1.12)$$

$$\bullet OH + O^-_{2ads} \longrightarrow HO_2\bullet + O^-_{ads} \quad (1.13)$$

$$O_{2ads} \longrightarrow 2O_{ads} \quad (1.14)$$

$$Ti^{3+} + O_{ads} \longrightarrow Ti^{4+} + O^-_{ads} \quad (1.15)$$

1.7 Research Objectives

The research objectives are as follows:

1. To develop an excellent TiO_2 based catalysts that able to degrade toxic VOCs into non-toxic components.
2. To study the effectiveness of TiO_2 doped with various types of first row transition metals towards the degradation of dichloromethane, chloroform, carbon tetrachloride and a mixture of carbon tetrachloride and chloroform.
3. To study the kinetic and the model of the degradation of dichloromethane, chloroform and carbon tetrachloride.

1.8 Scope of Study

The scopes of research are as follows:

1. TiO_2 will be prepared in the form of thin film using the sol-gel method through dip coating technique.
2. Characterization of catalysts using various techniques includes XRD, SEM, EDX and UV/Vis spectroscopy.
3. Degradation of dichloromethane, chloroform, carbon tetrachloride and a mixture of carbon tetrachloride and chloroform using prepared catalysts. Experiments will be carried out using UV light with ~ 354 nm wavelength, under atmospheric pressure and at room temperature.
4. A possible model of the photocatalytic degradation of dichloromethane, chloroform and carbon tetrachloride will be proposed.

CHAPTER 3

EXPERIMENTAL

3.0 Catalysts Preparation

3.1 Preparation of TiO_2 Sol-Gel

The precursor solution for TiO_2 sol for coatings was prepared using a modification of the sol-gel method reported by Kato (Kato, 1994). 6 g Polyethylene glycol (2000) was dissolved in 600 mL ethanol in a volumetric flask (1000 mL). The solution was then stirred continuously until the polyethylene glycol was fully dissolved. 85.2 g titanium tetraisopropoxide, 31.8 g diethanolamine and 5.4 mL deionized water were added to the solution. The mixture was then stirred continuously using a magnetic stirrer in order to achieve a stable, transparent and homogeneous sol-gel. The sol-gel was then used to prepare doped and undoped TiO_2 thin films.

3.2 Preparation of TiO_2 Thin film

Hollow pyrex glass cylinders were used as the support substrates. The hollow pyrex glass cylinders were cleaned with acetone, followed by ethanol and finally oven dried prior to dip-withdrawal process. The TiO_2 thin films were prepared manually by the dip-withdraw method. 135 mL sol-gel was added into a beaker (200 mL). The hollow glass cylinder was then dipped into the sol-gel and left for a minute in the sol before extraction. The thin film was dried at ambient temperature in a desiccator for 10 minutes before repeating the process. The complete dip-withdraw cycle was repeated 5 times. The dipping and withdrawing processes must be constant in order to ensure the formation of a homogeneous thin film on the support. The thin film was then dried in the oven at 80°C for 1 hour. Finally, the thin film was calcined in the furnace with an elevated temperature of 2°C/min up to 500°C and kept at this temperature for 1 hour.

3.2.3 Preparation of Catalysts with Dopants

3.2.4 To determine the weight of Ti^{4+} in the sol-gel, a clean container was weighted before 10 mL sol-gel was poured into it. This was followed by the calcination of

the solgel in a furnace with an elevated temperature of 2°C/min up to 500°C and maintained for 1 hour. After it was cooled to room temperature, it was weighted once again. The calcination and weighing processes were repeated until no differences in weights were observed. The measured weight was the weight of Ti^{4+} in the sol-gel. This Ti^{4+} weight will be used in the determination of the ratio of TiO_2 against dopants weight. In the preparation of catalyst with dopants, the metal salt was weighted into a 200 mL beaker based on the required amount and dissolved with 135 mL sol-gel. The mixture was stirred till homogeneous. Further procedures in the preparation of thin film catalysts with dopants were similar to those used in preparing undoped TiO_2. All the solutions were transparent. Coloured solutions were caused by the presence of metal ions. For instance, the solution which was green in colour was caused by the presence of Fe^{2+} ions. Meanwhile, the solution which was chocolate in colour was caused by the presence of Mn^{2+} ions.

3.3 Photocatalytic Measurements

3.3.1 Calibration

The calibration process was carried out using vacuum pump and calibration glass container with exactly 1000 mL. The samples used were dichloromethane, chloroform and carbon tetrachloride. Before calibration was conducted, the glass container must be vacuumed for a few minutes prior to use. This was important to ensure that all gases and pollutants that might be present in the glass container was eliminated. Then, a certain amount of sample was injected into the glass container through the septum. One of the taps of the container was then opened and kept open until the “hissing” sound disappeared to ensure that the pressure inside the container was equivalent to the ambient pressure. The sample was left to evaporate for a few minutes. A 50 μL sample was injected out from the container and analyzed using GC-FID. The resulting peak area was recorded. This process was repeated for a different sample volume. A calibration graph of peak area versus concentration was drawn.

3.3.2 Photocatalytic Degradation Testing

All photocatalytic degradation experiments of dichloromethane, chloroform and carbon tetrachloride were conducted in a home built fixed bed annulus glass reactor with exactly 1000 mL. The reactor is equipped with an electromagnetic pump to circulate the sample, a glass compartment to place the catalyst and UV light and a septum for injection of sample into the reactor. The UV radiation that was used in the photocatalytic degradation experiments was provided by a light source from a 6 W black lamp (Toshiba Litec Co.). The wavelength is ~ 354 nm. Reactor effluent was collected using a Hamilton gastight syringe and analyzed every 10 minutes for 90 minutes using GC-FID. All experiments were carried out under room temperature (28-30°C).

The gas chromatographic apparatus used in conjunction with the photocatalytic degradation study was a Shimadzu GC-14A gas chromatograph which was coupled with a Shimadzu chromatopac 4A. The GC was equipped with a 2.0 m of 15 % carbowax on Csorb WNAW 80-100 GLT Mesh packed column and a flame ionization detector (FID). The carrier gas was helium at pressure of 2.75 Kg/cm^2. Gases used in the flame were air and hydrogen at pressure of 0.5 Kg/cm^2. The detection, column and injection temperatures were 200°C, 95°C and 150°C respectively. The remaining samples were analyzed every 10 minutes for 90 minutes using GC. The concentration of VOC (ppm) was measured by integrating the peak area.

3.4 Mechanistic Study

3.4.1 Kinetic Study

The procedures followed in conducting the kinetics study were similar to those in the photocatalytic degradation experiments. The experiments were conducted at ambient temperature and pressure. The photoreactor was vacuumed prior to use. Total illumination time of each photocatalytic degradation process was 10 minutes. Each sample was analyzed at 2 minutes intervals using GC-FID. Six different concentrations (0.2 µL, 0.4 µL, 0.5 µL, 0.6 µL, 0.8 µL and 1.0 µL) of each sample were degraded individually. The kinetics study of dichloromethane, chloroform and carbon tetrachloride was carried out using undoped TiO_2, Fe^{2+}, Fe^{3+}, Mn^{2+}, Cu^{2+}, Zn^{2+}-doped

TiO_2, Cu^{2+}/ Fe^{3+}/TiO_2 and Zn^{2+}/Fe^{3+}/TiO_2. A graph of reciprocal initial rate ($1/r^0$) versus reciprocal initial concentration ($1/C^0$) that gives *k* as the L-H rate constant and *K* as the Langmuir adsorption constant of the VOCs in the photocaalytic degradation reaction was drawn.

3.4.2 Determination of Model for the Photocatalytic Degradation of VOCs

Gas chromatography-mass spectrometry (GC-MS) is a combination of two techniques to form a single method of analyzing mixtures of chemicals. The gas chromatography separates the components of a mixture while the mass spectroscopy characterizes each of the components individually. As the individual compounds elute from the GC column, they enter the ionization chamber in the mass spectroscopy. In the ionization chamber, sample molecules are subjected to bombardment by a stream of high-energy electrons, converting some of the molecules to ions. The ions with a particular mass to charge ratio (m/z) are detected by a device which is able to count the number of ions which strike it. The detector's output is amplified and fed to a recorder.

The trace from the recorder is a mass spectrum which is a graph of the number of particles detected as a function of mass to charge ratio. Since most fragments have a charge of +1, therefore, the m/z usually represents the molecular weight of the fragment (Gudzinowicz, 1976).

In this study, A Hewlett-Packard Systems 5890 Series II GC and 5989 A MS were used to analyze fragments that may form during the photocatalytic degradation of the VOCs. The GC-MS is equipped with a 25 m crosslinked methyl siloxane capillary column. Standard addition method was used to predict the reaction model for the photocatalytic degradation of the VOCs. The isothermal temperatures of the oven, injection port and detector were 200°C, 250°C and 250°C respectively.

The procedure used in predicting possible reaction model for the VOCs photocatalytic degradation is similar to those used in the photocatalytic degradation experiments. The experiments were conducted at ambient temperature and pressure. The photoreactor was vacuumed prior to use. The total illumination time for each photocatalytic degradation process was 90 minutes.

3.5 Catalysts Characterization

3.5.1 Ellipsometer

In this research, a single wavelength (632.8 nm) Gaerther Scientific Corporation ellipsometer model L116S was used to measure the thickness and refractive index of thin films. The data obtained from the ellipsometer measurements were processed using the software for ellipsometric analysis. Catalysts coated on glass plates were used as samples. The thickness of thin films was used to calculate the optical band gap values for the thin films.

3.5.2 UV-Vis Spectroscopy (Band Gap Measurements)

The optical band gap, E_g of thin films can be determined using the spectra of measured absorption coefficient, α of the thin films. The α near the absorption edge was derived from the measured transmittance (T) and reflectance (R) factors of the thin films. The α can be obtained by using the following relationship:

$$T = (1 - R^2)\exp(-\alpha d) \qquad (3.1)$$

where d is the thickness of thin film. The calculation to obtain α value was shown in Appendix A. The transmittance and reflectance data were obtained from the optical spectra recorded using a UV-Vis-NIR Shimadzu UV-3101PC Spectrophotometer in the wavelength range of 300-800 nm (Appendix B and C). The optical band gap, E_g values for all catalyst samples were determined by plotting $(\alpha h\nu)_{1/2}$ versus the equivalent energy at the wavelength, λ. h is planck constant while ν is frequency. The resulting diagram was called Tauc's Plot. The respective band gaps were obtained by extrapolation of the Tauc plot dataset to $(\alpha h\nu)_{1/2} = 0$.

3.5.3 Scanning Electron Microscopy (SEM) / Electron Dispersive X-ray Analysis (EDX)

In this study the surface morphology of the catalysts was characterized using SEM, but by selecting only the best catalyst (Zn^{2+} co-doped Fe^{3+}/TiO_2) for characterization. The samples were gold-coated to ensure conductivity. They were then

placed on an aluminium sample stub using double sided carbon tape as adhesive and coated with gold in a Bio Rad SEM coating system using a gold sputterer at 10^{-1} Mbar.

The current flow during the coating process was 30 mA. Then, the gold-coated sample was placed in a specimen chamber under vacuum (5 bar) and the SEM analysis was conducted using a Philip XL40 microscope interfaced with a PC through Philip XL with version 5.01 software. The sample was bombarded using an electron gun with a tungsten filament under 30 kV resolution. A Philips graphic video recorder model GP-850 recorded an image with a 5k magnification. The EDX, model Ametek, USA, version 3.32 XL, is linked to the SEM and uses X-ray to identify trace amounts of elements on the surface of the scanned test specimen. In this study, all doped and undoped TiO_2 thin films were characterized using EDX. All data obtained from EDX were analyzed based on the emission lines of the elements recorded on the diffractogram. These lines were then referred to the Periodic Table from Link X-ray Analytical Systems for elemental identification.

CHAPTER 4

RESULTS AND DISCUSSION

4.1 Retention Time from GC Analysis and Photolysis of Dichloromethane, Chloroform and Carbon Tetrachloride

Individual gas sample was injected into the reactor and left to vaporize. The gas sample was then injected into the GC-FID, and sharp peak was found. The retention time for dichloromethane, chloroform and carbon tetrachloride were 1.358, 1.743 and 1.063 minutes respectively. (Refer Table 4.1)

Table 4.1: Retention times from GC analysis for dichloromethane, chloroform and carbon tetrachloride.

Sample	Retention Time / min
Dichloromethane	1.358
Chloroform	1.743
Carbon tetrachloride	1.063

In the photolysis experiment, UV light was used in the absence of catalysts in order to ensure that the measured activity was photocatalytic in nature (Table 4.2). As shown in Table 4.2, no photolysis was detected in the first 30 and 60 minutes. In addition, the measured photolysis at 90 minutes was rather small, in which only 0.73 % and 1.13 % were detected for dichloromethane and carbon tetrachloride respectively while for chloroform, the photolysis was almost negligible. This indicated that all gas samples could not be directly decomposed by UV light of maximum wavelength used in this study (354 nm).

Table 4.2: % Photolysis of dichloromethane, chloroform and carbon tetrachloride.

Time (minutes)	**Photolysis (%)**		
	Dichloromethane	Chloroform	Carbon Tetrachloride
30	0	0	0
60	0	0	0
90	0.73	0	1.13

4.2 Calibration Graph for Dichloromethane, Chloroform and Carbon Tetrachloride

The glass cylinder was vacuumed prior to use to ensure that no gases or pollutants were present. The volume of gas samples (μL) used in the calibration experiments were expressed in terms of concentration (ppm). The calculation is given in Appendix D. Figure 4.1 shows the calibration graph of dichloromethane, chloroform and carbon tetrachloride. Excellent straight lines which intercept on the origin were obtained in calibration graph. The R^2 and the obtained equations for dichloromethane, chloroform and carbon tetrachloride were shown in Table 4.3. The R^2 of the lines were 0.9903, 0.997 and 0.9939 for dichloromethane, chloroform and carbon tetrachloride respectively. The obtained equations were used to calculate the concentration of dichloromethane, chloroform and carbon tetrachloride in further experiments.

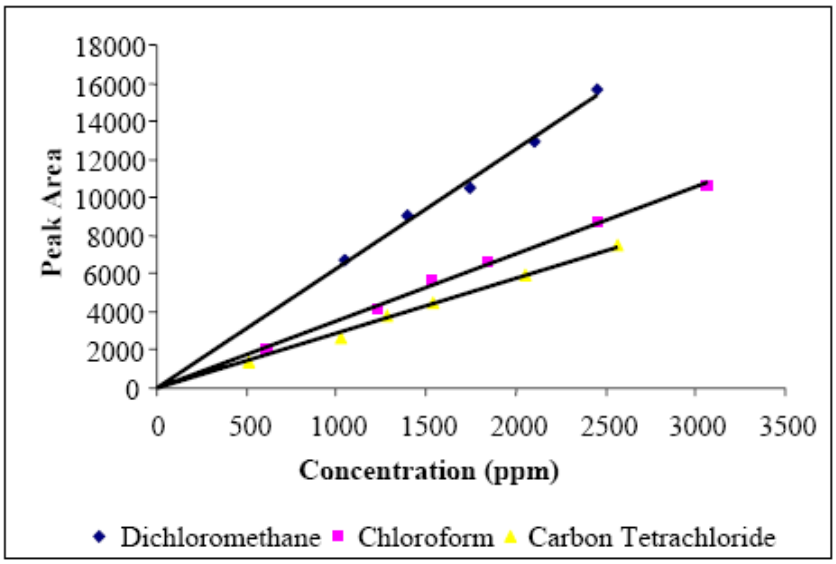

Figure 4.1: Calibration graph of peak area versus concentration for dichloromethane, chloroform and carbon tetrachloride.

Table 4.3: R_2 and the equation for dichloromethane, chloroform and carbon tetrachloride.

VOCs	Equations	R^2
Dichloromethane	y = 5.661x	0.9903
Chloroform	y = 3.4785x	0.997
Carbon tetrachloride	y = 2.8911x	0.9939

4.3 Optimum Dopant Ratios

In photocatalytic degradation experiments, TiO_2 doped with various metal ions ratios were used as catalysts. It was interesting to note that when the photocatalytic degradation experiments were conducted, a trend appeared in that only catalysts with optimum dopant ratios resulted in appreciable degradation. It can be further observed that the concentration of sample decreased with increasing of degradation time. Value of % degradation at any particular time can be calculated using the following formula:

$$\% \text{ of degradation} = \frac{[\text{sample}]_0 - [\text{sample}]_t}{[\text{sample}]_0} \times 100$$

whereby, $[\text{sample}]_0$: Initial concentration of sample

$[sample]_t$: Concentration of sample at particular time

Five dopant ratios were prepared when Fe^{2+} and Mn^{2+} were used as dopant in the photocatalytic degradation of dichloromethane, which ranged from 1:0.0003 to 1: 0.01 dopant ratios. However, only 3 dopant ratios were prepared for the Fe^{3+}-doped TiO_2, Cu^{2+}-doped TiO_2, Zn^{2+}-doped TiO_2, Zn^{2+} co-doped Fe^{3+}/TiO_2 and Cu^{2+} co-doped Fe^{3+}/TiO_2. All photocatalytic degradation processes were conducted for 90 minutes.

4.3.1 Dichloromethane

Figures 4.2-4.6 compare the percentage degradation of dichloromethane using catalysts TiO_2 doped with various metal ions ratios. Figures 4.7 and 4.8 show the comparison of percentage degradation of dichloromethane using catalysts Zn^{2+} co-doped Fe^{3+}/TiO_2 and Cu^{2+} co-doped Fe^{3+}/TiO_2 respectively. According to Figures 4.2-4.6, the curves indicate that metal ion doped TiO_2 displayed preferable photoactivity compared to undoped TiO_2 except for Mn^{2+}-doped TiO_2. From Figure 4.2, it can be seen that Fe^{2+}-doped TiO_2 with 1:0.0005 mole ratio showed the highest degradation of dichloromethane with 33.79 % dichloromethane was degraded. This was followed by Fe^{2+}-doped TiO_2 with 1:0.005 mole ratio and 1:0.01 mole ratio. Fe^{2+}-doped TiO_2 with 1:0.0003 mole ratio gave slightly higher degradation of dichloromethane than pure TiO_2 in which only 20.93 % dichloromethane was degraded.

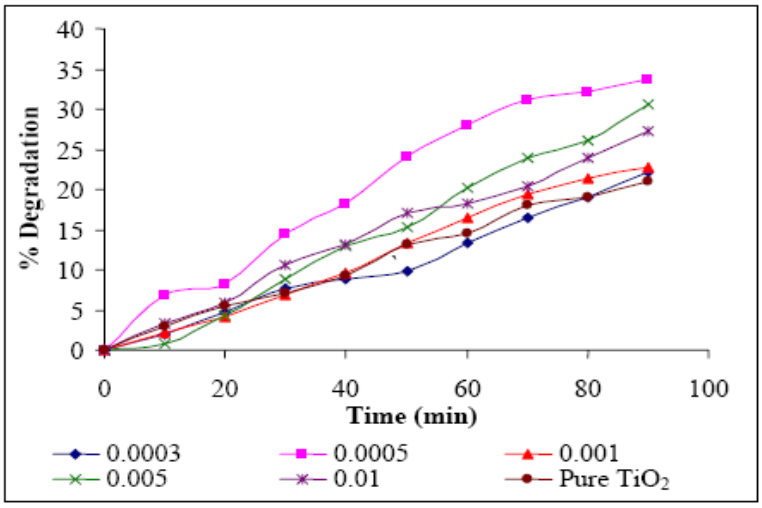

Figure 4.2: % Degradation of dichloromethane using Fe^{2+}-doped TiO_2 at various dopant concentrations.

Figure 4.3 depicts the % degradation of dichloromethane using Mn^{2+}-doped TiO_2 as catalyst. It was found that Mn^{2+}-doped TiO_2 gave lower degradation than pure TiO_2

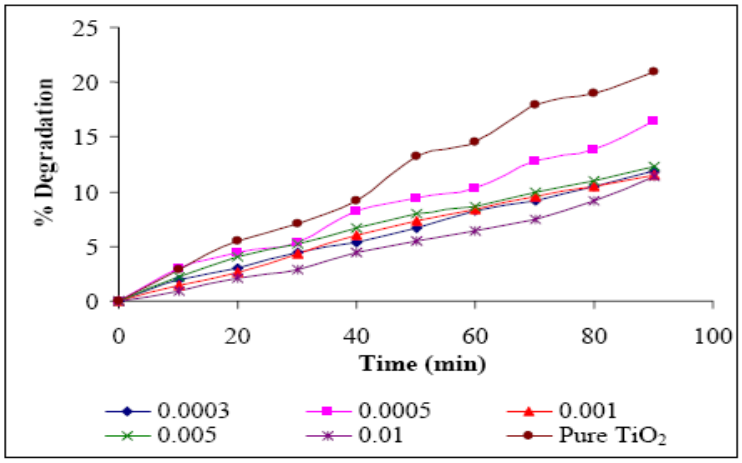

Figure 4.3: % Degradation of dichloromethane using Mn^{2+}-doped TiO_2 at various dopant concentrations.

Among all dopant ratios, Mn^{2+}-doped TiO_2 with 1:0.0005 mole ratio showed the highest degradation of dichloromethane. Meanwhile, Mn^{2+}-doped TiO_2 with 1:0.01 mole ratio gave the lowest degradation of dichloromethane. When Mn^{2+}-doped TiO_2 with 1:0.0003 and 1:0.005 mole ratios were used, only 11.95 % and 12.31 % dichloromethane had been degraded. From Figure 4.5, it can be observed that when Cu^{2+}-doped TiO_2 was used as catalyst in the photocatalytic degradation of dichloromethane, the optimum dopant ratio was 1:0.0005 mole ratio where 34.3 % dichloromethane was degraded. However, when Cu^{2+}-doped TiO_2 with 1:0.0003 and 1:0.001 mole ratios were used as catalyst, 31.84 % and 32.81 % dichloromethane were degraded respectively. According to Figure 4.6, it was found that Zn^{2+}-doped TiO_2 with 1:0.0005 mole ratio gave the highest degradation among all dopant ratios where 34.89 % dichloromethane was degraded. For Zn^{2+}-doped TiO_2 with 1:0.0003 mole ratio, 34.01 % dichloromethane was degraded. Among all dopant ratios, Zn^{2+}-doped TiO_2 with 1:0.001 mole ratio showed the lowest degradation of dichloromethane where 33.98 % dichloromethane had been degraded.

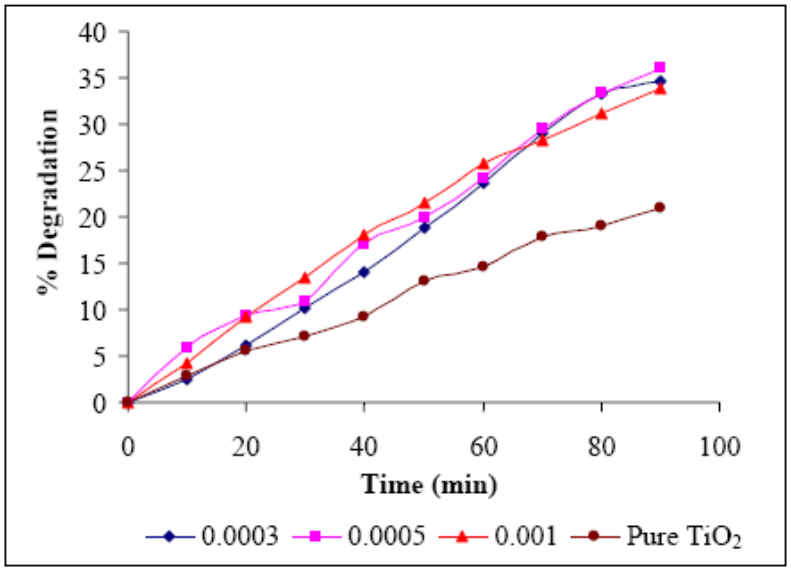

Figure 4.4: % Degradation of dichloromethane using Fe^{3+}-doped TiO_2 at various dopants

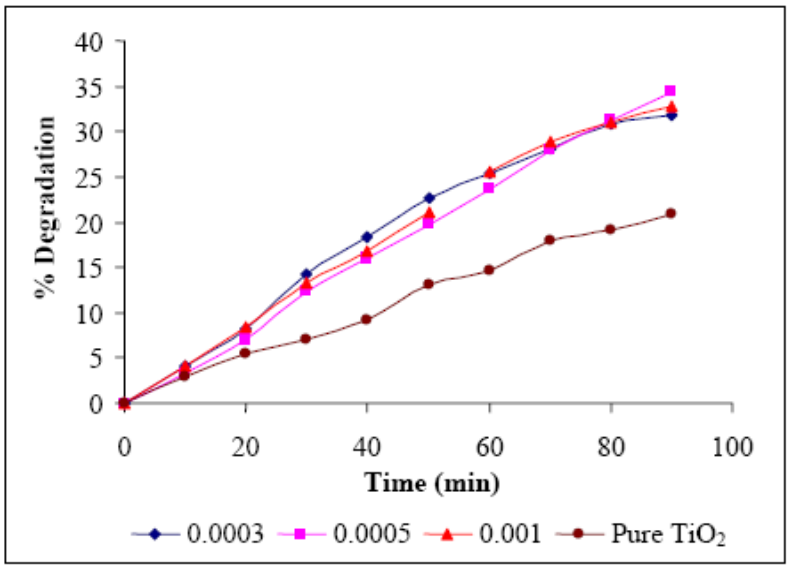

Figure 4.5: % Degradation of dichloromethane using Cu^{2+}-doped TiO_2 at various dopant concentrations.

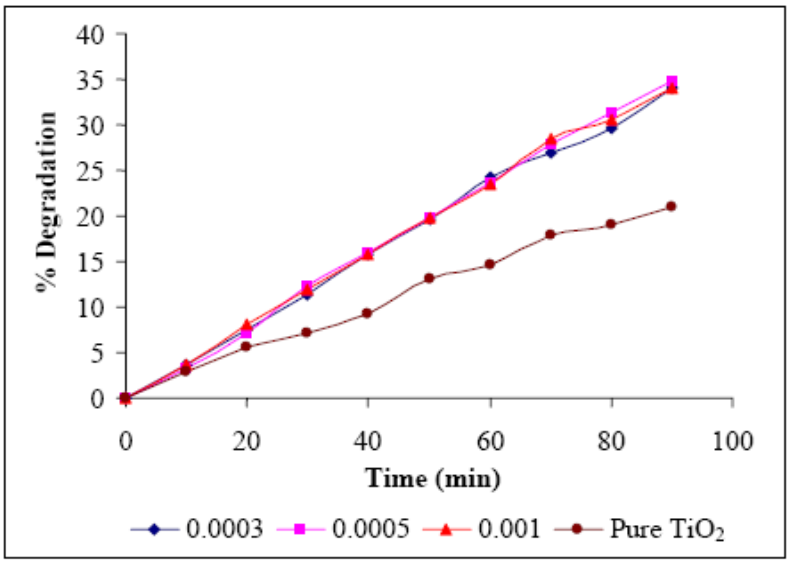

Figure 4.6: % Degradation of dichloromethane using Zn^{2+}-doped TiO_2 at various dopant concentrations.

Since the optimum dopant ratio for Fe^{3+} was 1:0.0005 mole ratio, therefore, in the preparation of co-dopant catalysts, the dopant ratio for Fe^{3+} was fixed at 1:0.0005 mole ratio while the co-dopant ratios for Zn^{2+} and Cu^{2+} were varied. Figure 4.7 and 4.8 depicted that the optimum dopant ratios for Zn^{2+} co-doped Fe^{3+}/TiO_2 and Cu^{2+} co-doped Fe^{3+}/TiO_2 were 1:0.0005:0.0005 mole ratios. When Fe^{3+}-doped TiO_2 with optimum dopant ratio was used, 36.02 % dichloromethane was degraded (Figure 4.4). However, when Zn^{2+} co-doped Fe^{3+}/TiO_2 and Cu^{2+} co-doped Fe^{3+}/TiO_2 with optimum dopant ratios were used, it was found that the % degradation of dichloromethane had been increased to 41.05 % and 36.76 % dichloromethane respectively (Figures 4.7 and 4.8).

Besides, the % degradation of dichloromethane using Zn^{2+} co-doped Fe^{3+}/TiO_2 and Cu^{2+} co-doped Fe^{3+}/TiO_2 as catalyst was also higher than that using single Zn^{2+} and Cu^{2+}- doped TiO_2 (Figure 4.5 and 4.6). Both of the Zn^{2+} co-doped Fe^{3+}/TiO_2 and Cu^{2+} codoped Fe^{3+}/TiO_2 with 1:0.0005:0.0003 and 1:0.0005:0.001 mole ratios gave less than 35 % degradation of dichloromethane.

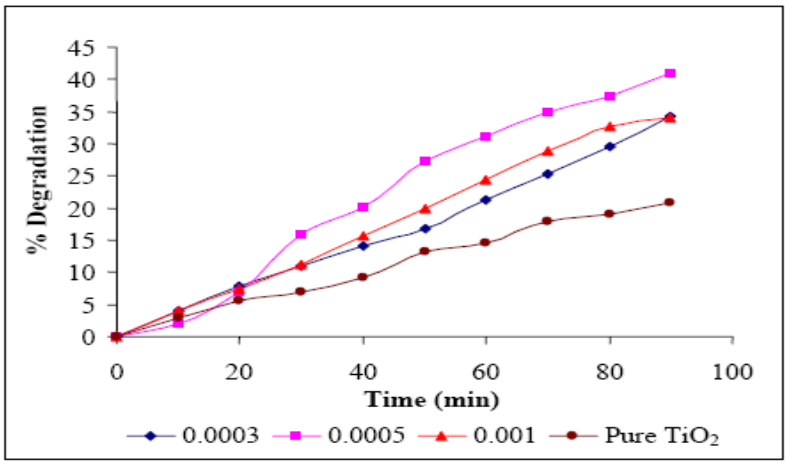

Figure 4.7: % Degradation of dichloromethane using Zn^{2+} co-doped Fe^{3+}/TiO_2 at various dopant concentrations.

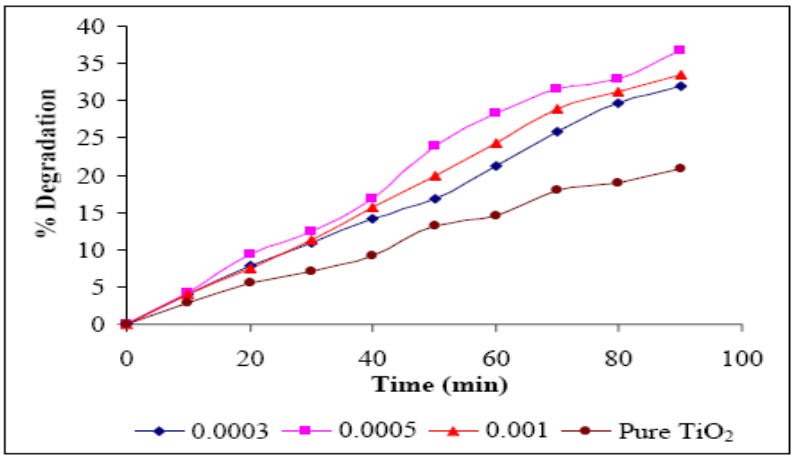

Figure 4.8: % Degradation of dichloromethane using Cu^{2+} co-doped Fe^{3+}/TiO_2 at various dopant concentrations.

4.3.2 Chloroform

In the determination of optimum dopant ratio in the photocatalytic degradation of chloroform, Fe^{3+}, Zn^{2+}, Cu^{2+}, Fe^{2+}, Mn^{2+}-doped TiO_2, Zn^{2+} co-doped Fe_{3+}/TiO_2 and Cu^{2+} co-doped Fe^{3+}/TiO_2 were tested. Figures 4.9-4.13 depict the photocatalytic degradation of chloroform using Fe^{2+}, Mn^{2+}, Fe^{3+}, Zn^{2+} and Cu^{2+}-doped TiO_2 respectively while Figures 4.14 and 4.15 show the photocatalytic degradation of chloroform using Zn^{2+} codoped Fe^{3+}/TiO_2 and Cu^{2+} co-doped Fe^{3+}/TiO_2.

It can be seen that a dopant ratio of 1:0.0005 showed higher degradation of chloroform when Zn^{2+}, Cu^{2+}, Fe^{2+}, Mn^{2+} and Fe^{3+}-doped TiO_2 were used. When Fe^{2+}-doped TiO_2 was used, catalysts with dopant ratios of 1:0.0005 gave the best degradation performance, with 34.21 % chloroform degraded, followed by the catalyst with 1:0.001 mole ratio and finally with 1:0.0003 mole ratio which showed 30.84 % and 29.8 % degradation respectively (Figure 4.9).

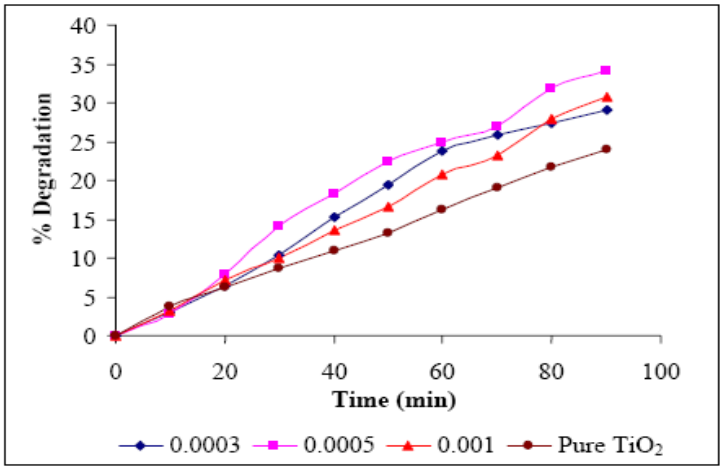

Figure 4.9: % Degradation of chloroform using Fe^{2+}-doped TiO_2 at various dopant concentrations.

Figure 4.10 shows that Mn^{2+}-doped TiO_2 with 1:0.0005 dopant ratio showed higher degradation of chloroform than other dopant ratios. However, pure TiO_2 showed higher degradation of chloroform than Mn^{2+}-doped TiO_2. Pure TiO_2 showed 23.87 % degradation of chloroform while Mn^{2+}-doped TiO_2 with various dopant ratios used in this study only showed less than 20 % degradation of chloroform.

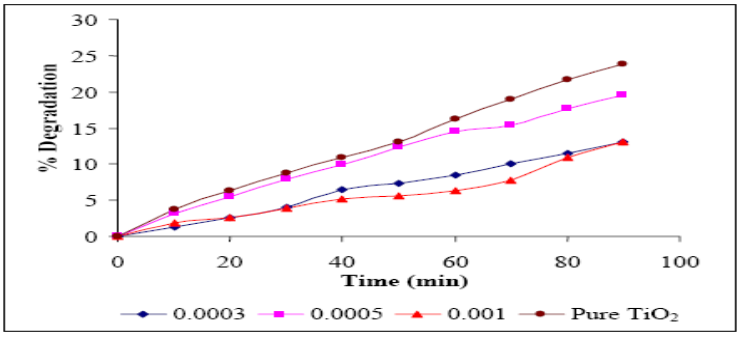

Figure 4.10: % Degradation of chloroform using Mn^{2+}-doped TiO_2 at various dopant concentrations.

Figure 4.11 shows the photocatalytic degradation of chloroform using Fe^{3+}-doped TiO_2 as catalysts. Fe^{3+}-doped TiO_2 with 1:0.0005 mole ratio gave the best degradation of chloroform among other Fe^{3+} dopant ratios in which 43.10 % chloroform had been degraded. Fe^{3+}-doped TiO_2 with 1:0.0003 and 1:0.001 dopant ratios gave 35.74 % and 35.11 % degradation respectively. Figures 4.12 and 4.13 show the % degradation of chloroform using Zn^{2+} and Cu^{2+}-doped TiO_2 as catalysts. From Figure 4.12, it can be seen that the optimum dopant ratio for Zn^{2+}-doped TiO_2 was 1:0.0005 mole ratio, where 36.98 % chloroform had been degraded. Meanwhile, Zn^{2+}-doped TiO_2 with 1:0.0003 and 1:0.001 mole ratios showed 34.43 % and 34.77 % degradation of chloroform respectively. When Cu^{2+}-doped TiO_2 was used as catalyst in the photocatalytic degradation of chloroform, it was found that Cu^{2+}-doped TiO_2 had an optimum dopant ratio of 1:0.0005, where 36.14 % chloroform was degraded (Figure 4.13).

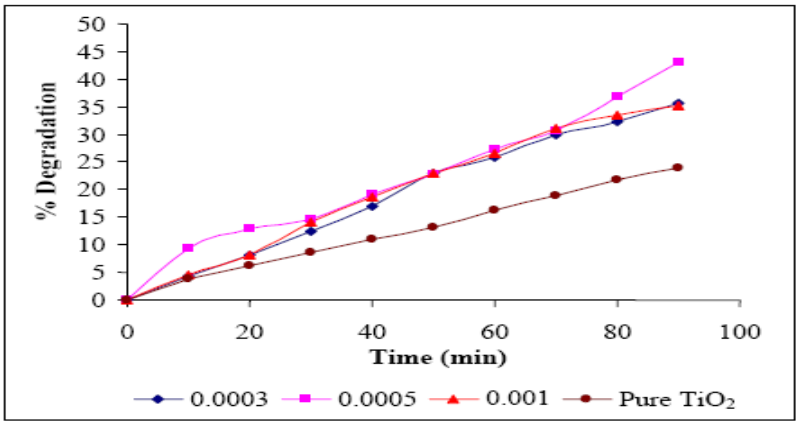

Figure 4.11: % Degradation of chloroform using Fe^{3+}-doped TiO_2 at various dopant concentrations.

Figures 4.14 and 4.15 depict the degradation of chloroform using Zn^{2+} co-doped Fe^{3+}/TiO_2 and Cu^{2+} co-doped Fe^{3+}/TiO_2 respectively. Both of the Zn^{2+} co-doped Fe^{3+}/TiO_2 and Cu^{2+} co-doped Fe^{3+}/TiO_2 catalysts had an optimum dopant ratio of 1:0.0005:0.0005 where 49.45 % and 42.55 % chloroform was degraded respectively. It was found that all Zn^{2+} co-doped Fe^{3+}/TiO_2 and Cu^{2+} co-doped Fe^{3+}/TiO_2 with 1:0.0005:0.0003 and 1:0.0005:0.001 mole ratios gave less than 40 % degradation of chloroform.

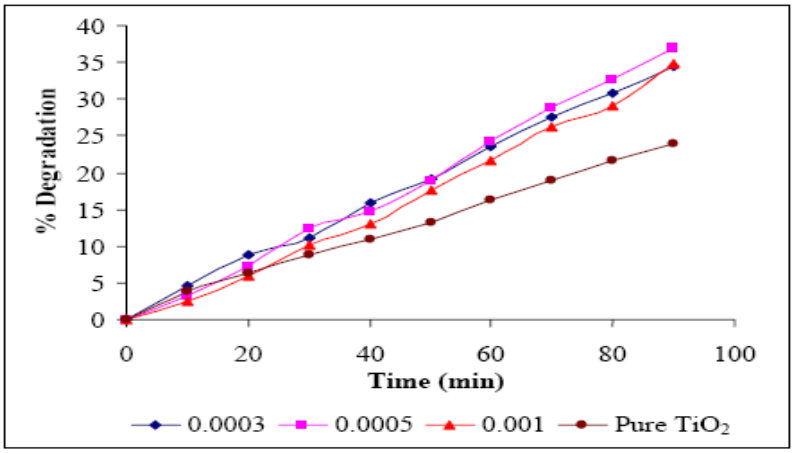

Figure 4.12: % Degradation of chloroform using Zn^{2+}-doped TiO_2 at various dopant concentrations.

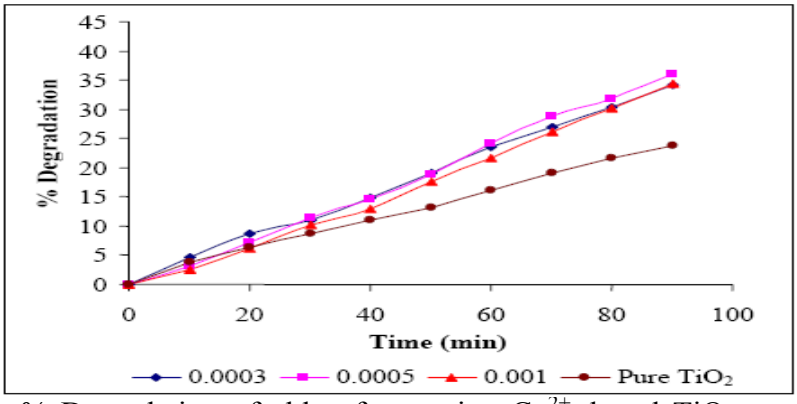

Figure 4.13: % Degradation of chloroform using Cu^{2+}-doped TiO_2 at various dopant concentrations.

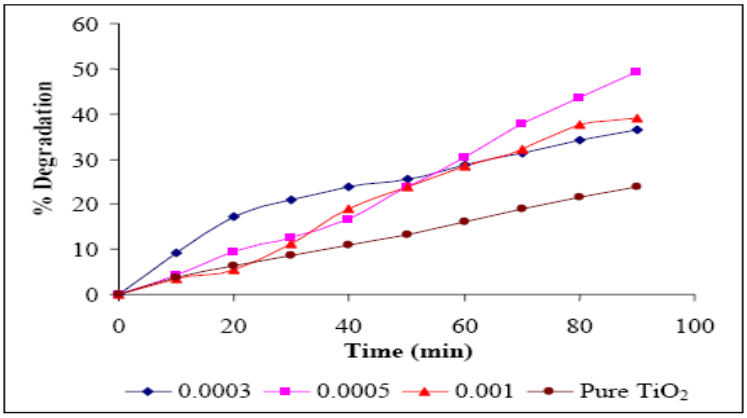

Figure 4.14: % Degradation of chloroform using Zn^{2+} co-doped Fe^{3+}/TiO_2 at various dopant concentrations.

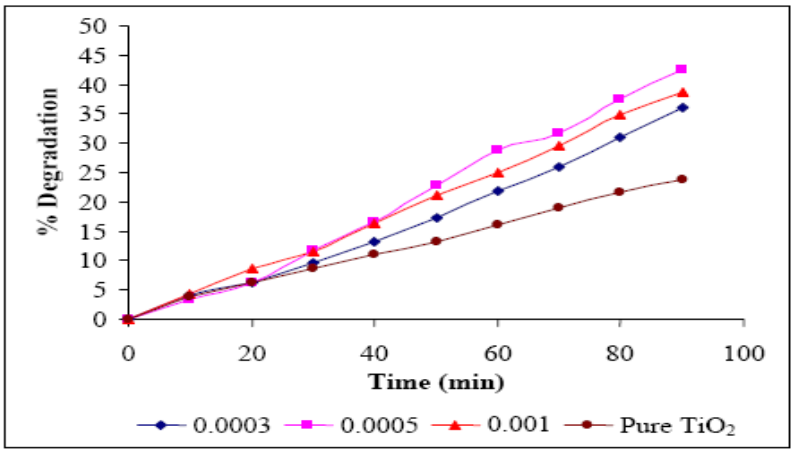

Figure 4.15: % Degradation of chloroform using Cu^{2+} co-doped Fe^{3+}/TiO_2 at various dopant concentrations.

4.3.3 Carbon Tetrachloride

Figures 4.16, 4.17 and 4.18 depict the photocatalytic degradation of carbon tetrachloride using Mn^{2+}, Fe^{2+} and Fe^{3+}-doped TiO_2 as catalysts. From Figure 4.16, it can be seen that the degradation of carbon tetrachloride using pure TiO_2 showed higher degradation than Mn^{2+}-doped TiO_2. Among 1:0.0005, 1:0.0003 and 1:0.001 Mn^{2+} dopant ratios, it was noted that the optimum dopant ratio for Mn^{2+}-doped $TiO_2$was 1:0.0005 mole ratio.

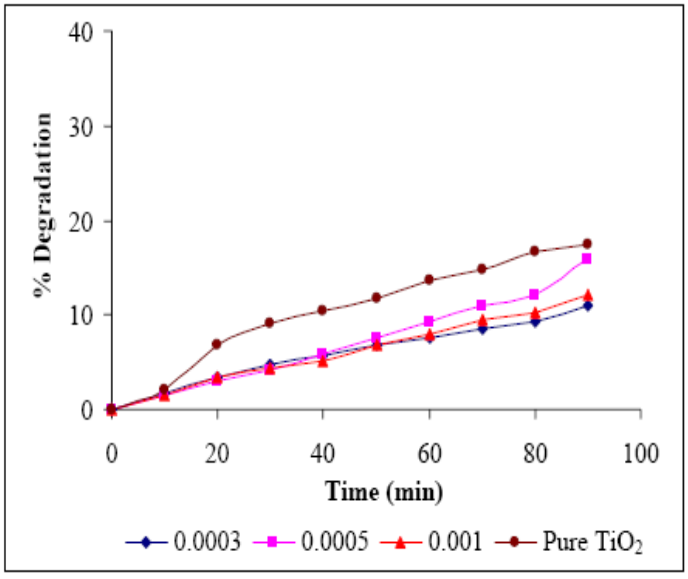

Figure 4.16: % Degradation of carbon tetrachloride using Mn^{2+}-doped TiO_2 at various dopant concentrations.

Figure 4.17 shows the photocatalytic degradation of carbon tetrachloride using Fe^{2+}-doped TiO_2 as catalyst. When Fe^{2+}-doped TiO_2 were used, the degradations of carbon tetrachloride were lower than undoped TiO_2 except Fe^{2+}-doped TiO_2 with 1:0.0005 mole ratio. From Figure 4.17, it can be seen that the optimum dopant ratio for Fe^{2+}-doped TiO_2 was 1:0.0005 mole ratio where 20.80 % carbon tetrachloride had been degraded. Fe^{2+}-doped TiO_2 with 1:0.0003 and 1:0.001 mole ratios only showed 13.42 % and 12.36 % degradation of carbon tetrachloride.

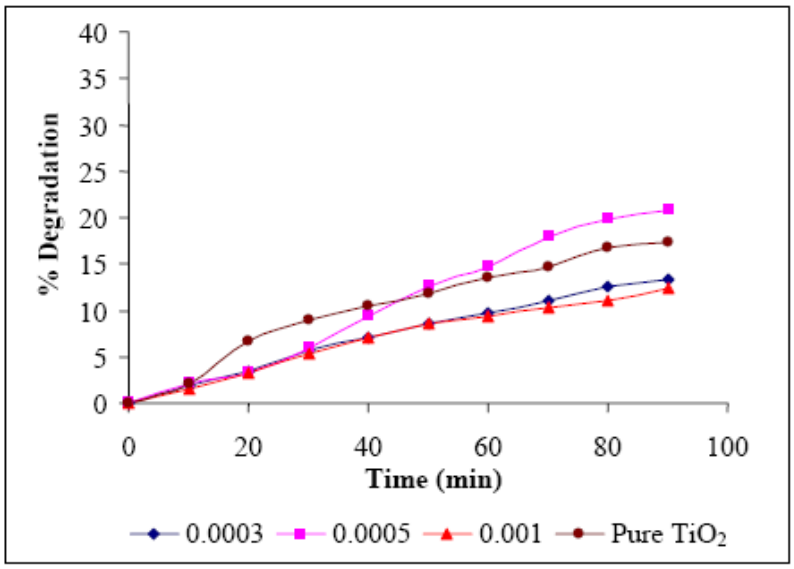

Figure 4.17: % Degradation of carbon tetrachloride using Fe^{2+}-doped TiO_2 at various dopant concentrations.

Figure 4.18 depicts the photocatalytic degradation of carbon tetrachloride using Fe^{3+}-doped TiO_2. It can be seen from Figure 4.18 that the optimum dopant ratio for the degradation of carbon tetrachloride was 1:0.0005 mole ratio, with 35.42 % carbon tetrachloride degraded. This was followed by Fe^{3+}-doped TiO_2 with 1:0.001 and 1:0.0003 mole ratio and finally pure TiO_2.

Figures 4.19 and 4.20 compare the % degradation of carbon tetrachloride when Zn^{2+}-doped TiO_2 and Cu^{2+}-doped TiO_2 with various dopant ratios were used. From the figures, it was found that both Zn^{2+}-doped TiO_2 and Cu^{2+}-doped TiO_2 catalysts with 1:0.0005 mole ratios gave the best degradation of carbon tetrachloride where 27.44 % and 25.67 % carbon tetrachloride was degraded respectively. This was followed by the Cu^{2+}-doped TiO_2 and Zn^{2+}-doped TiO_2 catalysts with 1:0.001 mole ratios and then by the Cu^{2+}-doped TiO_2 and Zn^{2+}-doped TiO_2 catalysts with 1:0.0003 mole ratios. Pure TiO_2 gave the lowest degradation of carbon tetrachloride. It was found that only 17.40 % of carbon tetrachloride was degraded when pure TiO_2 was used as catalyst.

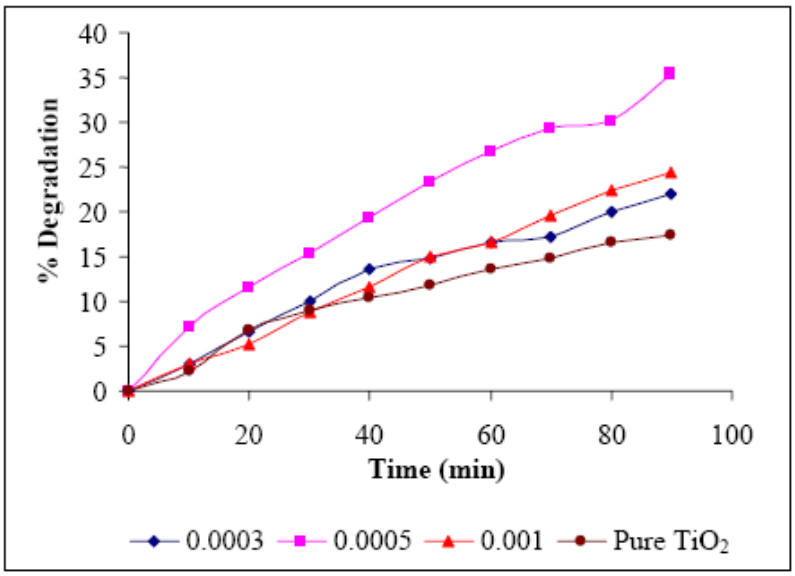

Figure 4.18: % Degradation of carbon tetrachloride using Fe^{3+}-doped TiO_2 at various dopant concentrations.

The influence of the second dopant ion in co-doped TiO_2 to the photocatalytic degradation process is demonstrated in Figures 4.21 and 4.22. It can be seen that both Zn^{2+} co-doped Fe^{3+}/TiO_2 and Cu^{2+} co-doped Fe^{3+}/TiO_2 had an optimum ratio of 1:0.0005:0.0005, where 37.84 % and 33.88 % carbon tetrachloride had been degraded respectively. For Zn^{2+} co-doped Fe^{3+}/TiO_2 and Cu^{2+} co-doped Fe^{3+}/TiO_2 with 1:0.0005:0.0003 mole ratios, the % degradation of carbon tetrachloride were 32.89 % and 29.10 % respectively. When Zn^{2+} co-doped Fe^{3+}/TiO_2 and Cu^{2+} co-doped Fe^{3+}/TiO_2

with 1:0.0005:0.001 mole ratios were used, 32.73 % and 31.03 % degradation of carbon tetrachloride were obtained respectively.

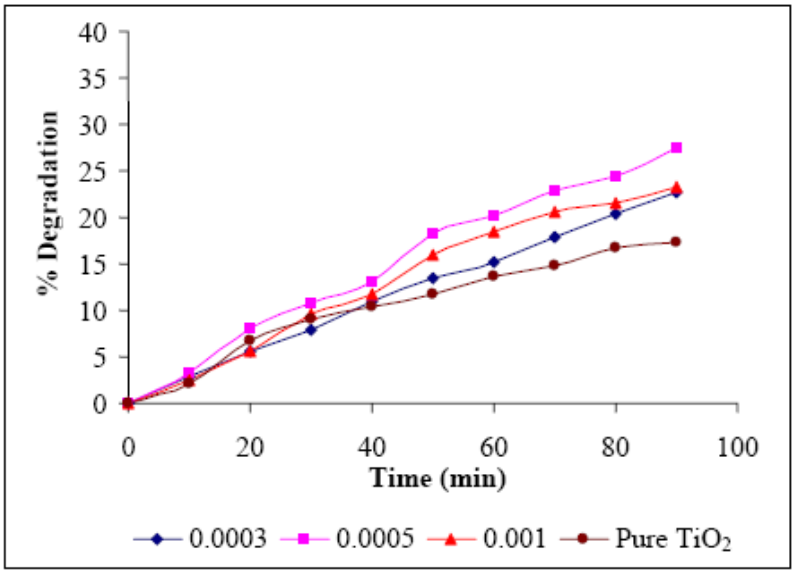

Figure 4.19: % Degradation of carbon tetrachloride using Zn^{2+}-doped TiO_2 at various dopant concentrations.

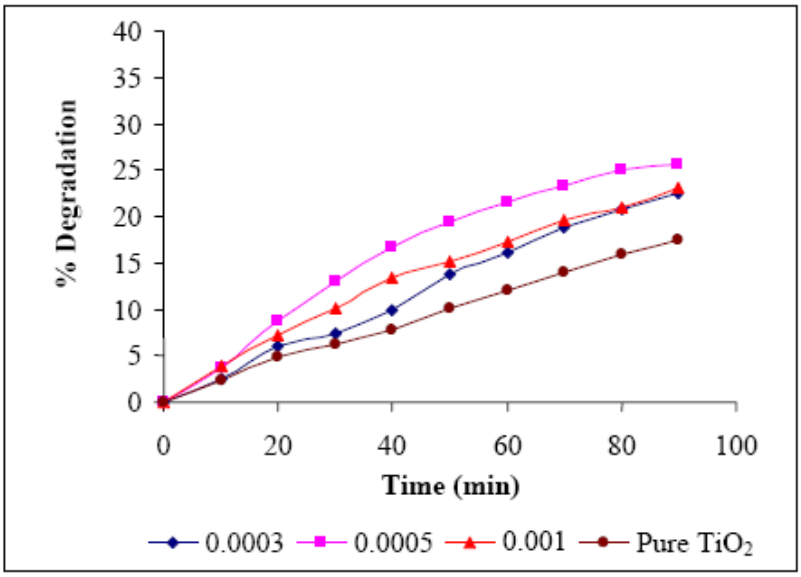

Figure 4.20: % Degradation of carbon tetrachloride using Cu^{2+}-doped TiO_2 at various dopant concentrations.

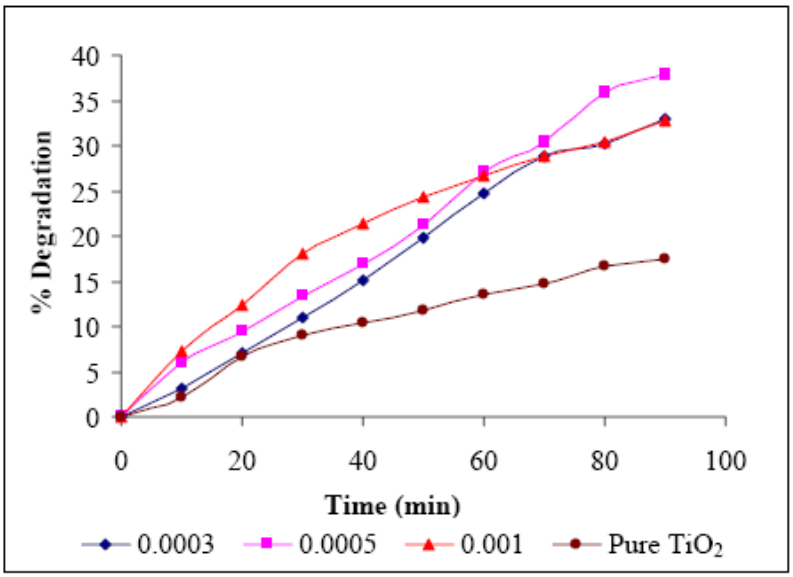

Figure 4.21: % Degradation of carbon tetrachloride using Zn^{2+} co-doped Fe^{3+}/TiO_2 at various dopant concentrations.

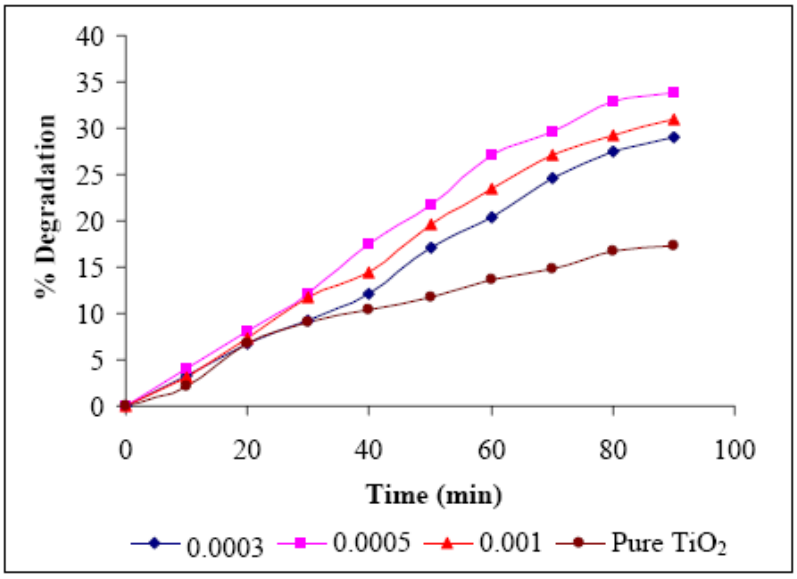

Figure 4.22: % Degradation of carbon tetrachloride using Cu^{2+} co-doped Fe^{3+}/TiO_2 at various dopant concentrations.

In a typical photocatalytic degradation experiment, the high degree of recombination between photogenerated holes and electrons was a major limiting factor controlling the photocatalytic degradation efficiency. Below the optimum dopant ratio,

the addition of metals as dopant can promote interfacial charge transfer process through the Equation 1.1 - 1.2. This migration of the generated electron to the metal particles can increase the lifetime of the holes and suppress electron-hole recombination and consequently, be beneficial for the photocatalytic degradation processes.

However, when the concentrations of dopants ion are above the optimum dopant ratio, photocatalytic activity decreases and this can be seen in Figures 4.2 - 4.22. This means that heavy doping may result in the dopant atoms becoming recombination centres, thus reducing the photocatalytic efficiency. Besides, the detrimental effect of high metal ion concentrations on the degradation rate also can be explained by several factors. In a photocatalytic degradation process, the •OH radicals exist in the catalyst are used to degrade the pollutants. When the concentrations of dopants ion are above the optimum dopant ratio, the metallic species can reoxidize the reduced metal ions by •OH radicals or h_+ (Eq. 4.1-4.2), forcing the reducing amount of •OH radicals to degrade the pollutants. The large number of metallic species will also compete with oxygen to react with generated electrons, consequently reducing the formation of •OH through Equation 4.3 - 4.8 (Litter, 1999). In the review of heterogeneous photocatalysis done by Litter in 1999, Litter noted another reason for the deleterious effect of high concentrations of Cu^{2+}, Ni^{2+} and Fe^{2+} was the filter effect due to UV light absorption of the species.

$$M^{(n-1)+} + h_{vb}^{+} \longrightarrow M^{n+} \quad (4.1)$$

$$M^{(n-1)+} + (\bullet OH) \longrightarrow M^{n+} + OH^{-} \quad (4.2)$$

$$e_{cb}^{-} + O_{2\,ads} + H^{+} \longrightarrow HO_2\bullet \rightleftharpoons O_2^{-}\bullet + H^{+} \quad (4.3)$$

$$HO_2\bullet + e_{cb}^{-} + 3H^{+} \longrightarrow 2H_2O \quad (4.4)$$

$$2HO_2\bullet \longrightarrow H_2O_2 + O_2 \quad (4.5)$$

$$H_2O_2 + O_2^{-}\bullet \longrightarrow HO\bullet + O_2 + OH^{-} \quad (4.6)$$

$$H_2O_2 + h\nu \longrightarrow 2HO\bullet \quad (4.7)$$

$$H_2O_2 + e_{cb}^{-} \longrightarrow HO\bullet + OH^{-} \quad (4.8)$$

4.4 Effects of Metal Ions (M^{n+})

In a photocatalytic degradation process, photogenerated electrons and holes will recombine; therefore suppressing the recombination of electron-hole pairs and prolonging the lifetime of carriers are essential for improving the efficiency of the

catalyst. For this reason, various studies have been carried out to increase the lifetime of the carriers and one such method employs transition metals as dopants.

Figure 4.23 shows the % degradation of dichloromethane using Cu^{2+}, Zn^{2+}, Mn^{2+}, Fe^{2+}, Fe^{3+}-doped TiO_2, Zn^{2+} co-doped Fe^{3+}/TiO_2, Cu^{2+} co-doped Fe^{3+}/TiO_2 and undoped TiO_2 as catalysts. The photocatalytic degradation of dichloromethane was significantly better with Zn^{2+} co-doped Fe^{3+}/TiO_2 (41.05 %) compared to other doped and pure TiO_2 catalysts. This was followed by Cu^{2+} co-doped Fe^{3+}/TiO_2 and then Fe^{3+}- doped TiO_2. It was found that the addition of co-dopants resulted in better degradation of dichloromethane if compared with the addition of Zn^{2+} and Fe^{3+} or Cu^{2+} and Fe^{3+} alone.

However, the addition of Cu^{2+}, Zn^{2+} and Fe^{3+} had increased the TiO_2 photoactivity. 36.02 % of CH_2Cl_2 were degraded when Fe^{3+}-doped TiO_2 was used in the photocatalytic degradation process, 34.89 % and 34.30 % dichloromethane was degraded with Zn^{2+} and Cu^{2+}-doped TiO_2 respectively. Besides, Fe^{2+}-doped TiO_2 had increased the degradation of dichloromethane if compared with pure TiO_2 in which 33.79 % degradation of dichloromethane was obtained. However, addition of Mn^{2+} decreased the degradation of dichloromethane. When pure TiO_2 was used during the photocatalytic degradation process, only 20.93 % CH_2Cl_2 was degraded.

Figure 4.24 indicates the % degradation of chloroform using Cu^{2+}, Zn^{2+}, Mn^{2+}, Fe^{2+}, Fe^{3+}-doped TiO_2, Cu^{2+} co-doped Fe^{3+}/TiO_2, Zn^{2+} co-doped Fe^{3+}/TiO_2 and undoped TiO_2 as catalysts. It shows that Cu^{2+}, Zn^{2+}, Fe^{2+}, Fe^{3+}-doped TiO_2, Cu^{2+} co-doped Fe^{3+}/TiO_2 and Zn^{2+} co-doped Fe^{3+}/TiO_2 give better degradation of chloroform than pure TiO_2. Meanwhile, Mn^{2+}-doped TiO_2 showed poor degradation in the photocatalytic degradation of chloroform, with only 19.57 % chloroform was degraded. Zn^{2+} co-doped Fe^{3+}/TiO_2 showed the best level of chloroform degradation among all doped TiO_2 catalysts that were used in the photocatalytic degradation processes. From Figure 4.24, it can be noticed that addition of Zn^{2+} and Fe^{3+} as co-dopant into TiO_2 enhanced the degradation efficiency of TiO_2 from 23.87 % to 49.45 %. Fe^{3+}-doped TiO_2 catalyst gave lower degradation of chloroform if compared with Zn^{2+} co-doped Fe^{3+}/TiO_2 but slightly higher than Cu^{2+} co-doped Fe^{3+}/TiO_2.

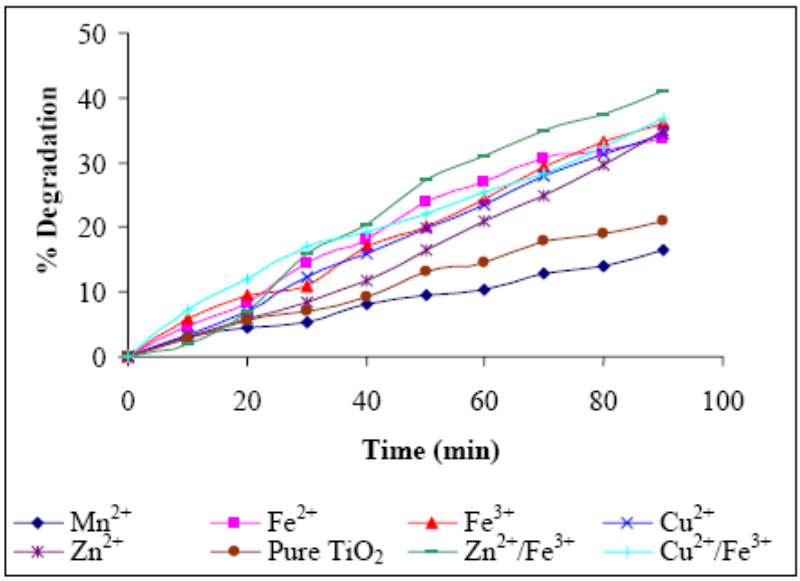

Figure 4.23: % Degradation of dichloromethane using Cu^{2+}, Zn^{2+}, Mn^{2+}, Fe^{2+}, Fe^{3+}-doped TiO_2, Cu^{2+} co-doed Fe^{3+}/TiO_2, Zn^{2+} co-doped Fe^{3+}/TiO_2 and undoped TiO_2 as catalysts.

Figure 4.25 depicts the % degradation of carbon tetrachloride using Cu^{2+}, Zn^{2+}, Mn^{2+}, Fe^{2+}, Fe^{3+}-doped TiO_2, Cu^{2+} co-doped Fe^{3+}/TiO_2, Zn^{2+} co-doped Fe^{3+}/TiO_2 and undoped TiO_2 as catalysts. Among all doped, co-doped and pure TiO_2, Zn^{2+} co-doped Fe^{3+}/TiO_2 showed the best photocatalytic activity where 37.84 % carbon tetrachloride was degraded. This was followed by Fe^{3+}-doped TiO_2 and then Cu^{2+} co-doped Fe^{3+}/TiO_2. Photocatalytic degradation of carbon tetrachloride using Fe^{2+} and Fe^{3+}-doped TiO_2 as catalysts were slightly slower than that of chloroform, which was 20.80 % and 35.42 % respectively. The addition of Cu^{2+} and Zn^{2+} increased the degradation of carbon tetrachloride, with 25.67 % and 27.44 % carbon tetrachloride degraded. However, pure TiO_2 showed higher photocatalytic degradation of carbon tetrachloride than using Mn^{2+}-doped TiO_2 as catalysts.

4.4.1 Effect of $Zn^{2+}/Fe^{3+}/TiO_2$

In the photocatalytic degradation process, a good dopant must be able to act as both electron and hole trap, so that the recombination process between photogenerated

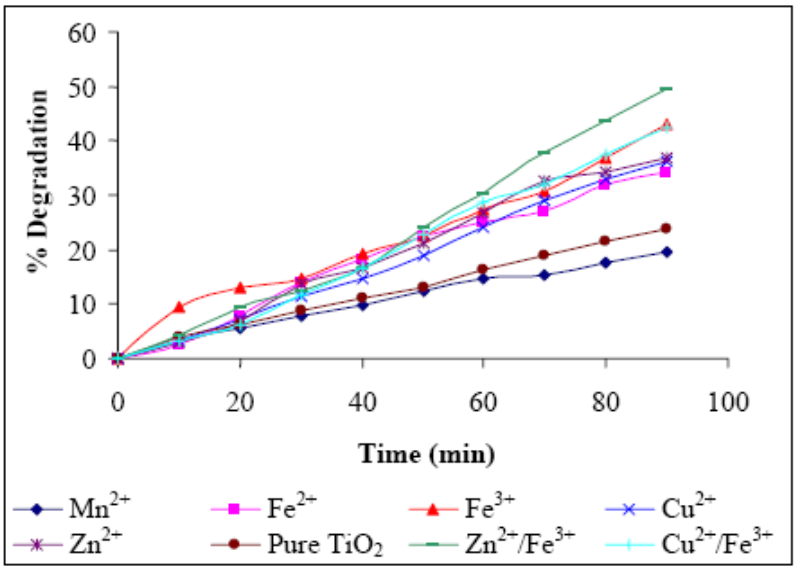

Figure 4.24: % Degradation of chloroform using Cu^{2+}, Zn^{2+}, Mn^{2+}, Fe^{2+}, Fe^{2+}-doped TiO_2, Cu^{2+} co-doped Fe^{3+}/TiO_2, Zn^{2+} co-doped Fe^{3+}/TiO_2 and undoped TiO_2 as catalysts.

electrons and holes can be suppressed, thus increasing the photoactivity of the catalyst (Eq. 1.1 and 1.2). From Figures 4.23-4.25, it can be observed that Zn^{2+} co-doped Fe^{3+}/TiO_2, Fe^{3+}-doped TiO_2 and Cu^{2+} co-doped Fe^{3+}/TiO_2 showed better degradation of dichloromethane, chloroform and carbon tetrachloride than Cu^{2+}, Zn^{2+}, Mn^{2+}, Fe^{2+}, Fe^{3+}-doped TiO_2. An increase in the photocatalytic activity is observed in the case of Zn^{2+} codoped Fe^{3+}/TiO_2. Such an improvement implies that there is a synergistic effect in photocatalytic activity when both Fe^{3+} and Zn^{2+} are co-doped into TiO_2. The effect may be explained by the cooperative operation of the Fe^{3+} and Zn^{2+} in trapping charge carriers and mediating interfacial charge transfer process. Zn^{2+} and Fe^{3+} dopants in TiO_2 can be randomly dispersed on the TiO_2 surface in the form of their oxides (Yuan, 2002).

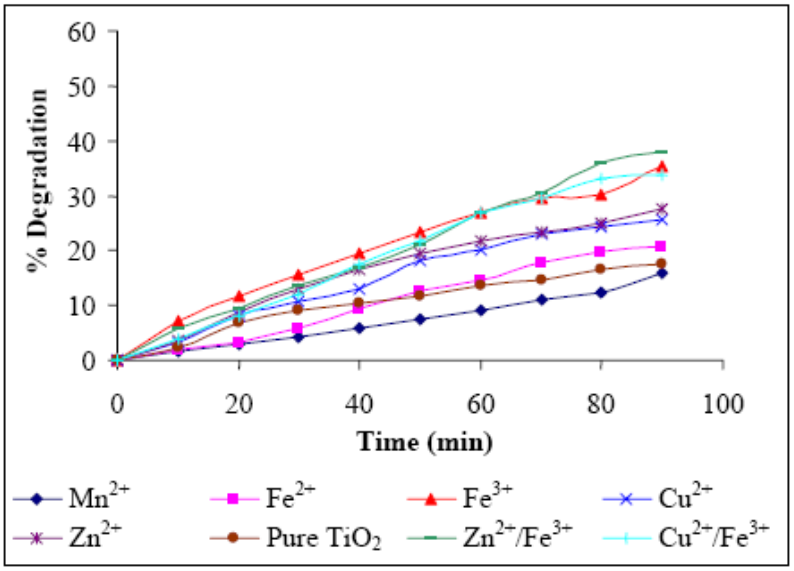

Figure 4.25: % Degradation of carbon tetrachloride using Cu^{2+}, Zn^{2+}, Mn^{2+}, Fe^{2+}, Fe^{3+}-doped TiO_2, Cu^{2+} co-doped Fe^{3+}/TiO_2, Zn^{2+} co-doped Fe^{3+}/TiO_2 and undoped TiO_2 as catalysts.

Due to the difference in the energy band position, the dispersed oxides on the TiO_2 surface will involve some charges transfer between them and TiO_2 during illumination. The valence band of TiO_2 is lower than ZnO but the conduction band of TiO_2 is higher than Fe_2O_3, so the photogenerated holes can move into ZnO while the photogenerated electrons can move into Fe_2O_3. Since Zn^{2+} co-doped Fe^{3+}/TiO_2 can trap electrons and holes, it is not surprising that its photoactivity is higher.

4.4.2 Effect of Fe^{3+}/TiO_2

The Fe^{3+}/Fe^{4+} energy level lies within the band gap, however the Fe^{2+}/Fe^{3+} energy level is closed to the conduction band. Therefore, Fe^{3+} can act as both electron and hole traps as shown in Equation 4.9 and 4.10.

$$Fe^{3+} + h^{+} \longrightarrow Fe^{4+} \qquad (4.9)$$

$$Fe^{3+} + e^{-} \longrightarrow Fe^{2+} \qquad (4.10)$$

This process reduces the recombination rate of holes and electrons and thus enhances the photoactivity of Fe^{3+}. Besides, the trapped hole embodied in Fe^{4+} also can oxidize the VOCs.

4.4.3 Effect of $Cu^{2+}/Fe^{3+}/TiO_2$

In the photocatalytic degradation process, the usage of Cu^{2+} co-doped Fe^{3+}/TiO_2 as catalyst resulted in a better degradation of the studied VOCs compared to single dopant catalysts except for Fe^{3+}-doped TiO_2. Since the valence band of TiO_2 is lower than the energy band for Fe^{3+}/Fe^{4+} while the conduction band of TiO_2 is higher than the energy band for Cu^{2+}/Cu^0, therefore, Fe^{3+} will trap photogenerated holes to form Fe^{4+} while Cu^{2+} will trap the photogenerated electrons. (Refer Figure 1.2). As a consequence, the recombination rate between photogenerated holes and electrons can be suppressed and the photoactivity of $Cu^{2+}/Fe^{3+}/TiO_2$ becomes higher.

4.4.4 Effect of Mn^{2+}/TiO_2

In the photocatalytic degradation of under studied VOCs, addition of Zn^{2+}, Cu^{2+}, Mn^{2+} and Fe^{2+} gave lower degradation of dichloromethane, chloroform and carbon tetrachloride than Cu^{2+} co-doped Fe^{3+}/TiO_2, Zn^{2+} co-doped Fe^{3+}/TiO_2 and Fe^{3+}-doped TiO_2. As stated earlier, a good dopant must be able to trap photogenerated electrons and holes. Zn^{2+}, Cu^{2+}, Mn^{2+} and Fe^{2+} were unable to act as electron and hole traps, so the photoactivity was lower. An experiment on phenol degradation using Zn^{2+}, Mn^{2+}, Fe^{3+}, Co^{3+}, Cr^{3+}, Ce^{3+}, Al^{3+}, Li^{+} and Pt^0-doped TiO_2 as catalyst was conducted (Brezova, 1997). They reported that Mn^{2+} inhibited the degradation of phenol. Mn^{2+} is the most stable oxidation state of manganese. When Mn^{2+} loses an electron to a hole, Mn^{3+} will be created. Since the energy difference between Mn^{2+} and Mn^{3+} is small, so this electron transfer process is not desirable. Therefore, the separation of the photogenerated electron and hole is not effective, and as a consequence, photocatalytic degradation of under studied VOCs was poor.

4.4.5 Effect of Cu^{2+}/TiO_2

The presence of transition metal ions in photocatalytic reactions was reviewed (Litter, 1999). It was found that Cu^{2+} can act positively or negatively depending on the concentration; large amounts of Cu^{2+} will be detrimental. The result obtained gives good agreement with this statement since in the photocatalytic degradation of dichloromethane, chloroform and carbon tetrachloride, the usage of Cu^{2+} as dopant enhanced the photocatalytic activity although the photocatalytic activity was lower than Cu^{2+} co-doped Fe^{3+}/TiO_2, Zn^{2+} co-doped Fe^{3+}/TiO_2 and Fe^{3+}-doped TiO_2. Cu^{2+} only can trap the electrons to form Cu^{+} and then Cu^{0} (Eq. 4.11).

$$Cu^{2+} + e^{-} \longrightarrow Cu^{+} + e^{-} \longrightarrow Cu \qquad (4.11)$$

However, Cu^{2+} is unable to trap photogenerated holes, as a result, the degradations of dichloromethane, chloroform and carbon tetrachloride were lower than the catalysts with dopant which can trap electrons and holes.

4.4.6 Effect of Fe^{2+}/TiO_2

According to Figure 1.2, the energy level for Fe^{2+}/Fe^{3+} is closed to the conduction band, so Fe^{2+} is expected to trap photogenerated holes to form Fe^{3+} during the photocatalytic degradation process. Since Fe^{2+} is unable to trap electrons, therefore, the photoactivity of Fe^{2+}-doped TiO_2 was lower than Cu^{2+} co-doped Fe^{3+}/TiO_2, Zn^{2+} codoped Fe^{3+}/TiO_2 and Fe^{3+}-doped TiO_2.

$$Fe^{2+} + h^{+} \longrightarrow Fe^{3+} \qquad (4.12)$$

4.4.7 Effect of Zn^{2+}/TiO_2

The effect of Zn^{2+}-doped TiO_2, Fe^{2+}-doped TiO_2 and Zn^{2+} co-doped Fe^{3+}/TiO_2 in the degradation of phenol had been studied (Yuan, 2002). It was found that Zn^{2+}-doped TiO_2 showed higher degradation of phenol than pure TiO_2 but lower than Zn^{2+} co-doped Fe^{3+}/TiO_2. However, when photocatalytic degradation of dichloromethane, chloroform and carbon tetrachloride was conducted, it was noticed that in comparison with pure TiO_2, Zn^{2+} co-doped Fe^{3+}/TiO_2 and TiO_2 doping with Zn^{2+}, Zn^{2+}-doped TiO_2 can slightly

improve the photocatalytic degradation but the % degradation was lower than Zn^{2+} co-doped Fe^{3+}/TiO_2. Zn^{2+} dopant in TiO_2 can be randomly dispersed on the TiO_2 surface in the form of zinc oxides. These oxides which dispersed on the TiO_2 surface can involve some charges transfer between them and TiO_2 during illumination due to the difference in the energy band position. As the valence band of TiO_2 is lower than that of ZnO, therefore, the photogenerated holes can be transferred from TiO_2 to ZnO. As a result, charge separation of the photogenerated carriers can be promoted and enhanced the photocatalytic activity of Zn^{2+}/TiO_2 (Yuan, 2002).

It can be concluded from the above observations (Figure 4.23, 4.24, 4.25) that a dopant can give different effects to different VOCs. Zn^{2+} co-doped Fe^{3+}/TiO_2 seems to be more suitable for the photocatalytic degradation of dichloromethane, chloroform and carbon tetrachloride than other doped and undoped TiO_2 in this study. Mn^{2+}-doped TiO_2 was found to be detrimental to the photocatalytic degradation of dichloromethane, chloroform and carbon tetrachloride.

4.5 Effect of VOCs

It was found that different VOCs will have different levels of degradation although the same catalyst was used in the photocatalytic degradation experiment. In this study, dichloromethane, chloroform and carbon tetrachloride had been chosen for the studies. Table 4.4 depicted the % degradation of dichloromethane, chloroform and carbon tetrachloride when doped and undoped TiO_2 were used. From Table 4.4, some differences in the levels of degradation of chloroform, dichloromethane and carbon tetrachloride were found. It can be seen that the rate of degradation of the studied chlorinated hydrocarbons follows the order: $CHCl_3 > CH_2Cl_2 > CCl_4$. It is reported that chloroform will show Cl• sensitized degradation when its concentration was above 500 ppm (Feiyen, 2002). Since the concentration of chloroform that was used in the photocatalytic degradation process was more than 500 ppm, the degradation of chloroform was expected to undergo Cl• sensitized degradation (Eq. 4.13- 4.14).

$$CHCl_3 + h\nu \longrightarrow CHCl_2\bullet + Cl\bullet \quad (4.13)$$

$$CHCl_3 + Cl\bullet \longrightarrow CCl_3\bullet + HCl \quad (4.14)$$

Dichloromethane was expected to undergo Cl• sensitized degradation since its structure is quite similar to chloroform. However, when photocatalytic degradation experiments using dichloromethane and chloroform were conducted, chloroform showed higher levels of degradation than dichloromethane. This can be explained by the different number of chlorine atoms in both dichloromethane and chloroform. Since dichloromethane has 2 chlorine atoms in its structure, Cl• sensitized degradation was lower than in the degradation of chloroform which has 3 chlorine atoms in its structure. Carbon tetrachloride showed the lowest levels of degradation in this study. Carbon tetrachloride is a stable compound, in that chlorine radicals do not attack the C-Cl bond, hence a Cl• sensitized degradation does not happen in carbon tetrachloride.

T

Catalysts	**Dopant ratios**	**% Degradation**		
		CH_2Cl_2	$CHCl_3$	CCl_4
Mn^{2+}/ TiO_2	1:0.0003	11.95	13.06	10.94
	1:0.0005	**16.47**	**19.57**	**15.87**
	1:0.001	11.49	13.12	12.12
Fe^{2+}/ TiO_2	1:0.0003	22.08	29.08	13.42
	1:0.0005	**33.79**	**34.21**	**20.80**
	1:0.001	22.76	30.84	12.36
Fe^{3+}/ TiO_2	1:0.0003	34.53	35.74	22.07
	1:0.0005	**36.02**	**43.10**	**35.42**
	1:0.001	33.91	35.11	24.44
Zn^{2+}/ TiO_2	1:0.0003	34.01	34.43	22.77
	1:0.0005	**34.89**	**36.98**	**27.44**
	1:0.001	33.98	34.77	23.32
Cu^{2+}/ TiO_2	1:0.0003	31.84	34.27	22.46
	1:0.0005	**34.30**	**36.14**	**25.67**
	1:0.001	32.81	34.45	23.07
Zn^{2+}/Fe^{3+}/TiO_2	1: 0.0005: 0.0003	34.27	36.55	32.89
	1: 0.0005: 0.0005	**41.05**	**49.45**	**37.84**
	1: 0.0005: 0.001	34.06	39.02	32.73
Cu^{2+}/Fe^{3+}/TiO_2	1: 0.0005: 0.0003	31.87	36.11	29.10
	1: 0.0005: 0.0005	**36.76**	**42.55**	**33.88**
	1: 0.0005: 0.001	33.56	38.63	31.03
Pure TiO_2	-	20.93	23.87	17.40

4.6 Photocatalytic Degradation of Chloroform / Carbon Tetrachloride Mixtures

Although photocatalytic degradation of chloroform and carbon tetrachloride had been studied extensively, however, these studies are only limited to single contaminant feed. In a real industrial application, chlorinated VOCs are found in mixture. Therefore, photocatalytic degradation of chloroform and carbon tetrachloride mixtures had been carried out in this study. Only the best catalyst ($Zn^{2+}/Fe^{3+}/TiO_2$) was used in the photocatalytic degradation of the mixture. The initial concentration of chloroform used in the photocatalytic degradation process was 222 ppm for low and 528 ppm for high concentration of chloroform. Meanwhile, the initial concentration of carbon tetrachloride used in the photocatalytic degradation process was 203 ppm for low and 427 ppm for high concentration.

Studies the effect of adding carbon tetrachloride into the chloroform photocatalytic degradation process is shown in Figure 4.27. This figure depicts the % degradation of carbon tetrachloride and chloroform mixture using $Zn^{2+}/Fe^{3+}/TiO_2$ as catalyst. In the photocatalytic degradation process, two observations can be made. First, when the chloroform and carbon tetrachloride mixture was degraded, chloroform gave higher % degradation than carbon tetrachloride. Second, when the concentration of chloroform and carbon tetrachloride increased, the % degradation of both chloroform and carbon tetrachloride was decreased.

For low concentration of mixture, it was noted that 50.89 % and 43.87 % of chloroform and carbon tetrachloride were degraded respectively at 90 minutes. However, for high concentration of mixture, only 43.85 % and 35.32 % of chloroform and carbon tetrachloride was degraded respectively at 90 minutes. This indicates the dependency of photocatalytic activity on the concentration of VOCs. In the photocatalytic degradation process, the amount of chloroform and carbon tetrachloride being degraded depends on the amount of hydroxyl radicals on the catalyst, which in turn depends on the number of holes generated on the catalyst. With a higher concentration of chloroform and carbon tetrachloride mixture, the generated hydroxyl radicals are insufficient to degrade the chloroform and carbon tetrachloride. On the other

hand, with lower concentration of the mixture, more chloroform and carbon tetrachloride can be degraded. Consequently, the % degradation of the mixture is higher.

According to Figure 4.27, the degradation of chloroform was higher than carbon tetrachloride. During illumination using the UV lamp, Cl• radicals were formed since the mixture contained chloroform and carbon tetrachloride (Eq. 4.14 and 4.15). The Cl• radicals do not attack C-Cl bonds in carbon tetrachloride, therefore, Cl• radicals formed during the illumination of UV lamp (Eq.4.15) may contribute to the degradation of chloroform; consequently, more chloroform was degraded.

$$CCl_4 + h\nu \longrightarrow Cl\bullet + \bullet CCl_3 \qquad (4.15)$$

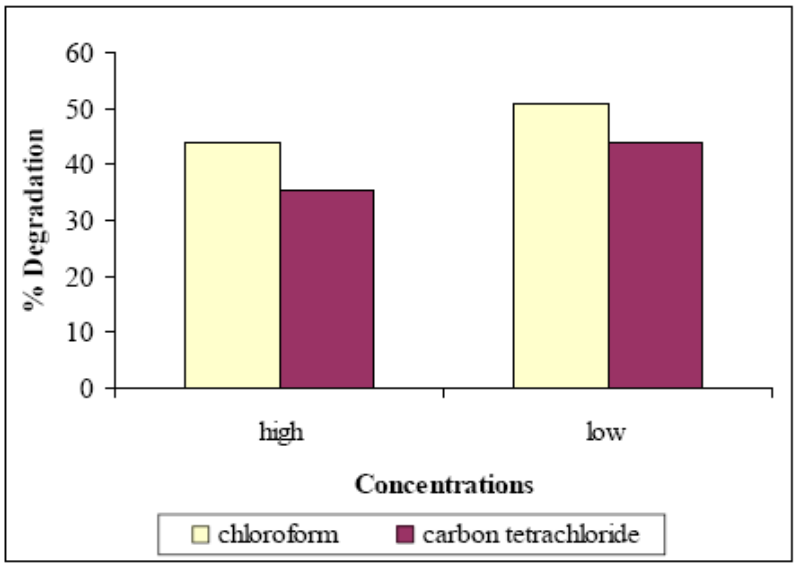

Figure 4.27: % Degradation of chloroform and carbon tetrachloride mixture at 90 minutes using $Zn^{2+}/Fe^{3+}/TiO_2$ as catalyst.

4.7 Kinetics Study

The photocatalytic degradation rate of dichloromethane, carbon tetrachloride and chloroform using doped and undoped TiO_2 depends on the adsorbed concentration of each gas sample. In general, the kinetics of photocatalytic degradation would follow the Langmuir-Hinshelwood kinetics model (Kim, 2002). Besides, this model has been shown to provide a quantitative kinetic treatment of many solid-gas reactions (Pichat,

2000). Since the photocatalytic degradation rates of dichloromethane, carbon tetrachloride and chloroform involved solid-gas reactions, therefore model L-H was suitable to be used in this study.

Figure 4.28 describes the reciprocal initial rate, $1/r_0$ versus reciprocal initial concentration, $1/C^0$ for photocatalytic degradation of dichloromethane. The plots for the chloroform and carbon tetrachloride are shown in Figure 4.29 and 4.30 respectively. The rate (mole $L^{-1}min^{-1}$) was calculated for the first 10 minutes of the photoillumination process. A linear plot of reciprocal initial rate versus reciprocal initial concentration (Figure 4.28, 4.29, 4.30) indicates a good fitting of the L-H model to the experimental data thus confirming the L-H nature of the photocatalytic degradation reaction. Figure 4.28 shows that the initial degradation rate resulting from Fe^{3+}-doped TiO_2 was lower than Mn^{2+}, Fe^{2+}-doped TiO_2 and pure TiO_2. Although the initial rate of Fe^{3+}-doped TiO_2 was lower than other sample catalysts, the amount of dichloromethane degraded was higher. This was also found to be the case in the degradation of dichloromethane using $Zn^{2+}/Fe^{3+}/TiO_2$ as catalyst. The initial rate of $Zn^{2+}/Fe^{3+}/TiO_2$ was the lowest among all sample catalysts but the yield of degradation was the highest.

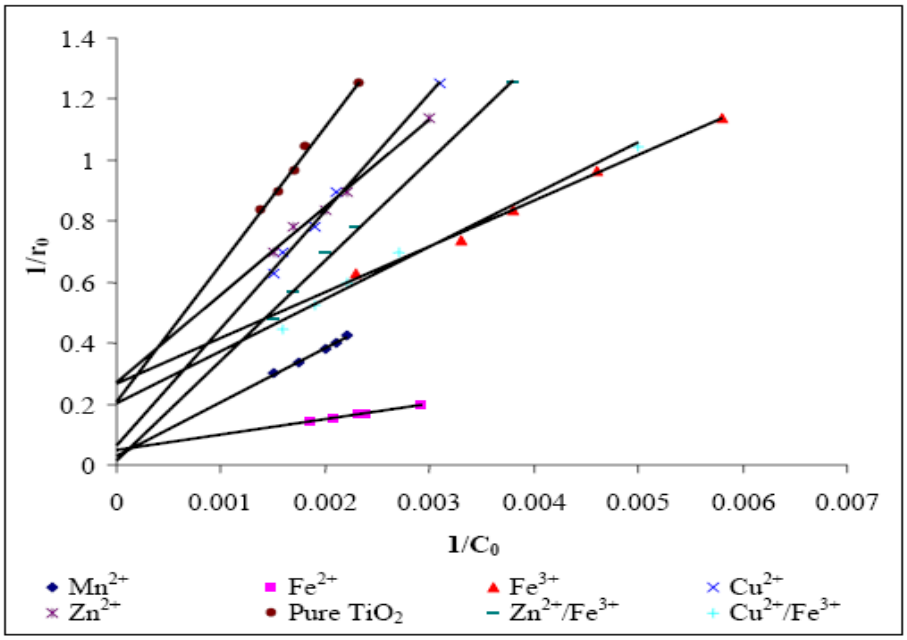

Figure 4.28: $1/r^0$ versus $1/C^0$ plot for dichloromethane degradation.

Figure 4.29 indicates the plot of reciprocal initial rate, $1/r_0$ versus reciprocal initial concentration, $1/C^0$ for chloroform. According to Figure 4.29, $Zn^{2+}/Fe^{3+}/TiO_2$ had the lowest initial degradation rate and this was followed by Zn^{2+}/TiO_2. Meanwhile, Mn^{2+}/TiO_2 had the highest initial rate but the % degradation of chloroform using Mn^{2+}/TiO_2 was the lowest.

Figure 4.30 shows the plot of reciprocal initial rate, $1/r^0$ versus reciprocal initial concentration, $1/C^0$ for carbon tetrachloride. For carbon tetrachloride degradation, the catalyst with the highest initial degradation rate was pure TiO_2 while the catalyst with lowest initial rate was $Cu^{2+}/Fe^{3+}/TiO_2$. It was found that pure TiO_2 had the highest initial rate. However, the degradation of carbon tetrachloride using doped TiO_2 was higher than pure TiO_2 except for Mn^{2+}/TiO_2. This indicates that the photocatalytic degradation process with high initial rate does not necessary lead to high degradation of VOCs.

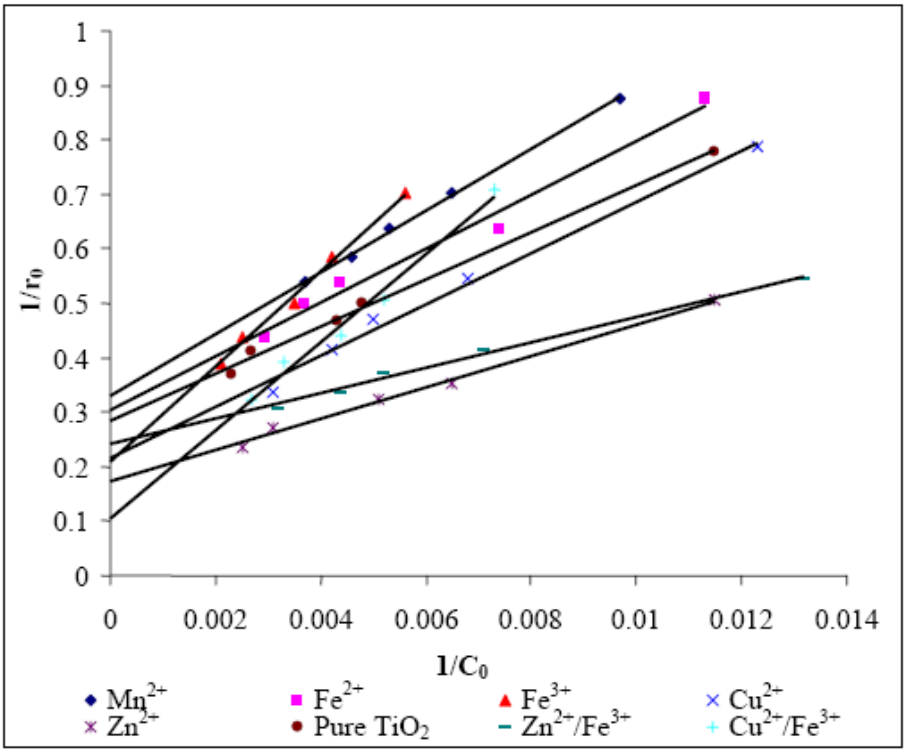

Figure 4.29: $1/r^0$ versus $1/C^0$ plot for chloroform degradation.

The kinetic parameters *k* and *K* were obtained from the intercept of the curve with the x-axis and the slope respectively. Table 4.5, 4.6 and 4.7 depict the obtained equations, the *k* and *K* values for the degradation of dichloromethane, chloroform and

carbon tetrachloride respectively using doped and undoped TiO_2 as catalyst. By substituting the *k* and *K* values into Equation 1.8, the relationship between r_0 and C^0 is obtained.

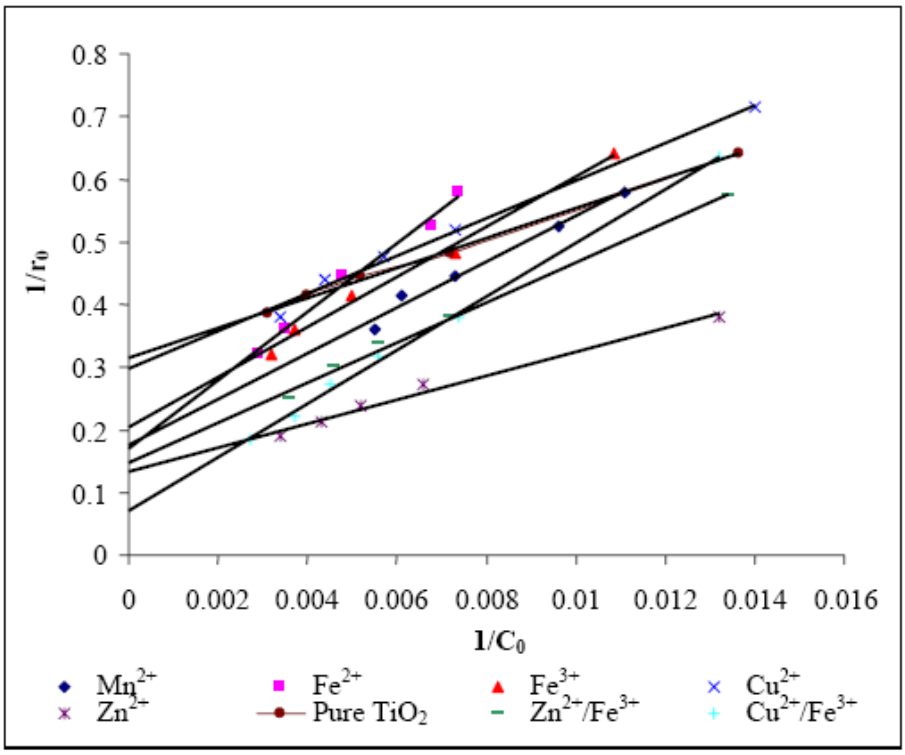

Figure 4.30: $1/r^0$ versus $1/C^0$ plot for carbon tetrachloride degradation.

It is interesting to note that the photocatalytic degradation rate is related to *k* and *K* values; therefore, a higher adsorption constant does not always result in a higher reaction rate. Although it could be thought that a high rate constant leads to a rapid reaction, the reaction rate based on the Langmuir- Hinsshelwood kinetic model (Eq. 1.8) depends simultaneously on *k* and *K*. As an example, carbon tetrachloride degradation using Fe^{3+}-doped TiO_2 had a higher adsorption constant than Fe^{2+}-doped TiO_2 but the reaction rate of Fe^{3+}-doped TiO_2 was lower than carbon tetrachloride degradation using Fe^{2+}-doped TiO_2, consequently, the multiplied products of *k* and *K* of Fe^{3+}-doped TiO_2 was higher than that of Fe^{2+}-doped TiO_2 (Table 4.7).

Table 4.5: Langmuir-Hinshelwood parameters and equations for the photocatalytic degradation of dichloromethane.

Catalysts	Equations	*k* (ppm/min)	*K* (ppm^{-1})
Mn^{2+}/TiO_2	y = 177.5x + 0.0286	34.97	1.61×10^{-4}
Fe^{2+}/TiO_2	y = 50.785x + 0.0481	20.79	9.47×10^{-4}
Fe^{3+}/TiO_2	y = 150.13x + 0.2659	3.76	1.77×10^{-3}
Cu^{2+}/TiO_2	y = 384.59x + 0.0663	15.08	1.72×10^{-4}
Zn^{2+}/TiO_2	y = 287.26x + 0.2723	3.67	9.48×10^{-4}
$Zn^{2+}/Fe^{3+}/TiO_2$	y = 328.57x + 0.0143	69.93	4.35×10^{-3}
$Cu^{2+}/Fe^{3+}/TiO_2$	y = 170.51x + 0.2044	4.89	1.20×10^{-3}
Pure TiO_2	y = 449.27x + 0.2085	4.80	4.64×10^{-4}

Table 4.6: Langmuir-Hinshelwood parameters and equations for the photocatalytic degradation of chloroform.

Catalysts	Equations	*k* (ppm/min)	*K* (ppm^{-1})
Mn^{2+}/TiO_2	y = 56.394x + 0.3317	3.01	5.88×10^{-3}
Fe^{2+}/TiO_2	y = 49.499x + 0.3037	3.29	6.14×10^{-3}
Fe^{3+}/TiO_2	y = 87.98x + 0.2079	4.81	2.36×10^{-3}
Cu^{2+}/TiO_2	y = 47.108x + 0.2157	4.64	4.58×10^{-3}
Zn^{2+}/TiO_2	y = 28.876x + 0.1718	5.82	5.95×10^{-3}
$Zn^{2+}/Fe^{3+}/TiO_2$	y = 23.387x + 0.241	4.15	1.03×10^{-2}
$Cu^{2+}/Fe^{3+}/TiO_2$	y = 80.955x + 0.1036	9.65	1.28×10^{-3}
Pure TiO_2	y = 43.19x + 0.2847	3.51	6.59×10^{-3}

The recombination of the photogenerated electron and hole is very fast (on the picosecond timescale), and thus interfacial electron transfer is possible only when the donor or acceptor is preadsorbed before photocatalysis (Alberici, 1997). The preliminary adsorption of VOCs is a very important pre-requisite for highly efficient degradation but this requirement seems not to be sufficient to determine an efficient degradation.

Table 4.7: Langmuir-Hinshelwood parameters and equations for the photocatalytic degradation of carbon tetrachloride.

Catalysts	Equations	k (ppm/min)	K (ppm^{-1})
Mn^{2+}/TiO_2	y = 36.456x + 0.1759	5.69	4.82×10^{-3}
Fe^{2+}/TiO_2	y = 54.242x + 0.1707	5.86	3.15×10^{-3}
Fe^{3+}/TiO_2	y = 39.98x + 0.2035	4.91	5.09×10^{-3}
Cu^{2+}/TiO_2	y = 30.143x + 0.2966	3.37	9.84×10^{-3}
Zn^{2+}/TiO_2	y = 19.056x + 0.1342	7.45	7.04×10^{-3}
$Zn^{2+}/Fe^{3+}/TiO_2$	y = 31.859x + 0.1486	6.73	4.66×10^{-3}
$Cu^{2+}/Fe^{3+}/TiO_2$	y = 42.797x + 0.0705	14.18	1.65×10^{-3}
Pure TiO_2	y = 23.99x + 0.3145	3.18	1.31×10^{-2}

For carbon tetrachloride degradation using TiO_2 as catalyst, it was found that the adsorption constant for pure TiO_2 was higher than that for Fe^{3+}-doped TiO_2 (Table 4.7) but the degradation of carbon tetrachloride using Fe^{3+}-doped TiO_2 was more efficient (Figure 4.25). Therefore, the preliminary adsorption of VOCs is not the major limiting factor in photocatalytic degradation.

In order to determine the order of the degradation of carbon tetrachloride, dichloromethane and chloroform, a graph of ln [C] versus time was plotted. Figures 4.31, 4.32 and 4.33 depict the graph of ln [C] versus time for dichloromethane, chloroform and carbon tetrachloride degradation respectively. The initial concentrations of dichloromethane were ranged from 430-733 ppm, 88-337 ppm for chloroform and 126-403 ppm for carbon tetrachloride. When a graph of ln [C] versus time was plotted, a straight line was obtained (Figure 4.31, 4.32, 4.33). This indicates that the VOCs in this study degrade according to first-order kinetics. In order to confirm this, the Langmuir-Hinshelwood model can be used (Eq. 1.8). From equation 1.8, when $KC >> 1$, the rate law is reduced to zero-order (Eq.1.9), however, when $KC << 1$, the apparent kinetics becomes first-order (Eq.1.10).

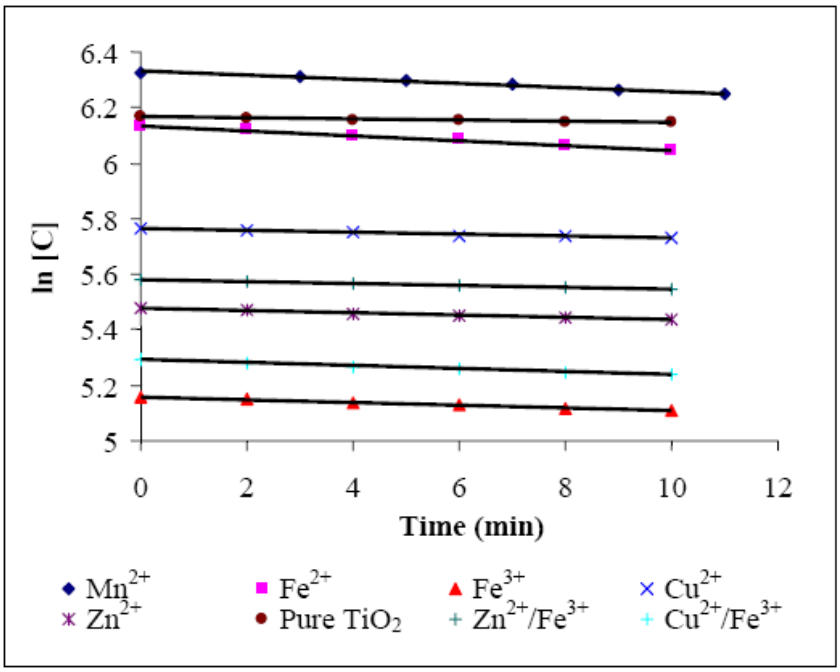

Figure 4.31: Graph of ln [C] versus time for dichloromethane degradation.

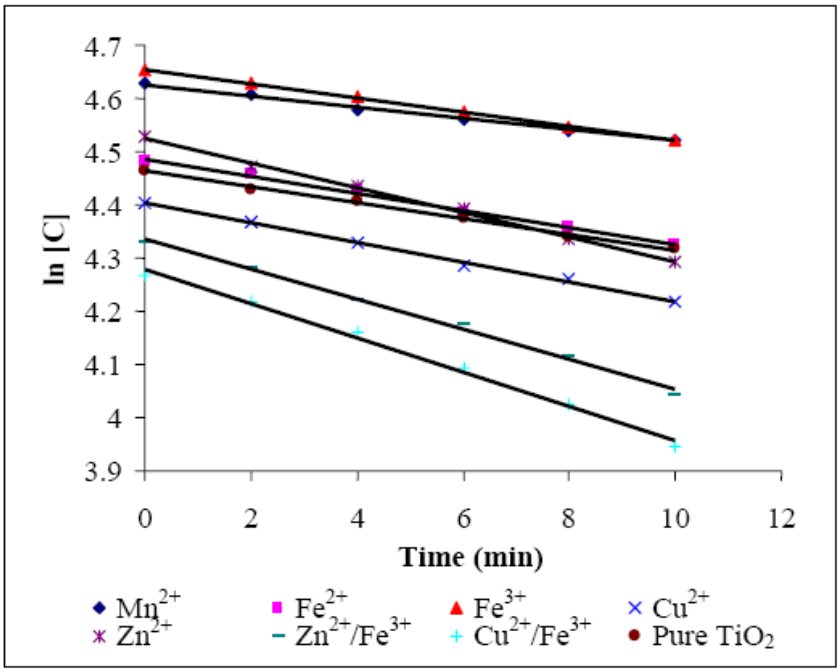

Figure 4.32: Graph of ln [C] versus time for chloroform degradation.

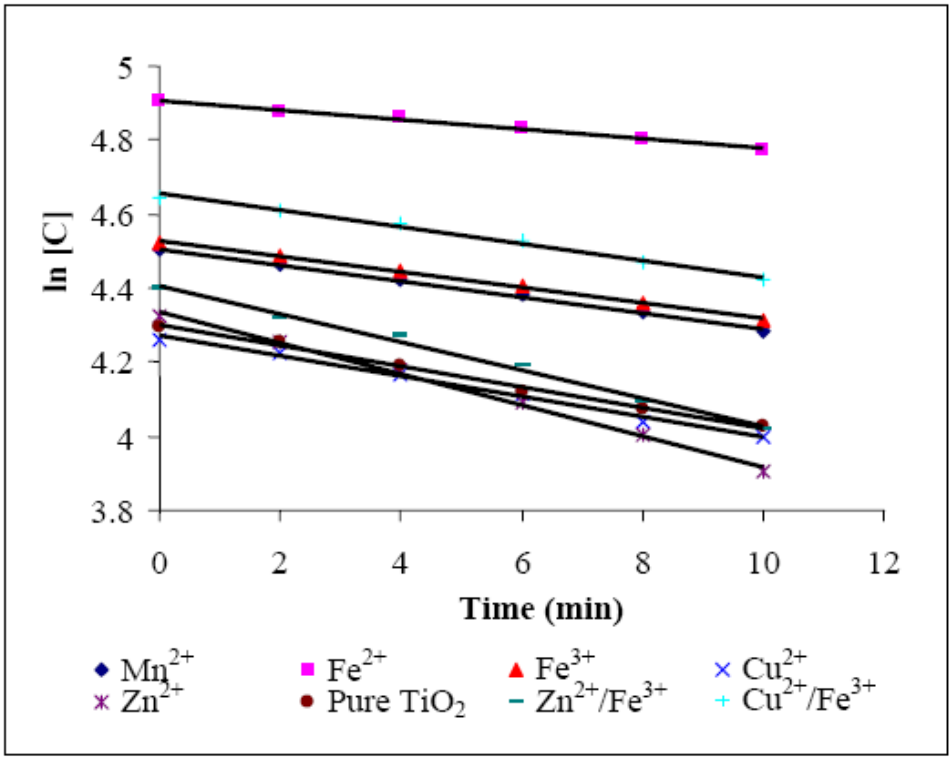

Figure 4.33: Graph of ln [C] versus time for carbon tetrachloride degradation.

Table 4.8, 4.9 and 4.10 show the R^2 and equation obtained from the graph of ln [C] versus time for dichloromethane, chloroform and carbon tetrachloride degradation. From Table 4.8, 4.9 and 4.10, it can be seen that all the linear regression, R_2 are greater than 0.98.

Table 4.8: R^2 and equations obtained from the graph of ln [C] versus time for

Catalysts	Equations	R^2
Mn^{2+}/ TiO_2	y = -0.0076x + 6.3322	0.9898
Fe^{2+}/ TiO_2	y = -0.0088x + 6.1351	0.9990
Fe^{3+}/ TiO_2	y = -0.005x + 5.1569	0.9998
Cu^{2+}/ TiO_2	y = -0.0033x + 5.7616	0.9957
Zn^{2+}/ TiO_2	y = -0.0041x + 5.4761	0.9928
$Zn^{2+}/Fe^{3+}/TiO_2$	y = -0.0029x + 5.5776	0.9930
$Cu^{2+}/Fe^{3+}/TiO_2$	y = -0.0052x + 5.2919	0.9934
Pure TiO_2	y = -0.0019x + 6.1648	0.9974

Catalysts	Equations	R^2
Mn^{2+}/TiO_2	y = -0.0106x + 4.626	0.9953
Fe^{2+}/TiO_2	y = -0.016x + 4.4862	0.9958
Fe^{3+}/TiO_2	y = -0.0134x + 4.6552	0.9994
Cu^{2+}/TiO_2	y = -0.0185x + 4.4024	0.9960
Zn^{2+}/TiO_2	y = -0.0234x + 4.5262	0.9966
$Zn^{2+}/Fe^{3+}/TiO_2$	y = -0.0282x + 4.3351	0.9962
$Cu^{2+}/Fe^{3+}/TiO_2$	y = -0.0324x + 4.2795	0.9946
Pure TiO_2	y = -0.015x + 4.4641	0.9934

Table 4.10: R^2 and equation obtained from the graph of ln [C] versus time for carbon tetrachloride

Catalysts	Equations	R^2
Mn^{2+}/TiO_2	y = -0.0215x + 4.5071	0.9964
Fe^{2+}/TiO_2	y = -0.0129x + 4.906	0.9971
Fe^{3+}/TiO_2	y = -0.021x + 4.5276	0.9970
Cu^{2+}/TiO_2	y = -0.0277x + 4.2728	0.9911
Zn^{2+}/TiO_2	y = -0.0418x + 4.336	0.9961
$Zn^{2+}/Fe^{3+}/TiO_2$	y = -0.0383x + 4.4071	0.9921
$Cu^{2+}/Fe^{3+}/TiO_2$	y = -0.0224x + 4.6536	0.9911
Pure TiO_2	y = -0.0278x + 4.2987	0.9951

Table 4.11, 4.12 and 4.13 depict the *K*C values for dichloromethane, chloroform and carbon tetrachloride respectively, where *K* is the adsorption constant and C is the concentration of a particular VOC. It showed that when the concentration of sample used in the kinetics study was low, the *K*C values for dichloromethane, chloroform and carbon tetrachloride were less than 1. According to Equation 1.10, the apparent kinetics becomes first-order. However, when the concentration of sample was high, the *K*C value will become more than 1, indicating that the kinetic order is variable. Previous research also found that the degradation of chloroform below 600 ppm followed first-order kinetics (Feiyen, 2002). However, when the initial concentration of chloroform was

above 600 ppm, the reaction seemed to follow second-order kinetics with respect to chloroform concentration, indicating a possible change in the mechanism. From Table 4.13, it can be noticed that the *K*C value for degradation of carbon tetrachloride using pure TiO_2 and Cu^{2+}/TiO_2 is 0.92 and 0.70 respectively, which is higher than other sample catalysts. This is due to the adsorption constant (*K*) for pure TiO_2 and Cu^{2+}/TiO_2 are very high, consequently, the resulted *K*C values also become high. This indicates that not only the concentration of sample will result in the change of the mechanism but also the adsorption of the sample on the catalyst.

Table 4.11: *K*C values for dichloromethane.

Catalysts	K (ppm^{-1})	C (ppm)	K C
Mn^{2+}/TiO_2	1.61×10^{-4}	443.85	0.07
Fe^{2+}/TiO_2	9.47×10^{-4}	340.11	0.32
Fe^{3+}/TiO_2	1.77×10^{-4}	158.64	0.03
Cu^{2+}/TiO_2	1.72×10^{-4}	317.93	0.55
Zn^{2+}/TiO_2	9.48×10^{-4}	333.41	0.32
$Zn^{2+}/Fe^{3+}/TiO_2$	4.35×10^{-5}	264.62	0.01
$Cu^{2+}/Fe^{3+}/TiO_2$	1.20×10^{-3}	198.86	0.20
Pure TiO_2	4.64×10^{-4}	407.14	0.19

Table 4.12: *K*C values for chloroform.

Catalysts	K (ppm^{-1})	C (ppm)	K C
Mn^{2+}/TiO_2	5.88×10^{-3}	103.53	0.61
Fe^{2+}/TiO_2	6.14×10^{-3}	88.41	0.54
Fe^{3+}/TiO_2	2.36×10^{-3}	100.96	0.24
Cu^{2+}/TiO_2	4.58×10^{-3}	81.61	0.37
Zn^{2+}/TiO_2	5.95×10^{-3}	87.26	0.52
$Zn^{2+}/Fe^{3+}/TiO_2$	1.03×10^{-2}	75.97	0.78
$Cu^{2+}/Fe^{3+}/TiO_2$	1.28×10^{-3}	71.45	0.09
Pure TiO_2	6.59×10^{-3}	86.99	0.57

Catalysts	K (ppm^{-1})	C (ppm)	K C
Mn^{2+}/ TiO_2	3.15 x 10^{-3}	94.08	0.30
Fe^{2+}/ TiO_2	4.82 x 10^{-3}	116.22	0.56
Fe^{3+}/ TiO_2	5.13 x 10^{-3}	81.63	0.42
Cu^{2+}/ TiO_2	9.84 x 10^{-3}	71.36	0.70
Zn^{2+}/ TiO_2	7.04 x 10^{-3}	75.56	0.53
Zn^{2+}/Fe^{3+}/TiO_2	4.66 x 10^{-3}	74.51	0.35
Cu^{2+}/Fe^{3+}/TiO_2	1.65 x 10^{-3}	103.89	0.17
Pure TiO_2	0.0131	70.22	0.92

4.8 Model for the Photocatalytic Degradation of Chlorinated Hydrocarbons

When photocatalytic degradation of VOCs was conducted, the information obtained from the use of GC-MS can be used to predict the possible model of the photocatalytic degradation process. Table 4.14, 4.15 and 4.16 show the fragments obtained before and after illumination of UV light for dichloromethane, chloroform and carbon tetrachloride respectively. The fragments were analyzed using the integral form of the GC-MS spectra. Appendix E, F and G show the integral form of the GC-MS spectra for photocatalytic degradation of dichloromethane, chloroform and carbon tetrachloride respectively.

4.8.1 Dichloromethane

When photocatalytic degradation of dichloromethane was carried out, fragments listed in Table 4.14 were obtained. From the information obtained from GC-MS, we may propose a model for the photocatalytic degradation of dichloromethane as follows:
Chlorine radicals were formed during the illumination of dichloromethane using UV light. Chlorine radicals were expected to attack CH_2Cl_2 to initialize the degradation process (Eq. 4.16).

$$CH_2Cl_2 + h\nu \longrightarrow Cl\bullet + CH_2Cl^+ \longrightarrow CCl_2^+ + H_2 \quad (4.16)$$

$$Cl\bullet + CH_2Cl_2 \longrightarrow H_2 + CCl_3^+ \longrightarrow HCl + CHCl_2^+ \quad (4.17)$$

$$H_2O + h\nu \longrightarrow \bullet OH + H\bullet \quad (4.18)$$

$$CH_2Cl_2 + \bullet OH \longrightarrow OCl^+ + CH_3Cl^+ \quad (4.19)$$

$$CH_2Cl_2 + \bullet OH \longrightarrow H_2O + CHCl_2^+ \quad (4.20)$$

$$\bullet OH + CHCl_2^+ \longrightarrow OCl^+ + CH_2Cl^+ \quad (4.21)$$

$$CH_2Cl^+ + O_2 \rightleftharpoons CH_2ClOO^+ \quad (4.22)$$

$$2CH_2ClOO^+ \longrightarrow 2CH_2ClO^+ + O_2 \quad (4.23)$$

$$CH_2ClO^+ \longrightarrow HCOCl + H\bullet \quad (4.24)$$

$$CHCl_2^+ + O_2 \longrightarrow CHCl_2OO^+ \quad (4.25)$$

$$2CHCl_2OO^+ \longrightarrow 2CHCl_2O^+ + O_2 \quad (4.26)$$

$$CHCl_2O^+ \longrightarrow HCOCl + Cl\bullet \quad (4.27)$$

$$CCl_3^+ + O_2 \rightleftharpoons CCl_3O_2^+ \quad (4.28)$$

$$2CCl_3O_2^+ \longrightarrow 2COCl_2^+ + O_2 + 2Cl\bullet \quad (4.29)$$

$$COCl_2^+ + h\nu \longrightarrow CO + 2Cl\bullet \quad (4.30)$$

$$COCl_2^+ + H_2O \longrightarrow 2HCl + CO_2 \quad (4.31)$$

$$2Cl\bullet \longrightarrow Cl_2 \quad (4.32)$$

$$\bullet OH + H\bullet \longrightarrow H_2O \quad (4.33)$$

Besides, •OH will attack CH_2Cl_2 to form OCl^+ and CH_3Cl^+ through Equation 4.19 or H_2O and $CHCl^{2+}$ through Equation 4.20. In the photocatalytic degradation of dichloromethane, it is expected that CCl^{3+} will react with O_2 to form CCl_3O^{2+} (Eq. 4.28). However, CCl_3O^{2+} is not detected in this study (Appendix E). This may be due to the formation of fragments and their fast reaction times which renders them unable to be detected. $COCl^{2+}$ formed from CCl_3O^{2+} was expected to undergo photolysis (Eq. 4.30) in the presence of moist air. In the termination process, Cl• will recombine to form Cl_2 (Eq. 4.32) while H• will combine with •OH to form H_2O (Eq. 4.33). In this study, only a small amount of phosgene was detected (Table 4.14). This may due to the $COCl^{2+}$ formed during the photocatalytic degradation process was expected to undergo photolysis (Eq. 4.30).

Table 4.14: Fragments obtained during photocatalytic degradation of dichloromethane.

VOCs	Abundance				
	Fragments	$Zn^{2+}/Fe^{3+}/TiO_2$		Mn^{2+}/TiO_2	
		Before Illumination	After Illumination	Before Illumination	After Illumination
CH_2Cl_2	$CHCl_2^+$	143232	128688	142720	140864
	CH_2Cl^+	238144	225472	238592	241344
	CCl_3^+	193	144	182	135
	$CHCl_2OO^+$	37	34	28	22
	$CHCl_2O^+$	45	49	23	27
	CH_2ClO^+	59	26	49	-
	CCl_2^+	16368	15626	15102	15585
	OCl^+	67432	57600	69704	66600
	$COCl_2^+$	49	74	69	80
	CH_3Cl^+	9240	8133	9154	8863

4.8.2 Chloroform

When photocatalytic degradation of chloroform was conducted, the fragments listed in Table 4.15 were obtained. A possible model for the photocatalytic degradation of chloroform is given below. It was discovered that the fragments observed in this study were quite similar to

those detected in previous research. A research about photodegradation of chloroform and carbon tetrachloride using a low mercury lamp with 92 % output at 254 nm and 6 % at 185 nm had been conducted (Feiyen, 2002). No catalyst was used in the photodegradation process. Fragments such as $CHCl^{2+}$, CCl^{3+}, CCl_3O^{2+}, $CHCl_2OO^+$ and $CHCl_2O^+$ was observed in the research (Feiyen, 2002). However, in this study, a light source from a 6 W black lamp with ~ 354 nm wavelength was used. The catalysts used in this study were $Zn^{2+}/Fe^{3+}/TiO_2$ and Mn^{2+}/TiO_2. The fragments which were not observed in the research done by Feiyen but are observed in this study are $CHCl^{2+}$, CH_2Cl^+, CCl^{2+} and OCl^+ (Table 4.15).

$$CHCl_3 + h\nu \longrightarrow Cl\bullet + CHCl_2^+ \longrightarrow CCl_2^+ + HCl \quad (4.34)$$

$$H_2O + h\nu \longrightarrow \bullet OH + H\bullet \quad (4.35)$$

$$CHCl_2^+ + \bullet OH \longrightarrow OCl^+ + CH_2Cl^+ \quad (4.36)$$

$$CH_2Cl^+ + \bullet H \longrightarrow CH_3Cl^+ \quad (4.37)$$

$$Cl\bullet + CHCl_3^+ \longrightarrow CCl_3^+ + HCl \quad (4.38)$$

$$CHCl_3 + \bullet OH \longrightarrow H_2O + CCl_3^+ \quad (4.39)$$

$$CCl_3^+ + O_2 \rightleftharpoons CCl_3O_2^+ \quad (4.40)$$

$$2CCl_3O_2^+ \longrightarrow 2COCl_2 + O_2 + 2Cl\bullet \quad (4.41)$$

$$CHCl_2^+ + O_2 \longrightarrow CHCl_2OO^+ \quad (4.42)$$

$$2CHCl_2OO^+ \longrightarrow 2CHCl_2O^+ + O_2 \quad (4.43)$$

$$CHCl_2O^+ \longrightarrow HCOCl + Cl\bullet \quad (4.44)$$

$$COCl_2^+ + h\nu \longrightarrow CO + 2Cl\bullet \quad (4.45)$$

$$COCl_2^+ + H_2O \longrightarrow 2HCl + CO_2 \quad (4.47)$$

$$2Cl\bullet \longrightarrow Cl_2 \quad (4.48)$$

In the presence of UV light, the photocatalytic degradation of chloroform results in the formation of Cl• and $CHCl_{2+}$. Then, Cl• and CH_2Cl^{2+} will decompose into CCl^{2+} and HCl (Eq. 4.34). CH_2Cl^+formed from the photocatalytic degradation of chloroform can react with •OH to form CH_2Cl^+ (Eq. 4.36). CH_2Cl^+ reacts with •H to form CH_3Cl^+ through Equation 4.37. The integral form of the GC-MS spectra shows the presence of CH_2Cl^+ (Table 4.15).

Table 4.15: Fragments obtained during photocatalytic degradation of chloroform.

VOCs	Abundance of fragments				
	Fragments	$Zn^{2+}/Fe^{3+}/TiO_2$		Mn^{2+}/TiO_2	
		Before Illumination	After Illumination	Before Illumination	After Illumination
$CHCl_3$	CCl_3^+	3382	2280	2763	2366
	$CHCl_2^+$	11081	7833	9014	7426
	CH_2Cl^+	25728	18000	24168	20968
	$CHCl_2OO^+$	-	25	-	43
	$CHCl_2O^+$	60	36	34	56
	CCl_2^+	329728	221568	256768	224064
	OCl^+	187	189	181	206
	$COCl_2^+$	49	29	30	29
	CH_3Cl^+	10397	7896	9677	8430

When chloroform is degraded, it will not only be attacked by Cl• but also •OH to form H_2O and CCl^{3+} (Eq. 4.39). In the photocatalytic degradation of chloroform, CCl_3O^{2+} is expected to form from the reaction between O_2 and CCl_{3+} through (Eq. 4.40), however, CCl_3O^{2+} is not observed in this study. This may be due to the fast formation and reaction times which renders it unable to be observed. Phosgene formed from CCl_3O^{2+} was expected to undergo photolysis since the photocatalytic degradation of chloroform was carried out in ambient conditions which contain moist air, which was reported (Feiyen, 2002) as a prerequisite for the process of phosgene photolysis.

4.8.3 Carbon Tetrachloride

In this study, photocatalytic degradation of carbon tetrachloride using Zn_{2+}/Fe_{3+}/TiO_2 and Mn_{2+}-doped TiO_2 as catalyst produced the fragments as listed in Table 4.16. It can be seen that most of the fragments observed in this study are similar to those observed in the previous research. However, in this study, some new fragments such as OCl^+, $CHCl^{2+}$ and CH_2Cl^+were observed. From the information obtained from GC-MS, the possible model is presumed to be as follow:

$$CCl_4 + h\nu \longrightarrow Cl\bullet + CCl_3^+ \longrightarrow 2Cl\bullet + CCl_2^+ \quad (4.50)$$

$$H_2O + h\nu \longrightarrow \bullet OH + H\bullet \quad (4.51)$$

$$CCl_4 + H\bullet \longrightarrow HCl + CCl_3^+ \quad (4.52)$$

$$CCl_4 + \bullet OH \longrightarrow OCl^+ + CHCl_3^+ \quad (4.53)$$

$$CCl_3^+ + O_2 \rightleftharpoons CCl_3O_2^+ \quad (4.54)$$

$$2CCl_3O_2^+ \longrightarrow 2COCl_2 + O_2 + 2Cl\bullet \quad (4.55)$$

$$CCl_3^+ + H\bullet \longrightarrow HCl + CCl_2^+ \quad (4.56)$$

$$CCl_3^+ + H\bullet \longrightarrow Cl\bullet + CHCl_2^+ \quad (4.57)$$

$$CHCl_2^+ + \bullet OH \longrightarrow OCl^+ + CH_2Cl^+ \quad (4.58)$$

$$CH_2Cl^+ + \bullet H \longrightarrow CH_3Cl \quad (4.59)$$

$$^+CHCl_2 + O_2 \rightleftharpoons CHCl_2OO^+ \quad (4.60)$$

$$2CHCl_2OO^+ \longrightarrow 2CHCl_2O^+ + O_2 \quad (4.61)$$

$$CHCl_2O^+ \longrightarrow HCOCl + Cl\bullet \quad (4.62)$$

$$COCl_2^+ + h\nu \longrightarrow CO + 2Cl\bullet \quad (4.63)$$

$$COCl_2^+ + H_2O \longrightarrow 2HCl + CO_2 \quad (4.64)$$

$$2Cl\bullet \longrightarrow Cl_2 \quad (4.65)$$

$$\bullet OH + H\bullet \longrightarrow H_2O \quad (4.66)$$

$$H\bullet + OCl\bullet \longrightarrow HOCl \quad (4.67)$$

During the illumination of UV, the produced Cl• will react with CCl^{3+} to form Cl• and CCl^{2+} (Eq. 4.50). CCl_4 can be attacked by •OH to form OCl^+ and $CHCl^{3+}$ (Eq.4.53). The integral form of the GC-MS spectra shows the presence of OCl^+ (Table 4.16). Besides, CCl_4 can also attacked by H• to form HCl and CCl^{3+} (Eq. 4.52). CCl^{3+} produced in the photocatalytic degradation of carbon tetrachloride can react with O_2 to form CCl_3O^{2+} (Eq. 4.54) or react with H• to produce CCl^{2+} and $CHCl_{2+}$ (Eq.4.56 and 4.57). However, in this study, CCl_3O^{2+} is unable to be detected. $CHCl^{2+}$ formed from the reaction between CCl^{3+} and H• can react with O_2 to form $CHCl_2OO^+$ (Eq.4.60). Unfortunately, $CHCl_2OO^+$ is unable to be detected and this may be due to the fast reaction between $CHCl^{2+}$ and O_2 and the product decomposed to $CHCl_2O^+$ and O_2. Since the presence of $CHCl_2O^+$ is able to be identified (Table 4.16), therefore, $CHCl_2OO^+$ is presumed to be presence in the photocatalytic degradation of carbon tetrachloride. Table 4.16 shows that only a small amount of phosgene is detected. This may due to the phosgene is rapidly hydrolyzed to CO_2 and HCl in the presence of moisture.

4.9 Characterization

4.9.1 Film Thickness and Refractive Index

The film thickness and refractive index values of all the thin films are given in Table 4.17.

Table 4.16: Fragments obtained during photocatalytic degradation of carbon tetrachloride.

VOCs	Abundance of Fragments				
	Fragments	$Zn^{2+}/Fe^{3+}/TiO_2$		Mn^{2+}/TiO_2	
	-	Before Illumination	After Illumination	Before Illumination	After Illumination
CCl_4	CCl_3^+	179264	168000	178176	163456
	CCl_2^+	2471	2458	2161	2139
	$CHCl_2^+$	34352	33840	34584	32360
	$CHCl_2O^+$	43	25	27	31
	OCl^+	4369	4686	4562	4243
	CH_2Cl^+	28080	25840	27336	25352
	$COCl_2^+$	27	-	30	30
	$CHCl_3^+$	2015	1985	2081	1879

Unfortunately, the film thickness and thus the refractive index of $Zn^{2+}/Fe^{3+}/TiO_2$ and $Cu^{2+}/Fe^{3+}/TiO_2$ were unable to be measured. This is due to the lack of analytical software for ellipsometric analysis to determine the refractive index for those co-doped catalysts. The film thickness for all catalyst samples is between 227-251 nm and thus within the range of thin film since the limit of thin film thickness is 1000 nm. From the literature, the refractive index for pure TiO_2 is 2.1-2.7 (Takahashi, 1988; Bendavid, 2000; Mardare, 2002). According to Table 4.17, the obtained refractive index for pure TiO_2 is 2.2104 and this is within the range delineated in the literature. The refractive index for doped TiO_2 is lower than pure TiO_2.

When TiO_2 thin films were calcined at 500°C, their morphology can be classified as nanocrystalline anatase from the XRD (Oh, 2003a). Since all the thin films used in this study were also calcined at 500°C, therefore, it was expected that all the thin films were nanocrystalline anatase too. The porosities were calculated using the following equation:

$$Porosity = \left(1 - \frac{n^2 - 1}{n^2_d - 1}\right) \times 100\% \qquad (4.68)$$

where n_d is the refractive index of pore-free anatase (2.52) and n is the refractive index of the porous thin films (Oh, 2003a). From Table 4.17, it can be seen that the lower the refractive index, the higher the porosity of catalyst is. Addition of dopant into TiO_2 increases the porosity of the thin films. Fe^{2+}-doped TiO_2 shows the highest porosity among other catalyst samples. Thin films with high porosity had superior photoactivity when formic acid was used as testing sample (Oh, 2003a). When Mn^{2+}, Fe^{2+}, Fe^{3+}, Cu^{2+} and Zn^{2+}-doped TiO_2 were used in the photocatalytic degradation of dichloromethane, chloroform and carbon tetrachloride, only Fe^{2+}, Fe^{3+}, Cu^{2+} and Zn^{2+}-doped TiO_2 showed higher degradation of VOCs than pure TiO_2. Mn^{2+}-doped TiO_2 was detrimental to the degradation of VOCs although the porosity of Mn^{2+}-doped TiO_2 was found to be higher than pure TiO_2. This may be caused by the incomplete separation of the photogenerated electron and hole as explained in the Section 4.4.4.

4.9.2 UV-Visible Spectrum

The absorption spectrum for all optimum ratio metal ions doped TiO_2 and undoped TiO_2 were taken using the Shimadzu UV-Vis-NIR Scanning Spectrophotometer. Figure 4.34 shows the UV-Vis absorption spectrum wavelength in the range of 300-540 nm for doped and undoped TiO_2.

A slight shift to a higher wavelength or red shift was noted for Zn^{2+} co-doped Fe^{3+}/TiO_2 and Cu^{2+} co-doped Fe^{3+}/TiO_2. This indicates a decrease in band gap value of the respective catalysts. Meanwhile, Fe^{2+} and Mn^{2+}-doped TiO_2 showed a slight shift to a lower wavelength or blue shift indicating an increase in the band gap. However, for Zn^{2+}/TiO_2, Fe^{3+}/TiO_2 and Cu^{2+}/TiO_2, blue shift or red shift is unable to be differentiated since the absorption are very close (Figure 4.34). Zn^{2+} co-doped Fe^{3+}/TiO_2, Cu^{2+} co-doped Fe^{3+}/TiO_2, Fe^{3+}-doped TiO_2 and Zn^{2+}-doped TiO_2 have higher absorbances than pure TiO_2 at the visible region while Mn^{2+} doped TiO_2 and Fe^{2+} doped TiO_2 have lower absorbances than pure TiO_2 at the visible region. At wavelengths below 400 nm, the absorption increases rather quickly.

The red shift in optical energy gap is considered to be due to the following factors. The energy level for dopants lies below the conduction band edge (E_{cb}) and above valence band edge (E_{vb}) of TiO_2. The introduction of such energy levels in the band gap induces the red shift in the band gap transition and the visible light absorption through a charge transfer between a dopant and cb (or vb) or a d-d transition in the crystal field according the energy level. Previous research also found that addition of Fe^{3+} into TiO_2 had shifted the absorption edge into higher wavelengths (Jiang, 2002).

Table 4.17: Film thickness, refractive index and porosity of doped and undoped TiO_2

Catalyst Samples	Film Thickness (nm)	Refractive Index (n)	Porosity (%)
Mn^{2+}/TiO_2	227.09	2.1199	34.70
Fe^{2+}/TiO_2	251.45	2.1094	35.53
Fe^{3+}/TiO_2	243.40	2.0183	42.56
Cu^{2+}/TiO_2	228.54	2.1077	35.66
Zn^{2+}/TiO_2	251.48	2.1093	35.53
$Zn^{2+}/Fe^{3+}/TiO_2$	NA	NA	NA
$Cu^{2+}/Fe^{3+}/TiO_2$	NA	NA	NA
Pure TiO_2	236.09	2.2104	27.37

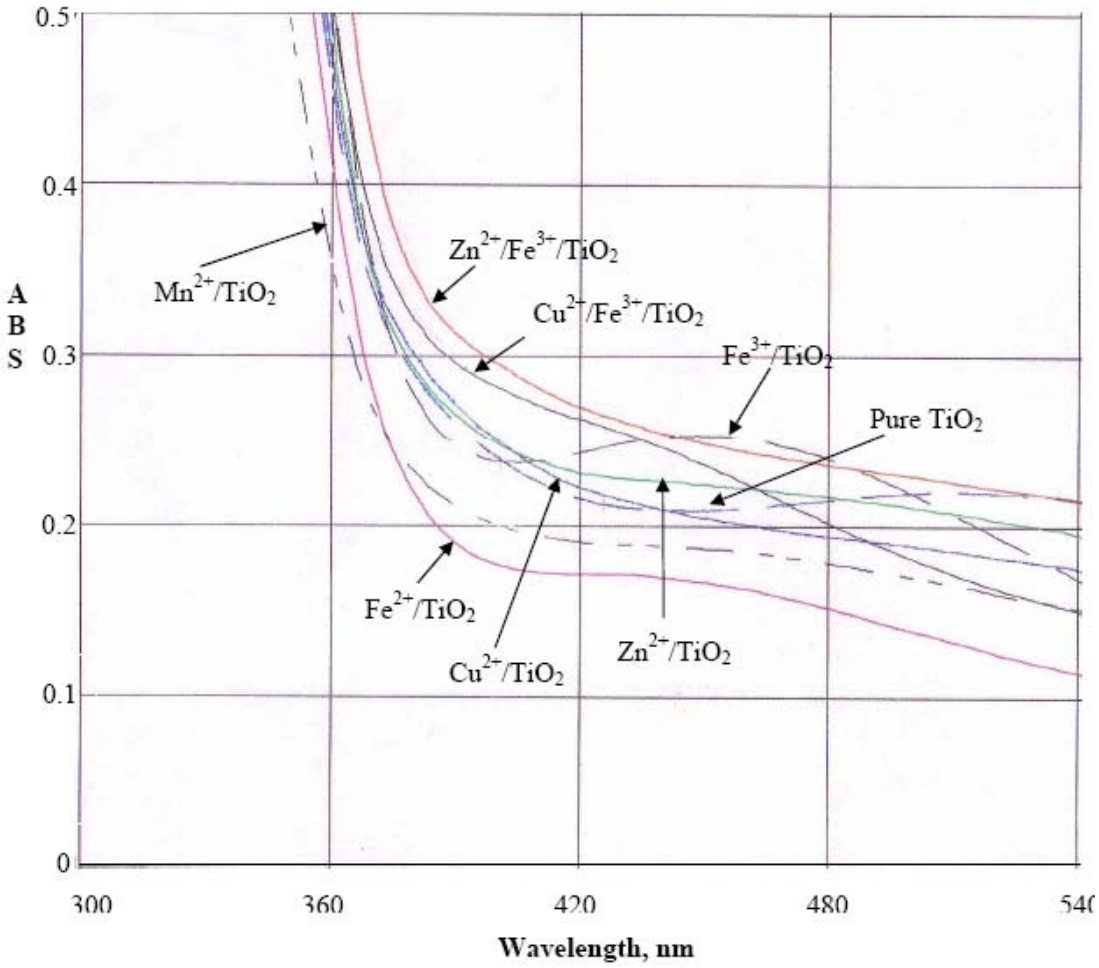

Figure 4.34: UV-Vis absorption spectra for doped and undoped TiO_2 thin films.

4.9.3 Determination of Band Gap

The optical band gaps, E_g values for all catalyst samples were determined by plotting $(\alpha h\nu)^{1/2}$ versus the equivalent energy at the wavelength, λ. (Amor, 1998). Since the thickness of Cu^{2+} co-doped Fe^{3+}/TiO_2 and Zn^{2+} co-doped Fe^{3+}/TiO_2 were unable to be determined, their α values were not calculated. As a consequence, the E_g for Cu^{2+} codoped Fe^{3+}/TiO_2 and Zn^{2+} co-doped Fe^{3+}/TiO_2 were not determined. Figure 4.35 shows the graph of $(\alpha h\nu)^{1/2}$ versus equivalent energy at particular wavelength for Fe^{3+}-doped TiO_2. The graph of $(\alpha h\nu)^{1/2}$ versus equivalent energy at particular wavelength for other thin films can be referred in Appendix H. It is noted that all obtained graphs have a similar curve. The respective values of E_g can be obtained by extrapolation to $(\alpha h\nu)^{1/2} = 0$. The E_g for all thin films are summarized in Table 4.18.

According to Table 4.18, the obtained band gap values are different in comparison to the well-known value of 3.2 eV for the TiO_2 anatase. In this study, the obtained band gap values are in the range of 3-3.05 eV, which is lower than the normal value of 3.2 eV but is close to the literature data. Most researchers obtained the indirect band gap values in the range of 3.05-3.4 eV (Chen, 1999; Mardare, 2000; Abou-Helal,2002). Also, the obtained indirect band gap values were 3.2, 2.95 and 2.7 eV for pure, 5 and 10 mole % Pb^{2+}-doped TiO_2 respectively (Rahman, 1999). The thin films were deposited on vitreous silica substrates using the sol-gel dip-coating method. From Table 4.18, it can be seen that the addition of Fe^{2+}, Fe^{3+} and Zn^{2+} increases the E_g value but the differences are insignificant. On other hand, the E_g values for Mn^{2+} and Cu^{2+} are similar to the ones obtained for pure TiO_2. If compared the indirect band gaps as shown in Table 4.18 with the UV-Vis spectra (Figure 4.34), it can be seen that absorption edges for some catalysts have been shifted to higher or lower wavelength, however, the differences in the indirect band gaps between these catalysts and pure TiO_2 are insignificant. As an example, Mn^{2+}/TiO_2 has shifted the absorption edge to lower wavelength, therefore, it is expected that the indirect band gap for Mn^{2+}/TiO_2 is higher than pure TiO_2.

However, it is found that the indirect band gap for Mn^{2+}/TiO_2 is similar with the indirect band gap for pure TiO_2. This may be due to the difference in film thicknesses for both catalysts. According to the Equation 3.1, film thickness plays an important role in the determination of absorption coefficient value (α). When film thickness is different, the absorption coefficient value will be changed too. Since indirect band gap can be obtained by extrapolation to $(\alpha h\nu)_{1/2} = 0$, therefore, different film thickness will lead to different absorption coefficient value which in turn will result in the changing of indirect band gap.

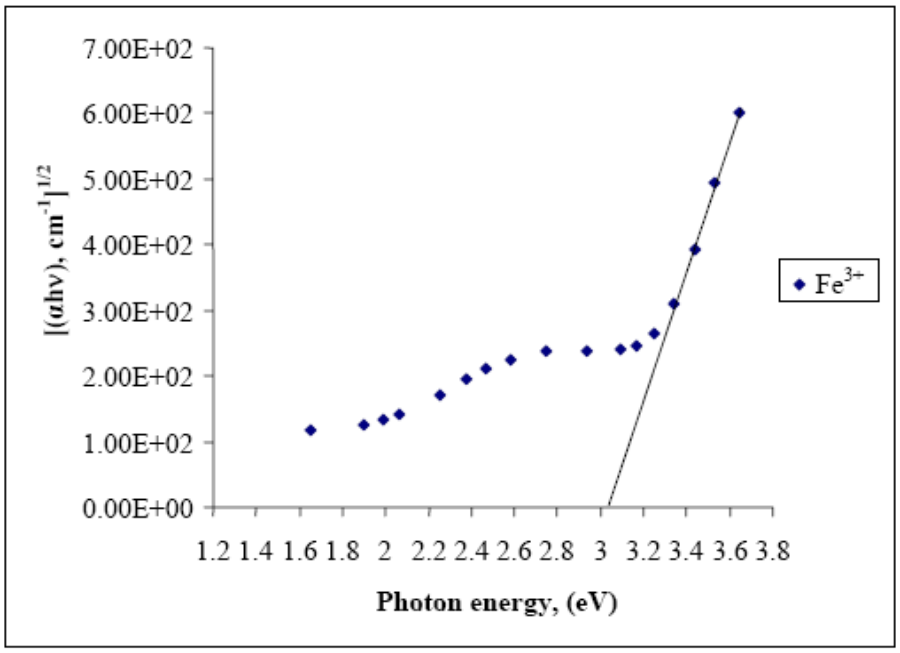

Figure 4.35: Tauc's plot for indirect band gap of Fe^{3+}-doped TiO_2.

4.9.4 Electron Dispersive X-ray Analysis (EDX)

Figure 4.36 shows the EDX spectrum for Zn^{2+} co-doped Fe^{3+}/TiO_2 thin film. DX. However, the ratio of Ti bounded to oxygen and bounded to dopant (Zn^{2+}, Fe^{2+}, Fe^{3+}, Mn2+, Cu^{2+}, Cu^{2+} co-doped Fe^{3+} and Zn^{2+} co-doped Fe^{3+}) could not be calculated using this method since the percentage amount of elements given in EDX data represents the total amount of that individual element in the respective samples for other thin film are given in Appendix H. All doped catalysts were observed by EDX. However, the ratio of Ti bounded to oxygen and bounded to dopant (Zn^{2+}, Fe^{2+}, Fe^{3+}, Mn^{2+}, Cu^{2+}, Cu^{2+} co-doped Fe^{3+} and Zn^{2+} co-doped Fe^{3+}) could not be calculated using this method since the percentage amount of elements given in EDX data represents the total amount of that individual element in the respective sample.

Table 4.18: The optical band gaps for pure TiO_2 and doped TiO_2.

Catalyst Samples	Optical band gaps, E_g (eV)
Mn^{2+}/ TiO_2	3.00
Fe^{2+}/ TiO_2	3.02
Fe^{3+}/ TiO_2	3.04
Cu^{2+}/ TiO_2	3.00
Zn^{2+}/ TiO_2	3.05
Pure TiO_2	3.00

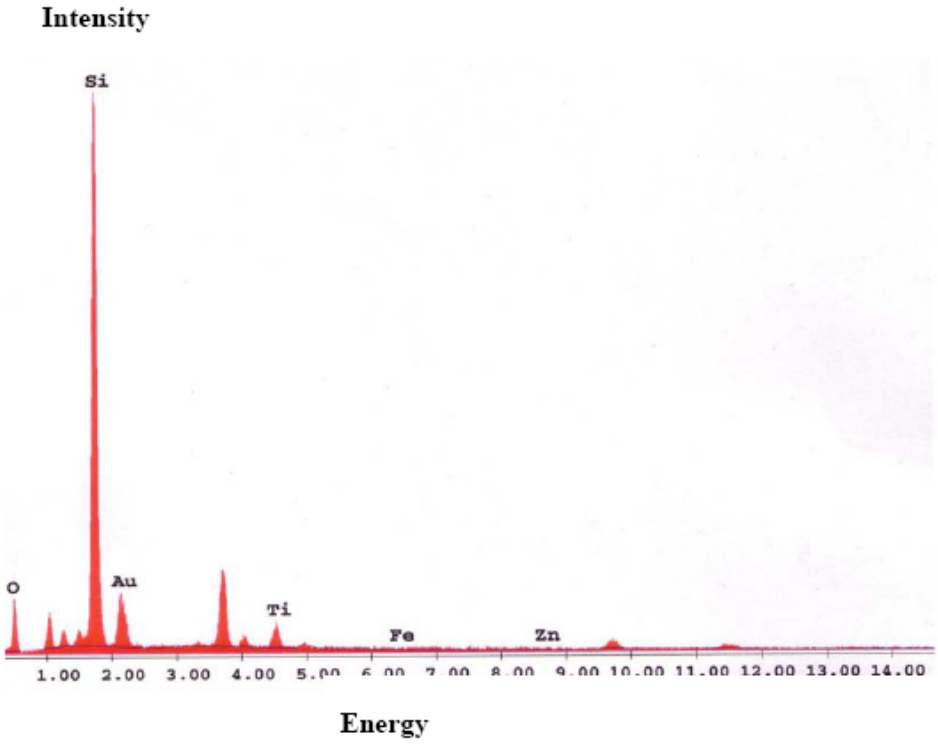

Figure 4.36: EDX spectrum for Zn^{2+} co-doped Fe^{3+}/TiO_2 thin film.

4.9.5 Scanning Electron Microscopy (SEM)

In the characterization of thin film using SEM, only the best catalyst was characterized. Figure 4.37 shows the SEM micrograph of Zn^{2+} co-doped Fe^{3+}/TiO_2 thin film. Scanning of Zn^{2+} co-doped Fe^{3+}/TiO_2 thin film was made with 5000 magnification

and 30 kV scanning voltage. According to Figure 4.37, it was found that pores are produced in the thin film. Pores are produced in the films because PEG contained in the sol-gel decomposes at 450°C (Sonawane, 2004). In the preparation of Zn^{2+} co-doped Fe^{3+}/TiO_2 thin film, PEG was added into the sol-gel and the catalyst was calcined at 500°C. Therefore, it is expected that pores exist in the catalyst and this has a good agreement with the obtained micrograph.

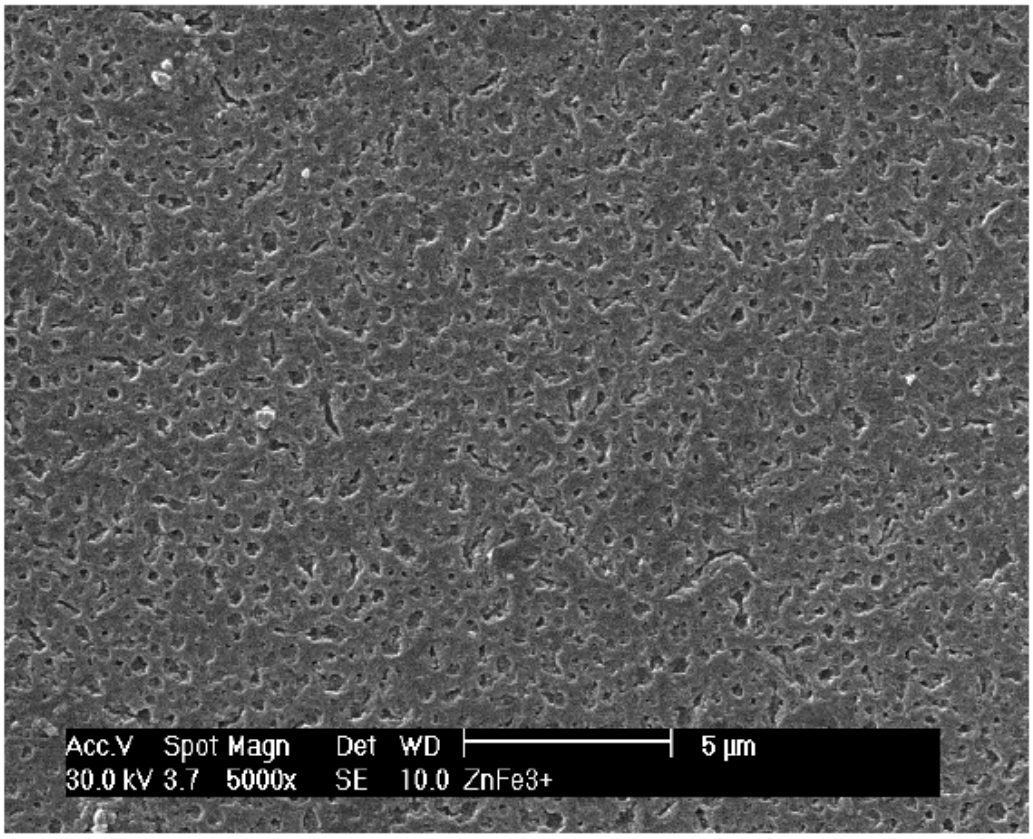

Figure 4.37: SEM micrograph of Zn^{2+} co-doped Fe^{3+}/TiO_2 thin film.

CHAPTER 5

CONCLUSIONS AND RECOMMENDATIONS

5.0 Conclusions

Transparent and non-abrasive doped and undoped TiO_2 thin films were successfully prepared using the sol-gel method. It was noted that the photocataytic degradation of under studied VOCs did not only depend on the concentration and type of dopant ions but also the type of VOCs. When doped catalysts with different dopant ratios were used, only catalysts with optimum dopant ratios gave the highest % degradation of studied VOCs. All Cu^{2+}, Fe^{2+}, Zn^{2+}, Fe^{3+}-doped TiO_2 had an optimum dopant ratio of 1:0.0005, while Zn^{2+} co-doped Fe^{3+}/TiO_2 and Cu^{2+} co-doped Fe^{3+}/TiO_2 showed an optimum dopant ratio of 1:0.0005:0.0005.

Catalysts such as Cu^{2+}, Fe^{2+}, Zn^{2+}, Fe^{3+}-doped TiO_2, Zn^{2+} co-doped Fe^{3+}/TiO_2 and Cu^{2+} co-doped Fe^{3+}/TiO_2 increased the photocatalytic degradation of dichloromethane, chloroform and carbon tetrachloride. The rate of degradation of the studied chlorinated hydrocarbons follows the order: $CHCl_3 > CH_2Cl_2 > CCl_4$. In the photocatalytic degradation of chloroform and carbon tetrachloride mixture, chloroform showed higher % degradation than carbon tetrachloride. When the concentrations of $CHCl_3$ and CCl_4 were increased, the % degradation of $CHCl_3$ and CCl_4 decreased.

Kinetic studies were carried out using doped and pure TiO_2 for each VOC. A linear plot of reciprocal initial rate versus reciprocal initial concentration results in a good fitting of the L-H model to the experimental data thus confirming the L-H nature of the photocatalytic degradation reaction. Although in the degradation of dichloromethane, the initial rate of Fe^{3+}-doped TiO_2 was lower than for other sample catalysts, the amount of dichloromethane degraded was higher. This indicates that a higher adsorption constant does not always result in a higher degradation rate. In order to determine the order of the degradation of carbon tetrachloride, dichloromethane and chloroform, a graph of In [C] versus time was plotted. The obtained data showed that the VOCs in this study degraded according to first-order kinetics.

GC-MS was used to analyze fragments that may form during the photocatalytic degradation of the VOCs. A possible model was proposed for the photocatalytic degradation of dichloromethane, chloroform and carbon tetrachloride. Structural and optical characterizations were conducted through SEM/EDX, UVVis spectrophotometeric and ellipsometric analyses. The thin film thickness and refractive index of Zn^{2+} co-doped Fe^{3+}/TiO_2 and Cu^{2+} co-doped Fe^{3+}/TiO_2 were unable to be determined using ellipsometry. As a consequence, the indirect band gap values for Cu^{2+} co-doped Fe^{3+}/TiO_2 and Zn^{2+} co-doped Fe^{3+}/TiO_2 were not determined.

The film thickness for all catalyst samples is between 227-251 nm and thus within the range of acceptable thin film dimensions since the limit of thin film thickness is 1000 nm. The refractive index for doped TiO_2 is lower than pure TiO_2. Refractive index can be used to calculate the porosity of the thin films. It was found that the lower the refractive index, the higher is the porosity. Fe^{3+} -doped TiO_2 shows the highest porosity among other catalyst samples. Thin films with high porosity had superior photoactivity. However, when Mn^{2+}, Fe^{2+}, Fe^{3+}, Cu^{2+} and Zn^{2+} doped TiO_2 were used in the degradation of dichloromethane, chloroform and carbon tetrachloride, only Fe^{2+}, Fe^{3+}, Cu^{2+} and Zn^{2+} doped TiO_2 showed higher degradation of VOCs than pure TiO_2.

Mn^{2+} doped TiO_2 was found to be detrimental to the degradation of VOCs although the porosity of Mn^{2+} doped TiO_2 was found to be higher than pure TiO_2. The absorption spectrum for all doped TiO_2 with optimum dopant ratio and undoped TiO_2 were taken using the Shimadzu UV-Vis-NIR Scanning Spectrophotometer. A slight shift to a higher wavelength or red shift was noted for Zn^{2+} co-doped Fe^{3+}/TiO_2, Cu^{2+} co-doped Fe^{3+}/TiO_2 and Cu^{2+} doped TiO_2. Meanwhile, Fe^{3+}, Fe^{2+}, Mn^{2+} and Zn^{2+} showed a slight shift to a lower wavelength.

The optical band gap, E_g values for all catalyst samples were determined by plotting $(\alpha h\nu)_{1/2}$ versus the equivalent energy at the wavelength, λ. It is noted that all obtained graphs have a similar curve. The obtained band gap values are in the range of 3-3.05 eV, which is lower than the normal value of 3.2 eV but is close to the literature data. It is expected that their photocatalytic activity will be lower than pure TiO_2.

However, when photocatalytic degradation of dichloromethane, chloroform and carbon tetrachloride were carried out, it was found that the photocatalytic activities of Fe^{3+}-doped TiO_2 and Zn^{2+}-doped TiO_2 were higher than pure TiO_2. Band gap, therefore, is not the main contributing factor to photocatalytic activity to doped and pure TiO_2. All doped catalysts were observed by EDX. However, the ratio of Ti bounds to oxygen and bounds to dopant (Zn^{2+}, Fe^{2+}, Fe^{3+}, Mn^{2+}, Cu^{2+} co-doped Fe^{3+} and Zn^{2+} co-doped Fe^{3+}) could not be calculated using this method. In the characterization of thin film using SEM, only the best catalyst was characterized. It was found that pores are produced in the thin film.

REFERENCES

Abou-Helal, M.O. and Seeber, W.T. (2002). Preparation of TiO_2 Thin Films by Spray Pyrolysis to be Used as a Photocatalyst. *Appl. Surf. Sci.* 195: 53-62.

Alberici, R.M. and Jardim, W.F. (1997). Photocatalytic Destruction of VOCs in The Gas-phase Using Titanium Dioxide. *Appl. Catal. B: Environ.* 14: 55-68.

Amor, S.B., Baud, G., Jacquet, M. and Pichon, N. (1998). Photoprotecive Titania Coatings on PET Substrates. *Surf. and Coatings Techol.* 102: 63-72.

Arana, J., Cabo, C.G.i., Dona-Rodriguez, J.M., Gonzalez-Diaz, O., Herrera-Melian, J.A. and Perez-Pena, J. (2004). FTIR Study of Formic Acid Interaction with TiO_2 and TiO_2 doped with Pd and Cu I Photocatalytic Processes. *Appl. Surf. Sci.*

Arana, J., Diaz, O. G., Dona Rodriguez, Saracho, M. M., Herrera Melian, J.A. and Perez Pena, J. (2001). Photocatalytic Degradation of Formic Acid Using Fe/ TiO_2 Catalysts: The Role of Fe^{3+}/ Fe^{2+} as TiO_2 Dopant Ions in the Degradation Mechanism. *Appl. Catal. B: Environ*. 32: 49-61.

Arroyo, R., Cordoba, G., Padilla, J. and Lara, V.H. (2002). Influence of Manganese Ions on The Anatase-rutile Phase Transition of TiO_2 Prepared by Sol-gel Process. *Mater. Lett.* 54: 397-420.

Bendavid, A., Martin, P.J., Takikawa, H. (2000). Deposition and Modification of Titanium Dioxide Thin Films by Filtered Arc Deposition. *Thin Solid Films.* 360: 102. 241-249.

Binder, L., Jantscher, W., Hofer, F. and Kothleitner, G. (1998). Production and Characterization of Ellectrolytically Doped Manganese Oxide. *J. Power Sources.* 70: 1-7.

Borgarello, E., Kiwi, J., Gractzel, M., Pelizzetti, E., Visca, M. (1982). Visible Light Induced Water Cleavage in Colloidal Solutions of Cr-doped TiO_2 Particles. J. Am. Chem. Soc. 104: 2996-3002.

Braun, A.M., Jakob, L. and Oliveros, E. (1993). Advanced Oxidation Processes: Concepts of Reactor Design. *AQUAAA,* 42: 166-173.

Brezova, V., Blazkova, A., Karpinsky, L., Groskova, J., Havlinova, B., Jorik, V. and Ceppan, M. (1997). Phenol Decomposition Using M_{n+}/TiO_2 Photocatalysts Supported by The Sol-gel Technique on Glass Fibres. *J. Photochem. Photobio. A: Chem.* 109: 177-183

Butler, E.C. and Davis, A.P. (1993). Photocatalytic Oxidation in Aqueous Titanium Dioxide Suspensions: The influence of Dissolved Transition Metals. *J. Photochem. Photobiol. A: Chem.* 70: 273-283.

Cardona, A.I., Candal, R., Sanchez, B., Avila, P. and Rebollar, M. (2004). TiO_2 on Magnesium Silicate Monolith: Effects of Different Preparation Techniques on the Photocatalytic Oxidation of Chlorinated Hydrocarbons. *Energy.* 29: 845-852.

Chen, C.H., Kelder, E.M., Schoonman, J. (1999). Electrostatc sol-Spray Deposition (ESSD) and Characterization of Nanostructured TiO_2 Thin Films. *Thin Solid films.* 342: 35-41.

Choi, W., Ko, J. Y., Park, H. and Chung, J. S. (2001). Investigation on TiO_2- coated Optical Fibers for Gas-phase Photocatalytic Oxidation of Acetone. *Appl. Catal. B: Environ*. 31: 209-220.

Dionysiou, D.D., Suidan, M.T., Bekou, E., Baudin, I., Laine, J.M. (2000). Effect of Ionic Strength and Hydrogen Peroxide on the Photocatalytic Degradation of 4-Chlorobenzoic Acid in Water. *Appl. Catal. B: Environ*. 26: 153-171.

Djeghri, N., Teichner, S. J. (1980). Heterogeneous Photocatalysis-the Photooxidation of 2-Methylbutane. *J. Catal.* 62: 99-106.

Dvoranova, D., Brezova, V., Mazur, M. and Malati, M. A. (2002). Investigations of Metal-doped Titanium Dioxide Photocatalysts. *Appl. Catal. B: Environ*. 37: 91-105.

Feiyen, C., Pehkonen, S.O. and Ray, M. B. (2002). Kinetics and Mechanisms of UV photodegradation of Chlorinated Organics in The Gas Phase. *Water Research.* 36:4203-4214.

Fu, X., Zeltner, W. A., Anderson, M. A. (1996). Applications in Photocatalytic Purification of Air. In: P.V. Kamat & D. Meisel (Eds.), Semiconductor nanoclusters. studies in surface science and catalysis Amsterdam. *Elsevier Sci.* 445–461.

Fox, M. A., Dulay, T. (1993). Heterogeneous Photocatalysis. *Chem. Rev.* 93: 341–357.

Gracia, F., Holgado, J.P., Yubero, F., Gonzales-Elipe, A.R. (2002). Phase Mixing in Fe/TiO_2 Thin Films Prepared by Ion Beam-induced Chemical Vapour Deposition:

Optical and Structural Properties. *Surf. Coatings Technol.* 158-159: 552-557.

Gudzinowicz, B.J., Gudzinowicz, M.J. and Martin, H.F. (1976). *Fundamentals of Integrated GC-MS.* New York: Marcel Dekker, Inc.

Hale, R.C., Greaves, J. (1992). Methods for the Analysis of Persistent Chlorinated Hydrocarbons in Tissues. *J. Chromatogr. Biomed. Appl*. 580: 257–278.

He, C., Xiong, Y., Chen, J. Zha, C. and Zhu, X. (2003). Photoelectrochemical Performance of Ag-TiO_2 / ITO Film and Photoelectrocatalytic Activity Towards the Oxidation of Organic Pollutants. *J. Photochem. Photobio. A: Chem.* 157: 71-79.

Hester, R. E., Harrison, R. M. (1995). *Volatile Organic Compounds in the Atmosphere.* London: The Royal Society of Chem.

Hirano, K., Asayama, H., Hoshino, A., Wakatsuki, H. (1997). Metal Powder Addition Effect on the Photocatalytic Reactions and the Photogenerated Electric Charge Collected at an Inert Electrode in Aqueous TiO_2 Suspensions. *J. Photochem. Photobio. A: Chem.* 110: 307-311.

Hoffmann, M.R., Martin, S.T., Choi, W., Bahnemann, D. W. (1995). Environmental Applications of Semiconductor Photocatalysis. *Chem. Reviews,* 95: 69–96.

Hong, H.S., Kim, D.H., Kim, S.J., Song, J. and Lee, K.S. (2004). Photocatalytic Behaviours and Structural Characterization of Nanocrystalline Fe-doped TiO_2

Synthesized by Mechanical Alloying. *J. Alloy and Compounds*

Jiang, H. and Gao, L. (2002) Enhancing The UV Inducing Hydrophilicity of TiO_2 Thin Film by Doping Fe Ions. *Mater. Chem. And Phys.* 77: 878- 881.

Karvinen, S. (2003). The Effects of Trace Elements on The Crystal Properties of TiO_2. *Solid State Sci*. 5: 811-819.

Kato, K. Tsuzuki, A. Taoda, H. Torii, Y., Kato, T. and Butsugan, Y. (1994). Crystal Structures of TiO_2 Thin Coatings Prepared from The Alkoxide Solution Via The Dipcoating Technique Affecting The Photocatalytic Decomposition of Aqueous Acetic Acid. *J. Mater. Sci.* 29: 5911-5915.

Kim, S. B. and Hong, S. C. (2002). Kinetic Study for Photocatalytic Degradation of Volatile Organic Compounds in Air Using Thin Film TiO_2 Photocatlyst. *Appl. Catal. B: Environ*. 35: 305-315.

Legrand-Buscema, C., Malibert, C. and Bach, S. (2002). Elaboration and Characterization of Thin Film of TiO_2 Prepared by Sol-gel Process. *Thin Solid Films.* 418: 79-84.

Legrini, O., Oliveros, E., Brawn, A.M. (1993). Photochemical Processes for Water Treatment. *Chem. Rev.* 93: 671-689.

Litter, M.I. (1999). Review Heterogeneous Photocatalysis Transition Metal Ions in Photocatalytic Systems. *Appl. Catal. B: Environ*. 23: 89-114.

Liu, T-C. and Cheng, T-I. (1995). Effects of SiO_2 on the Catalytic Properties of TiO_2 for the Incineration of Chloroform. *Catal. Today.* 26: 71-77.

Luo, Y. and Ollis, D. F. (1996). Heterogeneous Photocatalytic Oxidation of Trichloroethylene and Toluene Mixtures in Air: Kinetic Promotion and Inhibition, Time-dependent Catalyst Activity. *J. Catal.* 163: 1-11.

Malati, M. A., Wong, W. K. (1984). Doping TiO_2 for Solar Energy Applications. Surface Tech. 22: 305-322.

Mardare, D. (2002). Optical Constant of Heat Treated TiO_2 Thin Films. *Mater. Sci. Eng.* 95: 83-87.

Mardare, D., Tasca, M., Delibas, M., Rusu, G.I. (2000). On the Structural Properties and Optical Transmittance of TiO_2 R.F. Sputtered Thin Film. *Appl. Surf. Sci.* 156: 200-206.

Mills, A., Davies, R. H., Worsley, D. (1993). Water-Purification by Semiconductor Photocatalysis. *Chem. Soc. Reviews.* 22: 417–425.

Mills, A., Le Hunte, S. (1997). An Overview of Semiconductor Photocatalysis. *J.*

Photochem. Photobio. A: Chem. 108: 1-35.

Mirmohseni, A. and Oladegeragoze, A. (2004). Determination of Chlorinated Aliphatic Hydrocarbons in Air Using a Polymer Coated Quartz Crystal Microbalance Sensor. *Sens. Actuators B* 102: 261-70.

Monneyron, P., Manero, M-H., Foussard, J.-N. and Maurette, M.-T. (2003). Heterogeneous Photocatalysis of Butanol And Methyl Etyl Ketone-Characterization of Catalyst and Dynamic Study. *Chem. Eng. Sci.* 58: 971-978.

Navio, J.A., Colon, G., Trillas, M., Peral, J., Domenech, X., Testa, J. J., Padron, J., Rodriguez, D. and Litter, M. I. (1998). Heterogeneous Photocatalytic Reactions of Nitrite Oxidation and Cr(VI) Reduction on Iron-doped Titania Prepared by the Wet Impregnation Method. *Appl. Catal. B: Environ*. 16: 187-196.

Oh, S.H., Kim, D.J., Hahn, S.H., Kim, E.J. (2003a). Comparison of Optical and Photocatalytic Properties of TiO_2 Thin Films Prepared by Electron-beam Evaporation and sol-gel dip-coating. *Mater. Lett.* 57: 4151-4155.

Oh, S-M., Kim, S-S., Lee, J.E., Ishigaki, T. and Park, D-W. (2003b). Effect of Additives on Photocatalytic Activity of Titanium Dioxide Powders Synthesized by Thermal Plasma. *Thin Solid Films.* 435: 252-258.

Ollis, D. F. (1993). *Photocatalytic puriGcation and treatment of water and air.* Lausanne: Elsevier.

Palmisano, L., Schiavello, M., Selafani, A., Martin, C., Martin, I., Rives, V. (1994) Surface Properties of Iron-Titania Photocatalysts Employed for 4-Nitrophenol Photodegradation in Aqueous TiO_2 Dispersion. *Catal. Lett.* 24: 303-315.

Paola, A.D., Garcia-Lopez, E., Ikeda, S., Marci, G., Ohtani, B. and Palmisano, L. (2002) Photocatalytic Degradation of Organic Compounds in Aqueous Systems by Transition Metal Doped Polycrystalline TiO_2. *Catal. Today.* 75: 87-93.

Park, S.E., Joo, H. and Kang, J.W. (2003). Effect of Impurities in TiO_2 Thin Films on Trichloroethylene Conversion. *Solar Energy Mater. & Solar Cells.*

Papaefthimiou, P., Ioannides, T. and Verykios, X.E. (1998). Performance of Doped Pt/TiO_2 (W^{6+}) Catalyst for Combustion of Volatile Organic Compounds (VOCs). *Appl. Catal. B: Environ.* 15: 75-92.

Pichat, P., Disdier, J., Hong-Van, C., Goutailler, G. and Gaysse, C. (2000).

Purification/deodorization of Indoor Air and Gaseous Effluents by TiO_2 Photocatalysis. *Catal. Today.* 63: 363-369.

Pilchowski, K., Averkiou, C., Solutuschien, B. (1992). Adsorption of Vinyl-chloride on Activated Carbons, Adsorber Polymers and Zeolites 2. *Kinetics of Adsorption, J. Fur Praktische Chemie-Chemiker-Zeitung.* 334: 681-684

Pinard, L., Mijoin, J., Magnoux, P. and Guisnet, M. (2003). Oxidation of Chlorinated Hydrocarbons Over P Zeolite Catalysts 1-mechanism of Dichloromethane transformation Over PtNaY Catalysts. *J. Cat.* 215: 234-244.

Rahman, M.M., Krishna, K.M., Soga, T., Jimbo, T., Umeno, M. (1999). Optical Properties and X-ray Photoelectron Spectroscopic Study of Pure and Pb-doped TiO_2 Thin Films. *J. Phys. Chem. Solids.* 60: 201-210.

Ranjit, K.T. and Viswanathan, B. (1997). Synthesis, Characterization and Photocatalytic Properties of Iron-doped TiO_2 Catalysts. *J. Photochem. Photobiol. A: Chem.* 108: 79-84.

Sonawane, R.S., Kale, B.B. and Dongare, M.K. (2004). Preparation and photo-catalytic Activity of Fe-TiO_2 Thin Films Prepared by Sol-gel Dip Coating. *Mater. Chem. Phys.* 85: 52-57.

Takahashi, Y. and Matsuoka, Y. (1988). Dip-coating of TiO_2 Films Using a Sol Derived from Ti(O-*i*-Pr)$_4$-diethanolamine-H_2O-*i*-PrOH System. *J. Mater. Sci.* 23: 2259-2266.

Wang, K-H. and Hsieh,Y-H. (1998). Heterogeneous Photocatalytic Degradation of Trichloroethylene in Vapor Phase by Titanium Dioxide. *Pergamon Environ. International.* 24: 267-274.

Winkler, K., Radeke, K.H., Stach, H. (1996). Adsorption/Desorption Behavior of Organic-Water Pollutants onto an Adsorber Polymer. *Chem. Tech.* 48: 249–257.

Yang, P., Lu, C., Hua, N. and Du, Y. (2002). Titanium Dioxide Nanoparticles Codoped with Fe^{3+} and Eu^{3+} Ions for Photocatalysis. *Mater. Lett.* 57: 794- 801.

Yashin, Y.I., Yashin, A.Y. (1999). New Potentialities of Chromatography in the Determination of Pollutants in Potable Water. *J. Anal. Chem.* 54: 843-849.

Yuan, Z-h., Jia, J-h. and Zhang, L-d. (2002). Influence of Co-doping of Zn(II) + Fe(III) on the Photocatalytic Activity of TiO_2 for Phenol Degradation. *Mater. Chem. And*

Phys. 73: 323-326.

Zhang, S., Li, S.F.Y. (1996). Detection of Organic Solvent Vapors and Studies of Thermodynamic Parameters using Quartz Crystal Microbalance Sensors Modified with Siloxane Polymers. *Analyst.* 121: 1721–1726.

Zhang, W., Li, Y., Zhu, S. and Wang, F. (2004). Copper Doping in Titanium Oxide Catalyst Film Prepared by DC Reactive Magnetron Sputtering . *Catal. Today* 93-95: 589-594.

Zheng, S.K., Wang, T.M., Wang, C. and Xiang, G. (2002). Photocatalytic Activity Study of TiO_2 Thin Films with and Without Fe Ion Implantation. *Nucl. Instr. and Meth. In Phys. Res. B* 187: 479-484.

APENDICES

Appendix A: Calculation to Obtain α Value

$$T = (1 - R^2)\exp(-\alpha d)$$

$$\frac{T}{1 - R^2} = \exp(-\alpha d)$$

$$\ln\left(\frac{1 - R^2}{T}\right) = \alpha d$$

$$\alpha = \frac{\ln\left(\frac{1 - R^2}{T}\right)}{d}$$

T and R values for doped and undoped TiO_2 at particular wavelength can be obtained from Appendix B and C while the thin film thickness, d can be obtained from Table 4.17.

Example:

R for Mn^{2+}-doped TiO_2 at 500 nm is 0.27 while T at 500 nm is 0.68, the film thickness for Mn^{2+}-doped TiO_2 is 227.09 nm.

Appendix B: Reflectance data for doped and undoped TiO_2

$$\alpha = \frac{\ln\left(\frac{1-0.27^2}{0.68}\right)}{2.2709\times10^{-5}\,\text{cm}}$$

$\alpha = 13649.59\ \text{cm}^{-1}$

Wavelength (nm.)	R%
800.00	6.20
790.00	6.44
780.00	6.63
770.00	6.83
760.00	7.02
750.00	7.21
740.00	7.42
730.00	7.67
720.00	8.00
710.00	8.29
700.00	8.60
690.00	8.97
680.00	9.38
670.00	9.83
660.00	10.31
650.00	10.79
640.00	11.37
630.00	11.99
620.00	12.66
610.00	13.37
600.00	14.15
590.00	14.98
580.00	15.91
570.00	16.87
560.00	17.82
550.00	18.89
540.00	19.93
530.00	20.92
520.00	21.93
510.00	22.90
500.00	23.81
490.00	24.67
480.00	25.44
470.00	26.12
460.00	26.70
450.00	27.22
440.00	27.70
430.00	28.17
420.00	28.60
410.00	29.17
400.00	29.91
390.00	30.84
380.00	31.42
370.00	30.31
360.00	26.26
350.00	22.32
340.00	20.95
330.00	21.57
320.00	25.02
310.00	34.49
300.00	42.92

Appendix B1: Reflectance data for Fe^{3+}-doped TiO_2.

Wavelength (nm.)	R%
800.00	4.36
790.00	4.44
780.00	4.52
770.00	4.57
760.00	4.62
750.00	4.73
740.00	4.81
730.00	4.87
720.00	4.94
710.00	5.06
700.00	5.14
690.00	5.25
680.00	5.35
670.00	5.46
660.00	5.58
650.00	5.71
640.00	5.84
630.00	5.99
620.00	6.15
610.00	6.28
600.00	6.42
590.00	6.59
580.00	6.82
570.00	7.01
560.00	7.21
550.00	7.52
540.00	7.77
530.00	8.04
520.00	8.34
510.00	8.69
500.00	9.09
490.00	9.54
480.00	10.02
470.00	10.58
460.00	11.22
450.00	11.94
440.00	12.77
430.00	13.68
420.00	14.68
410.00	15.78
400.00	17.03
390.00	18.23
380.00	19.06
370.00	18.98
360.00	16.84
350.00	14.22
340.00	13.10
330.00	13.23
320.00	15.07
310.00	20.48
300.00	25.45

Appendix B2: Reflectance data for Fe^{2+}-doped TiO_2.

Wavelength (nm.)	R%
800.00	11.21
790.00	11.53
780.00	11.76
770.00	12.15
760.00	12.44
750.00	12.75
740.00	13.16
730.00	13.49
720.00	13.86
710.00	14.20
700.00	14.58
690.00	14.96
680.00	15.39
670.00	15.82
660.00	16.18
650.00	16.61
640.00	17.06
630.00	17.49
620.00	17.87
610.00	18.33
600.00	18.79
590.00	19.26
580.00	19.75
570.00	20.26
560.00	20.74
550.00	21.30
540.00	21.84
530.00	22.36
520.00	22.96
510.00	23.62
500.00	24.30
490.00	25.03
480.00	25.88
470.00	26.74
460.00	27.73
450.00	28.73
440.00	29.81
430.00	30.90
420.00	31.97
410.00	32.95
400.00	33.70
390.00	34.12
380.00	33.81
370.00	31.75
360.00	25.97
350.00	20.24
340.00	18.35
330.00	18.60
320.00	21.14
310.00	28.52
300.00	35.32

Appendix B3: Reflectance data for Cu^{2+}-doped TiO_2.

Wavelength (nm.)	R%
800.00	13.76
790.00	13.98
780.00	14.25
770.00	14.49
760.00	14.78
750.00	15.06
740.00	15.38
730.00	15.75
720.00	16.13
710.00	16.51
700.00	16.85
690.00	17.25
680.00	17.70
670.00	18.10
660.00	18.57
650.00	19.05
640.00	19.52
630.00	20.05
620.00	20.54
610.00	21.07
600.00	21.61
590.00	22.15
580.00	22.74
570.00	23.31
560.00	23.85
550.00	24.47
540.00	24.98
530.00	25.54
520.00	26.07
510.00	26.55
500.00	27.00
490.00	27.45
480.00	27.83
470.00	28.17
460.00	28.49
450.00	28.81
440.00	29.16
430.00	29.46
420.00	29.80
410.00	30.19
400.00	30.76
390.00	31.34
380.00	31.74
370.00	31.18
360.00	28.28
350.00	24.69
340.00	22.87
330.00	22.74
320.00	25.50
310.00	34.33
300.00	42.28

Appendix B4: Reflectance data for Mn^{2+}-doped TiO_2.

Wavelength (nm.)	R%
800.00	10.32
790.00	10.70
780.00	10.98
770.00	11.37
760.00	11.81
750.00	12.26
740.00	12.71
730.00	13.19
720.00	13.74
710.00	14.30
700.00	14.93
690.00	15.55
680.00	16.21
670.00	16.92
660.00	17.62
650.00	18.34
640.00	19.11
630.00	19.87
620.00	20.59
610.00	21.32
600.00	22.05
590.00	22.77
580.00	23.50
570.00	24.18
560.00	24.77
550.00	25.44
540.00	25.97
530.00	26.44
520.00	26.97
510.00	27.39
500.00	27.82
490.00	28.23
480.00	28.62
470.00	29.00
460.00	29.47
450.00	30.00
440.00	30.63
430.00	31.46
420.00	32.39
410.00	33.52
400.00	34.71
390.00	35.82
380.00	36.31
370.00	34.73
360.00	28.54
350.00	22.20
340.00	19.59
330.00	19.00
320.00	20.89
310.00	27.86
300.00	34.47

Appendix B5: Reflectance data for Zn^{2+}-doped TiO_2.

Wavelength (nm.)	R%
800.00	12.24
790.00	12.73
780.00	13.24
770.00	13.74
760.00	14.32
750.00	14.88
740.00	15.50
730.00	16.12
720.00	16.76
710.00	17.43
700.00	18.11
690.00	18.83
680.00	19.55
670.00	20.20
660.00	20.87
650.00	21.57
640.00	22.21
630.00	22.92
620.00	23.50
610.00	23.99
600.00	24.50
590.00	24.96
580.00	25.40
570.00	25.78
560.00	26.02
550.00	26.33
540.00	26.48
530.00	26.52
520.00	26.60
510.00	26.61
500.00	26.65
490.00	26.70
480.00	26.80
470.00	27.08
460.00	27.49
450.00	28.22
440.00	29.31
430.00	30.76
420.00	32.52
410.00	34.31
400.00	35.92
390.00	36.86
380.00	36.15
370.00	32.35
360.00	25.83
350.00	21.07
340.00	19.35
330.00	19.82
320.00	22.81
310.00	30.71
300.00	37.80

Appendix B6: Reflectance data for Zn^{2+} co-doped Fe^{3+}/TiO_2.

Wavelength (nm.)	R%
800.00	13.91
790.00	14.23
780.00	14.48
770.00	14.73
760.00	14.94
750.00	15.18
740.00	15.41
730.00	15.63
720.00	15.89
710.00	16.19
700.00	16.46
690.00	16.75
680.00	17.00
670.00	17.30
660.00	17.60
650.00	17.93
640.00	18.30
630.00	18.67
620.00	19.03
610.00	19.41
600.00	19.84
590.00	20.31
580.00	20.84
570.00	21.40
560.00	21.91
550.00	22.53
540.00	23.14
530.00	23.74
520.00	24.41
510.00	25.04
500.00	25.72
490.00	26.43
480.00	27.15
470.00	27.89
460.00	28.68
450.00	29.50
440.00	30.38
430.00	31.33
420.00	32.32
410.00	33.26
400.00	34.17
390.00	34.77
380.00	34.52
370.00	32.12
360.00	26.64
350.00	21.78
340.00	19.79
330.00	20.10
320.00	23.18
310.00	31.47
300.00	39.06

Appendix B7: Reflectance data for Cu^{2+} co-doped Fe^{3+}/TiO_2.

Wavelength (nm.)	R%
800.00	8.51
790.00	8.82
780.00	9.21
770.00	9.61
760.00	9.90
750.00	10.28
740.00	10.71
730.00	11.19
720.00	11.66
710.00	12.18
700.00	12.70
690.00	13.25
680.00	13.84
670.00	14.50
660.00	15.16
650.00	15.82
640.00	16.54
630.00	17.26
620.00	17.99
610.00	18.73
600.00	19.41
590.00	20.10
580.00	20.78
570.00	21.39
560.00	21.90
550.00	22.40
540.00	22.76
530.00	23.04
520.00	23.24
510.00	23.34
500.00	23.43
490.00	23.46
480.00	23.46
470.00	23.54
460.00	23.75
450.00	24.15
440.00	24.91
430.00	26.10
420.00	27.77
410.00	29.84
400.00	32.14
390.00	34.11
380.00	35.12
370.00	34.05
360.00	29.11
350.00	23.61
340.00	21.28
330.00	21.36
320.00	24.54
310.00	33.70
300.00	41.96

Appendix B8: Reflectance data for pure TiO_2.

Appendix C: Transmittance data for doped and undoped TiO_2

Wavelength (nm.)	T%
800.00	79.29
790.00	79.87
780.00	80.05
770.00	80.38
760.00	80.55
750.00	80.84
740.00	81.12
730.00	81.25
720.00	81.46
710.00	81.56
700.00	81.72
690.00	81.75
680.00	81.64
670.00	81.57
660.00	81.39
650.00	81.01
640.00	80.56
630.00	79.94
620.00	79.29
610.00	78.50
600.00	77.47
590.00	76.22
580.00	74.92
570.00	73.55
560.00	71.74
550.00	70.06
540.00	68.19
530.00	66.13
520.00	64.30
510.00	62.51
500.00	60.78
490.00	59.23
480.00	58.00
470.00	57.03
460.00	56.34
450.00	56.02
440.00	56.06
430.00	56.54
420.00	57.21
410.00	57.83
400.00	57.91
390.00	56.85
380.00	53.32
370.00	45.25
360.00	31.33
350.00	17.69
340.00	8.57
330.00	2.83
320.00	0.52
310.00	0.08
300.00	0.05

Appendix C1: Transmittance data for Fe^{3+}-doped TiO_2.

Wavelength (nm.)	T%
800.00	75.52
790.00	75.85
780.00	76.00
770.00	76.32
760.00	76.74
750.00	77.05
740.00	77.41
730.00	77.95
720.00	78.22
710.00	78.56
700.00	78.93
690.00	79.27
680.00	79.55
670.00	79.77
660.00	80.04
650.00	80.27
640.00	80.31
630.00	80.40
620.00	80.52
610.00	80.47
600.00	80.29
590.00	79.84
580.00	79.41
570.00	79.14
560.00	78.22
550.00	77.57
540.00	76.73
530.00	75.70
520.00	74.77
510.00	73.63
500.00	72.60
490.00	71.48
480.00	70.42
470.00	69.56
460.00	68.67
450.00	68.10
440.00	67.65
430.00	67.47
420.00	67.40
410.00	67.08
400.00	66.54
390.00	64.81
380.00	60.93
370.00	53.49
360.00	39.95
350.00	25.50
340.00	14.84
330.00	6.74
320.00	2.14
310.00	0.55
300.00	0.13

Appendix C2: Transmittance data for Fe^{2+}-doped TiO_2.

Wavelength (nm.)	T%
800.00	77.39
790.00	77.39
780.00	77.04
770.00	76.85
760.00	76.83
750.00	76.89
740.00	76.59
730.00	76.35
720.00	76.11
710.00	75.81
700.00	75.61
690.00	75.26
680.00	74.90
670.00	74.42
660.00	73.93
650.00	73.37
640.00	72.80
630.00	72.20
620.00	71.57
610.00	70.92
600.00	70.21
590.00	69.41
580.00	68.68
570.00	68.12
560.00	67.24
550.00	66.60
540.00	66.00
530.00	65.30
520.00	64.86
510.00	64.29
500.00	63.81
490.00	63.34
480.00	62.94
470.00	62.52
460.00	62.04
450.00	61.54
440.00	60.97
430.00	60.25
420.00	59.27
410.00	57.77
400.00	55.55
390.00	52.89
380.00	49.34
370.00	44.01
360.00	33.82
350.00	21.45
340.00	12.19
330.00	5.31
320.00	1.67
310.00	0.57
300.00	0.25

Appendix C3: Transmittance data for Cu^{2+}-doped TiO_2.

Wavelength (nm.)	T%
800.00	75.76
790.00	75.49
780.00	75.74
770.00	76.16
760.00	76.34
750.00	76.17
740.00	76.22
730.00	76.42
720.00	76.40
710.00	76.56
700.00	76.53
690.00	76.51
680.00	76.30
670.00	76.18
660.00	76.02
650.00	75.76
640.00	75.57
630.00	75.19
620.00	74.92
610.00	74.53
600.00	74.01
590.00	73.52
580.00	72.94
570.00	72.54
560.00	71.71
550.00	71.17
540.00	70.46
530.00	69.63
520.00	69.00
510.00	68.26
500.00	67.59
490.00	66.91
480.00	66.38
470.00	65.83
460.00	65.41
450.00	65.15
440.00	64.88
430.00	64.76
420.00	64.51
410.00	64.03
400.00	63.11
390.00	61.58
380.00	58.89
370.00	54.16
360.00	44.66
350.00	32.45
340.00	21.72
330.00	12.23
320.00	5.93
310.00	3.24
300.00	2.19

Appendix C4: Transmittance data for Mn^{2+}-doped TiO_2.

Wavelength (nm.)	T%
800.00	80.20
790.00	80.25
780.00	79.80
770.00	79.51
760.00	79.22
750.00	79.05
740.00	78.62
730.00	78.46
720.00	77.85
710.00	77.33
700.00	76.79
690.00	76.25
680.00	75.62
670.00	74.90
660.00	74.20
650.00	73.41
640.00	72.65
630.00	71.84
620.00	71.00
610.00	70.18
600.00	69.35
590.00	68.52
580.00	67.81
570.00	67.14
560.00	66.30
550.00	65.72
540.00	65.03
530.00	64.40
520.00	63.97
510.00	63.46
500.00	62.99
490.00	62.63
480.00	62.34
470.00	62.05
460.00	61.80
450.00	61.56
440.00	61.28
430.00	61.01
420.00	60.49
410.00	59.61
400.00	58.03
390.00	55.91
380.00	52.74
370.00	47.05
360.00	35.14
350.00	21.41
340.00	12.11
330.00	5.71
320.00	2.31
310.00	1.37
300.00	1.16

Appendix C5: Transmittance data for Zn^{2+}-doped TiO_2.

Wavelength (nm.)	T%
800.00	76.43
790.00	76.32
780.00	76.12
770.00	75.87
760.00	75.64
750.00	75.47
740.00	75.03
730.00	74.82
720.00	74.28
710.00	73.60
700.00	73.13
690.00	72.46
680.00	71.78
670.00	71.02
660.00	70.15
650.00	69.36
640.00	68.50
630.00	67.60
620.00	66.81
610.00	65.96
600.00	65.11
590.00	64.31
580.00	63.61
570.00	63.03
560.00	62.25
550.00	61.71
540.00	61.15
530.00	60.54
520.00	60.10
510.00	59.58
500.00	59.07
490.00	58.64
480.00	58.19
470.00	57.71
460.00	57.18
450.00	56.47
440.00	55.74
430.00	54.84
420.00	53.78
410.00	52.39
400.00	50.73
390.00	48.74
380.00	45.41
370.00	38.76
360.00	26.84
350.00	14.98
340.00	7.04
330.00	2.48
320.00	0.76
310.00	0.37
300.00	0.25

Appendix C6: Transmittance data for Zn^{2+} co-doped Fe^{3+}/TiO_2.

Wavelength (nm)	T%
800.00	74.35
795.00	74.36
790.00	74.48
785.00	74.48
780.00	74.39
775.00	74.36
770.00	74.50
765.00	74.56
760.00	74.59
755.00	74.48
750.00	74.42
745.00	74.34
740.00	74.43
735.00	74.52
730.00	74.58
725.00	74.55
720.00	74.48
715.00	74.38
710.00	74.39
705.00	74.43
700.00	74.45
695.00	74.48
690.00	74.39
685.00	74.40
680.00	74.33
675.00	74.30
670.00	74.25
665.00	74.24
660.00	74.21
655.00	74.15
650.00	74.12
645.00	74.11
640.00	74.04
635.00	73.95
630.00	73.88
625.00	73.81
620.00	73.73
615.00	73.68
610.00	73.61
605.00	73.50
600.00	73.35
595.00	73.22
590.00	73.05
585.00	72.92
580.00	72.81
575.00	72.70
570.00	72.53
565.00	72.19
560.00	71.81
555.00	71.51
550.00	71.30
545.00	71.02
540.00	70.53
535.00	70.03
530.00	69.53
525.00	69.04
520.00	68.50
515.00	67.90
510.00	67.26
505.00	66.59
500.00	65.88
495.00	65.20
490.00	64.44
485.00	63.66
480.00	62.87
475.00	62.09
470.00	61.29
465.00	60.49
460.00	59.67
455.00	58.90
450.00	58.17
445.00	57.48
440.00	56.79
435.00	56.17
430.00	55.56
425.00	55.09
420.00	54.59
415.00	54.11
410.00	53.50
405.00	52.86
400.00	52.15
395.00	51.41
390.00	50.48
385.00	49.32
380.00	47.73
375.00	45.49
370.00	42.17
365.00	37.32
360.00	31.56
355.00	25.46
350.00	19.85
345.00	15.02
340.00	10.78
335.00	7.25
330.00	4.52
325.00	2.66
320.00	1.57
315.00	1.00
310.00	0.69
305.00	0.50
300.00	0.36

Appendix C7: Transmittance data for Cu^{2+} co-doped Fe^{3+}/TiO_2.

Wavelength (nm.)	T%
800.00	77.88
790.00	77.69
780.00	77.71
770.00	77.89
760.00	77.55
750.00	77.45
740.00	77.35
730.00	77.27
720.00	76.70
710.00	76.07
700.00	75.52
690.00	74.69
680.00	73.94
670.00	73.07
660.00	72.04
650.00	71.04
640.00	69.96
630.00	68.86
620.00	67.83
610.00	66.69
600.00	65.63
590.00	64.62
580.00	63.67
570.00	63.02
560.00	62.07
550.00	61.46
540.00	61.00
530.00	60.55
520.00	60.44
510.00	60.31
500.00	60.49
490.00	60.65
480.00	60.98
470.00	61.40
460.00	61.65
450.00	61.91
440.00	61.94
430.00	61.64
420.00	61.04
410.00	59.71
400.00	57.85
390.00	55.22
380.00	51.72
370.00	46.57
360.00	36.03
350.00	23.26
340.00	13.37
330.00	5.97
320.00	1.96
310.00	0.73
300.00	0.50

Appendix C8: Transmittance data for pure TiO_2.

Appendix D: Calculation for Concentration of VOCs in Term of ppm

Weight: Density (g/mL) x V (mL)

Density: ℓ (g/mL) @ (Kg/L)

Nombor of moles = $\frac{Weight}{MW}$

At SATP, 1 mole of gas = 24.79 L

Concentration (ppm): mole x 24.79 L x 10^6

: y ppm

Example: Density of dichloromethane = 1.3266 g/mL

MW of dichloromethane = 84.93

When volume = 3 μL

Weight =

1.3266 g	1000 mL	3 μL	1 L
mL	1 L		1 x 10^6 μL

= 3.9798 x 10^{-3} g

Nombor of Moles = $\frac{3.9798 \times 10^{-3}\ g}{84.93}$

= 4.6860 x 10^{-5} mole

Therefore, 4.6860 x 10^{-5} mole = 24.79 L x 4.6860 x 10^{-5}

= 1.1617 x 10^{-3} L

Concentration (ppm) = 1.1617 x 10^{-3} x 1 x 10^6

= 1162 ppm

Appendix E: Comparision of Fragments Formed Before and After Illumination of UV Light for Dichloromethane.

Scan 57 (1.007 min): MYB4152.D
dichloromethane

m/z	abund.	m/z	abund.	m/z	abund.	m/z	abund.
10.15	94	20.60	4543	34.50	3157	47.35	44424
10.45	108	21.50	81	35.40	18680	48.30	19344
10.75	102	22.60	130	36.40	4962	49.30	238144 → CH_2Cl^+
11.05	110	23.60	108	37.40	6214	50.30	9240 → CH_3Cl^+
12.75	3177	25.05	491	38.40	1513	51.30	67432 → OCl^+
13.75	10011	26.05	531	40.35	44032	52.20	713
14.75	192128	28.55	919360	41.35	7945	53.20	76
16.60	53560	29.55	24440	42.35	5238	54.20	53
17.70	22792	30.55	832	43.35	964	54.50	43
18.60	94128	32.40	641024	44.35	6177	55.30	93
19.70	946	33.40	809	45.35	147	56.25	156

Scan 57 (1.007 min): MYB4152.D
dichloromethane

CH_2ClO^+ CCl_2^+

m/z	abund.	m/z	abund.	m/z	abund.	m/z	abund.
56.85	56	67.00	64	76.65	58	85.90	88896
57.95	48	67.80	63	77.25	40	86.90	2691
58.75	56	69.20	88	78.35	40	87.90	13525
59.55	41	70.10	763	78.95	31	88.85	183
60.15	64	70.70	49	79.45	55	89.95	39
61.15	74	71.30	80	80.50	62	90.95	33
62.65	59	72.00	561	81.00	44	91.15	32
63.25	57	72.95	53	81.90	1950	91.55	46
64.90	64	73.95	116	82.90	16368	92.85	51
65.40	59	74.95	33	83.90	143232	93.35	30
66.40	33	75.25	32	84.90	12404	93.95	31

Scan 57 (1.007 min): MYB4152.D
dichloromethane

$CHCl_2O^+$ $COCl_2^+$ $CHCl_2^+$

m/z	abund.	m/z	abund.	m/z	abund.	m/z	abund.
94.75	43	100.90	34	108.45	26	118.60	193 → CCl_3^+
95.35	42	101.60	30	109.85	21	119.60	277
95.85	49	102.70	31	111.05	24	120.65	58
96.30	36	103.20	31	111.85	38	121.55	127
96.90	59	104.10	24	112.50	24	122.75	38
97.70	44	105.25	45	113.80	30	123.25	25
98.80	61	105.85	28	114.30	50	123.65	22
99.40	26	107.35	32	115.70	32	124.35	22
100.00	45	107.65	27	115.90	37	125.05	21
100.30	30	107.95	26	116.60	157	125.85	35
100.60	32	108.25	27	117.60	283	126.05	31

Scan 57 (1.007 min): MYB4152.D
dichloromethane

$CHCl_2OO^+$

m/z	abund.	m/z	abund.	m/z	abund.	m/z	abund.
126.35	30	135.50	20	146.00	43	158.05	30
126.65	30	135.70	27	147.40	33	160.15	20
126.85	28	137.15	26	149.80	23	160.75	26
127.55	29	138.35	33	150.70	29	161.90	27
128.25	28	139.05	25	151.20	21	163.00	33
129.00	30	139.35	20	153.55	25	163.60	22
129.40	49	140.35	27	154.15	23	163.80	22
131.00	25	141.15	28	154.95	24	164.20	24
131.60	21	141.45	23	155.35	28	165.80	36
133.00	33	142.45	37	156.45	21	167.10	25
134.00	34	143.75	29	156.65	21	167.40	21

Scan 57 (1.007 min): MYB4152.D
dichloromethane

m/z	abund.	m/z	abund.	m/z	abund.	m/z	abund.
168.00	25	185.85	20	199.70	23	220.25	22
168.60	27	186.95	29	201.10	20	222.95	42
169.85	40	187.75	22	201.25	20	229.00	32
174.65	23	190.05	29	203.15	30	229.80	23
177.40	24	191.55	22	205.75	60	231.10	30

Appendix E1: Fragments obtained before illumination of UV light for dichloromethane using Zn^{2+} co-doped Fe^{3+}/TiO_2 as catalyst.

Scan 57 (1.008 min): MYB4167.D
dichloromethane

m/z	abund.	m/z	abund.	m/z	abund.	m/z	abund.
10.35	104	21.30	77	30.55	923	44.35	5860
10.65	94	21.80	44	32.50	623872	45.35	156
11.25	122	22.10	38	34.50	3314	47.35	37944
12.75	3758	22.70	83	35.40	17160	48.30	18520
13.85	8731	23.20	54	36.40	4520	49.30	225472
14.75	211840	23.50	65	37.40	5801	50.30	8133
16.60	52992	23.70	65	38.40	1473	51.30	57600
17.70	20912	24.25	107	40.35	46984	52.20	702
18.70	93224	25.05	462	41.35	7037	52.90	47
19.70	966	28.55	880192	42.35	4703	53.40	44
20.60	4437	29.55	22456	43.35	777	54.00	54

CH_2Cl^+
CH_3Cl^+
OCl^+

Scan 57 (1.008 min): MYB4167.D
dichloromethane

CH_2ClO^+

m/z	abund.	m/z	abund.	m/z	abund.	m/z	abund.
55.60	82	61.55	41	68.00	59	77.15	47
56.35	104	62.25	38	69.20	89	77.75	25
57.15	46	62.45	38	70.10	653	78.55	30
57.75	27	63.05	74	71.00	74	79.15	38
58.15	40	63.75	54	72.00	428	79.45	39
58.65	49	64.40	46	73.15	65	79.95	48
58.95	55	65.00	53	73.95	130	81.90	1810
59.15	46	65.50	26	74.85	41	82.90	15626
59.95	68	66.10	34	75.35	30	83.90	128688
60.45	51	66.70	43	75.85	45	84.90	11414
61.05	52	67.00	--	--	48	85.90	79536

CCl_2^+
$CHCl_2^+$

Scan 57 (1.008 min): MYB4167.D
dichloromethan

$COCl_2^+$

m/z	abund.	m/z	abund.	m/z	abund.	m/z	abund.
86.90	2604	94.75	66	102.60	38	111.25	31
87.90	11767	96.15	58	103.20	37	112.35	41
88.85	165	96.80	85	103.80	22	113.50	31
90.15	35	97.60	37	104.10	23	114.20	40
90.85	25	97.90	35	104.55	32	115.60	34
91.65	25	98.90	62	105.05	26	116.60	177
91.95	23	99.80	49	106.55	50	117.60	260
92.25	28	100.90	24	107.15	29	118.60	144
92.45	26	101.10	24	109.95	26	119.60	224
92.85	31	101.50	28	110.25	21	120.55	52
93.65	22	102.30	39	110.55	21	121.55	113

$CHCl_2OO^+$
CCl_3^+

Scan 57 (1.008 min): MYB4167.D
dichloromethane

$CHCl_2O^+$

m/z	abund.	m/z	abund.	m/z	abund.	m/z	abund.
122.45	29	133.00	27	145.20	27	158.35	21
123.45	23	133.20	26	148.50	28	159.05	30
124.15	23	133.60	32	149.30	22	159.55	21
125.45	35	134.30	22	150.60	30	160.45	28
126.15	22	135.70	23	151.30	34	161.90	26
127.45	41	136.30	23	152.20	34	162.10	28
128.15	29	137.05	29	152.85	27	162.80	24
128.70	26	137.35	36	154.95	22	165.00	31
129.50	46	137.55	28	156.05	31	165.70	20
130.30	24	140.25	22	157.15	23	168.40	20
131.50	47	140.85	21	158.05	22	168.70	21

Scan 57 (1.008 min): MYB4167.D
dichloromethane

m/z	abund.	m/z	abund.	m/z	abund.	m/z	abund.
169.85	22	182.80	23	198.80	21	242.50	24
170.15	26	183.70	27	205.75	51	245.80	20
171.15	28	184.50	23	206.85	23		
172.05	36	184.70	24	209.90	28		
173.05	25	187.15	34	212.00	20		

Appendix E2: Fragments obtained after illumination of UV light for dichloromethane using Zn^{2+} co-doped Fe^{3+}/TiO_2 as catalyst.

Scan 59 (1.040 min): MYB4133.D
dichloromethane

m/z	abund.	m/z	abund.	m/z	abund.	m/z	abund.
10.25	100	22.20	89	35.40	19056	48.30	19616
10.85	125	22.60	121	36.40	5025	49.30	238592
11.45	128	23.70	71	37.40	6174	50.30	9154
12.75	3393	23.95	82	38.40	1513	51.20	69704
13.75	9423	25.05	444	40.35	45632	52.20	810
14.75	200512	25.55	263	41.35	7546	53.30	40
16.60	51016	28.55	914752	42.35	5170	54.20	61
17.60	22576	29.55	21728	43.25	828	54.80	77
18.60	100312	30.55	876	44.35	6387	55.30	95
19.60	925	32.40	627392	45.35	175	56.25	147
20.60	4907	34.40	3250	47.35	41912	56.85	38

CH_2Cl^+

CH_3Cl^+

OCl^+

Scan 59 (1.040 min): MYB4133.D
dichloromethane

CH_2ClO^+

m/z	abund.	m/z	abund.	m/z	abund.	m/z	abund.
57.15	33	62.55	87	69.10	76	78.95	39
58.05	35	63.15	75	70.10	796	80.70	76
58.65	48	64.10	36	70.80	69	81.00	73
58.95	53	64.50	32	72.00	555	81.90	1822
59.25	49	64.70	37	73.15	63	82.90	15102
59.55	54	65.20	49	74.05	109	83.90	142720
60.05	32	66.30	36	74.75	34	84.90	11407
60.35	33	66.60	38	75.35	29	85.90	85568
60.55	35	66.90	35	75.85	37	86.90	2716
61.15	44	67.20	37	76.95	51	87.90	13249
61.65	28	68.00	31	77.95	42	88.85	264

CCl_2^+

$CHCl_2^+$

Scan 59 (1.040 min): MYB4133.D
dichloromethane

$COCl_2^+$

m/z	abund.	m/z	abund.	m/z	abund.	m/z	abund.
90.05	33	97.80	44	107.05	37	114.50	34
90.95	63	98.80	57	107.65	37	114.80	40
92.35	32	99.50	35	108.05	24	115.90	28
92.85	44	100.00	23	108.25	23	116.60	155
93.25	37	101.10	53	108.95	41	117.60	188
93.85	52	101.90	36	109.15	37	118.60	182
94.45	52	102.40	52	110.05	34	119.60	216
94.75	72	103.20	32	111.75	37	120.55	41
95.65	45	104.20	40	112.80	40	121.45	76
96.80	53	104.85	34	113.50	25	122.15	38
97.60	45	106.15	34	113.70	24	123.55	49

$CHCl_2OO^+$

CCl_3^+

Scan 59 (1.040 min): MYB4133.D
dichloromethane

$CHCl_2O^+$

m/z	abund.	m/z	abund.	m/z	abund.	m/z	abund.
125.45	31	133.60	23	144.70	25	153.95	25
126.55	46	135.30	23	145.10	28	154.45	43
127.45	50	135.60	28	147.30	28	155.05	22
128.05	22	136.20	24	147.90	31	155.35	24
128.25	22	137.15	26	148.40	29	156.15	20
128.70	22	138.85	31	149.10	29	156.75	29
128.90	23	140.55	21	150.20	22	157.45	33
129.50	39	141.15	20	150.40	22	159.55	25
131.00	26	141.65	34	150.90	21	159.85	23
131.50	34	142.65	25	151.70	22	161.30	26
132.40	47	144.55	22	152.10	26	162.80	23

Scan 59 (1.040 min): MYB4133.D
dichloromethane

m/z	abund.	m/z	abund.	m/z	abund.	m/z	abund.
163.80	26	177.80	24	205.75	54	237.85	23
166.60	23	182.40	26	215.40	31	240.15	25
169.45	20	186.05	21	215.60	29		
170.15	27	191.95	22	218.65	23		
170.95	30	192.35	22	219.55	28		

Appendix E3: Fragments obtained before illumination of UV light for dichloromethane using Mn^{2+}-doped TiO_2 catalyst.

Scan 58 (1.023 min): MYB4148.D
dichloromethane

m/z	abund.	m/z	abund.	m/z	abund.	m/z	abund.
10.15	108	22.20	61	36.40	4927	49.30	241344
10.65	135	22.70	101	37.40	7051	50.20	8863
12.75	3805	23.30	92	38.40	1576	51.30	66600
13.75	8878	25.05	520	40.35	45968	52.20	745
14.75	191808	28.55	904192	41.35	7560	53.40	48
16.60	53296	29.55	22656	42.35	5338	54.10	68
17.70	24232	30.55	913	43.35	931	55.20	79
18.60	106224	32.40	615296	44.35	6717	56.25	123
19.70	946	33.40	771	45.35	192	57.15	56
20.60	4271	34.50	3080	47.25	41440	57.95	54
21.40	85	35.40	18944	48.30	20064	58.25	48

CH_2Cl^+

OCl^+

Scan 58 (1.023 min): MYB4148.D
dichloromethane

CCl_2^+

m/z	abund.	m/z	abund.	m/z	abund.	m/z	abund.
59.05	44	66.70	33	75.65	46	85.90	90712
59.65	51	67.30	64	76.95	63	86.90	2723
60.95	82	68.10	51	78.15	31	87.90	13273
61.95	50	68.70	49	78.45	38	88.85	196
62.45	42	70.10	806	78.65	35	90.05	25
62.75	41	71.10	80	78.95	32	90.35	22
63.25	58	72.00	564	80.30	38	90.85	30
64.05	65	73.05	43	81.90	1933	91.55	44
64.20	69	74.05	95	82.90	15585	92.85	35
65.10	75	74.65	25	83.90	140864	93.65	42
66.30	54	75.15	41	84.90	12463	94.85	64

Scan 58 (1.023 min): MYB4148.D
dichloromethane

$COCl_2^+$

$CHCl_2OO^+$

$CHCl_2^+$

m/z	abund.	m/z	abund.	m/z	abund.	m/z	abund.
95.65	26	104.85	33	115.70	24	124.35	28
96.80	79	105.55	28	115.90	22	124.55	26
97.50	39	106.15	43	116.60	165	126.05	34
97.70	40	107.55	37	117.60	227	126.25	39
98.70	68	108.25	30	118.60	135	127.55	44
100.20	27	108.45	37	119.60	211	129.30	59
100.90	40	108.75	52	120.55	80	129.80	24
102.10	22	109.65	32	121.45	96	130.80	22
102.60	28	111.95	30	122.35	26	131.40	24
103.40	36	112.60	28	122.85	26	131.90	52
104.00	38	114.50	21	123.05	25	132.50	27

$CHCl_2O^+$

CCl_3^+

Scan 58 (1.023 min): MYB4148.D
dichloromethane

m/z	abund.	m/z	abund.	m/z	abund.	m/z	abund.
132.80	28	144.05	22	155.05	30	171.85	22
133.90	25	145.50	32	155.95	21	175.15	20
134.20	26	146.60	42	157.75	25	176.15	24
134.90	25	147.30	39	158.95	28	177.30	22
136.30	33	148.20	34	160.55	33	177.90	21
137.35	26	148.60	31	162.30	21	178.60	21
139.05	22	149.80	28	166.20	22	179.70	21
139.65	28	151.70	27	168.50	22	180.90	32
140.35	27	152.30	28	170.35	30	182.50	22
141.15	21	153.55	30	170.65	34	184.20	40
143.75	20	154.15	31	170.85	35	185.85	31

Scan 58 (1.023 min): MYB4148.D
dichloromethane

m/z	abund.	m/z	abund.	m/z	abund.	m/z	abund.
187.75	43	205.85	55				
188.75	27	206.85	29				
190.25	46	209.50	21				
194.50	20	215.70	26				
195.10	20	217.20	29				

Appendix E4: Fragments obtained after illumination of UV light for dichloromethane using Mn^{2+}-doped TiO_2 as catalyst.

Appendix F: Comparision of Fragments Formed Before and After Illumination of UV Light for Chloroform.

Scan 60 (1.050 min): MYB4069.D
chloroform

m/z	abund.	m/z	abund.	m/z	abund.	m/z	abund.
10.55	103	22.10	52	36.40	4656	49.20	25728
11.05	173	22.70	75	37.40	8035	50.20	10397
12.75	4038	23.95	124	38.40	1573	51.20	187
13.75	12773	24.55	147	40.35	46552	52.00	69
14.65	167168	24.85	161	41.35	805	53.00	70
16.60	48560	28.55	875072	41.85	952	53.20	68
17.60	10737	29.45	22928	42.75	622	53.80	24
18.60	44640	30.45	811	44.35	5677	54.30	39
19.60	373	32.40	635264	45.35	909	54.80	68
20.60	3971	34.40	3006	47.25	84320	55.20	51
21.40	79	35.40	26056	48.20	31688	55.50	63

CH_2Cl^+, CH_3Cl^+, OCl^+

Scan 60 (1.050 min): MYB4069.D
chloroform

CCl_2^+

m/z	abund.	m/z	abund.	m/z	abund.	m/z	abund.
55.80	55	66.20	38	76.55	36	86.90	28816
56.15	80	67.00	57	77.05	86	87.90	347
57.25	41	68.00	47	77.55	22	88.65	49
58.65	243	69.10	116	78.15	62	90.05	41
59.55	194	70.00	2113	79.15	57	91.05	46
60.55	96	72.00	1321	80.20	86	91.75	28
61.75	47	72.85	66	81.90	12175	92.25	31
62.25	103	73.95	287	82.90	329728	92.75	32
63.15	130	74.65	37	83.90	11081	93.25	23
64.05	73	75.55	52	84.90	201536	93.85	48
64.90	70	75.95	50	85.90	3438	94.35	38

Scan 60 (1.050 min): MYB4069.D
chloroform

$COCl_2^+$

$CHCl_2^+$

m/z	abund.	m/z	abund.	m/z	abund.	m/z	abund.
94.95	59	102.00	50	107.95	40	115.40	52
95.85	75	102.50	26	108.75	23	116.60	3473
96.70	24	102.70	31	109.45	38	117.60	6552
97.30	29	103.10	26	109.75	34	118.60	3382
97.80	53	103.30	28	110.95	38	119.60	6463
98.40	30	104.00	28	111.25	31	120.55	1198
98.90	49	104.55	40	111.85	33	121.55	1971
99.80	60	104.95	44	112.35	29	122.55	178
100.50	36	105.65	33	112.90	27	123.55	270
101.10	31	105.85	33	114.10	38	124.45	35
101.50	23	106.75	52	114.90	26	124.75	29

CCl_3^+

$CHCl_2O^+$

Scan 60 (1.050 min): MYB4069.D
chloroform

m/z	abund.	m/z	abund.	m/z	abund.	m/z	abund.
125.45	34	134.30	29	142.85	25	156.05	23
126.55	30	134.90	41	143.05	25	156.25	21
126.75	29	135.40	31	143.55	25	156.55	22
127.65	46	136.00	21	143.75	25	157.05	22
128.70	36	136.60	35	144.45	25	159.35	54
129.40	38	137.05	41	146.20	29	159.95	24
130.40	49	138.85	24	146.70	27	160.15	23
131.50	40	139.45	25	147.50	21	161.70	23
132.50	46	140.35	31	148.40	26	162.00	24
133.30	27	141.65	29	151.10	20	163.30	40
133.90	23	142.55	21	151.80	22	164.50	24

Scan 60 (1.050 min): MYB4069.D
chloroform

m/z	abund.	m/z	abund.	m/z	abund.	m/z	abund.
165.10	24	174.55	33	185.45	25	199.70	23
166.20	27	176.05	36	188.65	20	201.35	26
167.50	40	176.35	32	190.45	25	205.85	87
168.10	25	177.10	22	190.75	28	206.95	29
168.50	23	177.50	26	191.95	27	207.85	35

Appendix F1: Fragments obtained before illumination of UV light for chloroform using Zn^{2+} co-doped Fe^{3+}/TiO_2 as catalyst.

Scan 57 (1.012 min): MYB4087C.D
chloroform

m/z	abund.	m/z	abund.	m/z	abund.	m/z	abund.
10.85	99	22.60	117	36.40	4079	47.25	57888
11.75	217	23.50	71	37.40	6033	48.20	21840
12.75	3490	24.45	116	38.40	1245	49.20	18000
13.75	10952	25.15	133	40.35	43720	50.20	7896
14.75	179840	28.55	916416	41.35	657	51.20	189
16.60	62472	29.55	31480	41.85	697	52.40	63
17.60	127280	30.55	1184	42.35	588	53.20	23
18.60	557312	32.40	632768	42.75	591	54.50	46
19.60	4814	33.40	1486	43.35	345	54.80	49
20.60	5045	34.40	3315	44.35	7615	55.10	47
21.90	67	35.40	19656	45.35	409	55.40	51

CH_2Cl^+ CH_3Cl^+ OCl^+

Scan 57 (1.012 min): MYB4087C.D
chloroform

CCl_2^+

m/z	abund.	m/z	abund.	m/z	abund.	m/z	abund.
56.15	74	63.15	101	73.15	68	85.90	2306
57.05	52	64.20	29	73.95	251	86.90	20432
57.55	57	65.00	53	75.05	50	87.90	237
58.35	140	66.20	27	76.25	28	88.65	37
58.55	132	67.80	44	76.95	141	89.15	23
59.65	138	68.80	67	77.95	36	89.75	29
60.15	57	69.10	70	78.95	39	90.25	36
60.45	62	70.10	1303	81.90	8285	91.05	20
61.45	30	71.20	70	82.90	221568	91.25	21
62.25	57	72.00	1065	83.90	7833	91.55	21
62.55	64	72.95	66	84.90	135936	92.25	24

Scan 57 (1.012 min): MYB4087C.D
chloroform

$COCl_2^+$ $CHCl_2OO^+$ $CHCl_2^+$

m/z	abund.	m/z	abund.	m/z	abund.	m/z	abund.
92.95	27	100.40	23	110.85	25	122.65	111
93.95	33	100.90	57	111.45	31	123.55	179
94.75	28	102.10	33	112.40	40	124.25	23
95.95	85	102.80	38	113.70	28	124.55	38
96.40	24	104.10	27	115.50	25	126.15	45
96.60	24	104.95	23	116.60	2250	126.75	28
97.10	25	107.05	24	117.60	4129	127.55	29
97.60	26	107.65	20	118.60	2280	128.25	30
98.10	29	108.85	39	119.60	3814	129.50	44
99.20	26	109.05	33	120.55	730	129.70	44
99.90	36	109.95	26	121.55	1206	130.10	22

$CHCl_2O^+$ CCl_3^+

Scan 57 (1.012 min): MYB4087C.D
chloroform

m/z	abund.	m/z	abund.	m/z	abund.	m/z	abund.
130.40	22	148.60	23	166.60	23	192.05	29
131.30	33	148.90	27	169.15	32	192.75	20
133.10	23	149.70	24	171.85	27	193.60	27
133.70	31	150.50	24	174.45	20	198.00	23
135.80	24	153.55	32	178.00	24	198.90	21
136.85	28	154.35	23	179.10	28	199.80	20
138.15	26	156.95	39	184.40	31	201.45	22
140.75	24	157.55	27	186.55	25	203.75	25
140.95	24	159.05	28	189.25	26	205.85	87
144.90	30	159.65	20	189.55	22	207.05	36
147.80	24	163.10	20	190.15	26	209.15	22

Scan 57 (1.012 min): MYB4087C.D
chloroform

m/z	abund.	m/z	abund.	m/z	abund.	m/z	abund.
211.10	21						
213.00	28						
216.80	22						
219.65	20						
220.45	43						

Appendix F2: Fragments obtained after illumination of UV light for chloroform using Zn^{2+} co-doped Fe^{3+}/TiO_2 as catalyst.

Scan 58 (1.024 min): MYB4093.D
chloroform

m/z	abund.	m/z	abund.	m/z	abund.	m/z	abund.
10.45	128	22.70	171	37.40	8347	48.20	29536
10.95	96	23.30	71	38.40	1790	49.20	24168
12.75	4461	24.45	146	40.35	43888	50.20	9677
13.75	12783	28.55	887040	41.35	809	51.20	181
14.75	188480	29.45	25056	41.85	1135	52.20	55
16.60	53760	30.55	734	42.35	712	52.50	41
17.60	26736	32.40	654976	42.75	734	53.20	44
18.60	113656	33.40	747	43.35	470	54.00	48
19.60	509	34.40	3241	44.35	6729	54.60	44
20.60	4369	35.40	27072	45.35	451	54.90	50
21.80	70	36.40	5439	47.25	79648	55.10	52

CH_2Cl^+
CH_3Cl^+
OCl^+

Scan 58 (1.024 min): MYB4093.D
chloroform

m/z	abund.	m/z	abund.	m/z	abund.	m/z	abund.
55.40	40	62.25	39	71.00	63	81.90	10244
56.00	57	63.25	139	72.00	1269	82.90	256768
56.55	26	64.20	48	73.15	69	83.90	9014
56.85	32	65.10	51	73.95	286	84.90	164608
57.15	34	65.60	39	74.65	37	85.90	2734
57.55	65	66.20	49	75.25	60	86.90	24208
58.65	260	67.30	36	76.15	30	87.90	259
59.65	136	68.10	52	77.05	70	88.95	38
60.65	91	69.00	76	78.35	38	89.75	39
61.25	86	69.20	76	79.15	37	90.35	37
61.75	54	70.00	1700	79.75	43	91.55	50

CCl_2^+
$CHCl_2^+$

Scan 58 (1.024 min): MYB4093.D
chloroform

m/z	abund.	m/z	abund.	m/z	abund.	m/z	abund.
91.75	46	101.60	31	110.35	21	121.55	1691
93.15	38	102.50	44	110.95	28	122.55	142
93.95	35	103.50	39	111.75	23	123.55	154
94.85	38	104.30	61	112.90	36	125.65	21
96.05	38	105.15	24	113.90	32	126.45	33
96.70	29	105.65	34	114.90	28	126.65	37
98.10	22	105.85	34	116.60	2708	127.65	42
98.80	30	106.85	43	117.60	4893	129.50	40
99.40	27	108.75	23	118.60	2763	130.40	23
99.90	34	109.85	33	119.60	4743	131.10	40
100.60	54	110.05	26	120.55	830	132.40	45

$COCl_2^+$
$CHCl_2O^+$
CCl_3^+

Scan 58 (1.024 min): MYB4093.D
chloroform

m/z	abund.	m/z	abund.	m/z	abund.	m/z	abund.
133.40	43	141.35	38	152.70	23	165.20	24
133.70	30	143.35	25	152.95	30	165.80	32
133.90	28	143.85	23	154.65	37	166.50	28
134.40	34	144.15	20	157.15	35	167.90	26
135.50	35	145.90	34	158.35	21	168.50	24
136.50	24	148.30	22	158.95	24	169.25	37
136.65	25	148.50	25	162.40	21	169.55	23
137.85	32	148.80	28	163.40	22	170.45	24
138.15	34	150.20	25	163.60	24	171.05	21
139.25	40	151.80	47	164.70	30	171.45	21
139.95	34	152.40	33	164.90	30	176.85	26

Scan 58 (1.024 min): MYB4093.D
chloroform

m/z	abund.	m/z	abund.	m/z	abund.	m/z	abund.
178.80	35	192.35	27	205.75	92	241.90	24
180.70	23	193.60	45	206.75	39	242.90	24
182.40	35	195.10	22	207.65	20		
184.30	20	197.20	21	209.90	22		
185.95	36	199.20	23	217.55	38		

Appendix F3: Fragments obtained before illumination of UV light for chloroform using Mn^{2+}-doped TiO_2 as catalyst.

Scan 58 (1.025 min): MYB4121.D
chloroform

m/z	abund.	m/z	abund.	m/z	abund.	m/z	abund.
10.55	121	22.60	149	36.40	4838	47.25	67808
12.75	3689	23.95	103	37.40	6978	48.30	26480
13.75	11168	24.65	135	38.40	1673	49.20	20968
14.75	190336	25.55	167	40.35	45256	50.20	8430
16.60	55120	28.55	902400	41.35	597	51.20	206
17.60	28904	29.45	24832	41.85	869	51.80	65
18.60	129008	30.55	701	42.35	643	53.20	60
19.60	503	32.40	647168	42.85	625	53.80	33
20.60	4232	33.40	814	43.35	296	54.30	63
21.60	56	34.40	3180	44.35	10687	55.50	64
21.80	51	35.40	21736	45.35	302	56.00	54

CH_2Cl^+, CH_3Cl^+, OCl^+

Scan 58 (1.025 min): MYB4121.D
chloroform

m/z	abund.	m/z	abund.	m/z	abund.	m/z	abund.
56.95	50	65.80	34	75.65	29	82.90	224064
57.15	51	66.40	48	76.15	23	83.90	7426
58.55	179	67.00	46	76.45	20	84.90	147584
59.65	189	67.60	68	77.05	64	85.90	2449
60.25	71	69.10	64	77.55	43	86.90	20880
60.55	76	70.00	1602	78.25	41	87.90	216
61.65	48	71.10	59	79.25	48	88.85	47
62.25	33	72.00	1046	80.05	40	90.05	32
63.15	129	72.95	88	80.30	36	90.95	37
64.10	55	73.95	149	80.60	54	91.45	31
65.10	70	74.85	51	81.90	8682	92.45	25

CCl_2^+, $CHCl_2^+$

Scan 58 (1.025 min): MYB4121.D
chloroform

m/z	abund.	m/z	abund.	m/z	abund.	m/z	abund.
93.05	40	102.50	44	113.50	34	122.55	84
93.55	22	103.60	35	113.90	22	123.55	183
94.65	52	105.95	45	114.80	20	126.05	33
95.65	39	106.85	54	115.00	21	127.25	32
95.85	35	107.55	36	115.50	43	128.05	25
97.10	45	108.25	22	116.60	2396	128.45	46
98.00	23	108.85	36	117.60	4452	129.40	33
99.10	29	109.65	21	118.60	2366	131.60	29
99.80	56	109.95	21	119.60	4188	132.50	39
100.80	39	111.75	41	120.55	864	133.00	35
101.50	27	112.35	30	121.55	1417	134.40	24

$CHCl_2OO^+$, $COCl_2^+$, $CHCl_2O^-$, CCl_3^+

Scan 58 (1.025 min): MYB4121.D
chloroform

m/z	abund.	m/z	abund.	m/z	abund.	m/z	abund.
134.90	26	143.85	22	160.45	20	175.25	20
135.40	35	146.70	25	163.10	47	175.55	25
136.60	22	150.60	22	165.20	37	177.90	25
137.35	46	151.20	31	165.70	20	179.10	31
138.55	25	152.20	22	167.30	30	180.20	28
139.55	25	154.35	26	168.00	32	183.20	29
140.15	53	155.35	26	168.60	24	185.85	28
141.55	32	155.55	24	170.35	21	189.95	31
141.75	31	156.55	29	173.45	21	190.75	21
142.15	27	157.15	20	174.35	28	190.95	21
142.85	23	158.05	32	174.65	32	196.30	27

Scan 58 (1.025 min): MYB4121.D
chloroform

m/z	abund.	m/z	abund.	m/z	abund.	m/z	abund.
201.65	23	229.40	21				
202.45	25	229.90	28				
205.75	68	233.55	23				
206.75	33	238.35	29				
207.95	26						

Appendix F4: Fragments obtained after illumination of UV light for chloroform using Mn^{2+}-doped as catalyst.

Appendix G: Comparision of Fragments Formed Before and After Illumination of UV Light for Carbon Tetrachloride.

Scan 46 (1.031 min): MYB4193.D
carbon tetrachloride

m/z	abund.	m/z	abund.	m/z	abund.	m/z	abund.
10.25	49	22.50	75	35.40	25856	48.30	2111
10.75	113	23.10	53	36.40	2718	49.30	28080 → CH_2Cl^+
11.35	130	24.25	90	37.40	8267	50.20	692
12.75	4717	24.45	91	38.40	814	51.20	4369 → OCl^+
14.75	154112	25.15	135	40.35	40232	52.30	82
16.70	42832	28.55	861632	41.35	1285	53.20	32
17.70	22272	29.55	19184	42.35	1112	54.10	36
18.70	99248	30.55	589	43.35	419	55.40	40
19.60	415	32.40	582592	44.35	5931	56.00	46
20.60	3763	33.40	684	45.25	144	57.15	66
21.40	52	34.50	2761	47.35	41112	58.65	3232

Scan 46 (1.031 min): MYB4193.D
carbon tetrachloride

CCl_2^+

m/z	abund.	m/z	abund.	m/z	abund.	m/z	abund.
59.65	2862	67.00	32	77.65	33	88.85	42
60.65	1000	67.20	28	78.15	29	89.85	40
61.65	136	68.10	44	78.75	31	91.15	29
63.15	444	70.00	1626	79.65	47	91.35	28
64.05	50	72.10	996	81.90	40504	92.55	36
64.20	51	72.85	37	82.90	2471	92.75	34
65.10	87	73.95	238	83.90	34352	93.65	29
65.60	43	74.65	25	84.90	1569	94.15	35
66.10	21	74.85	27	85.90	9625	95.05	31
66.30	21	75.75	37	87.00	339	95.95	39
66.70	31	76.85	41	87.90	933	96.90	34

Scan 46 (1.031 min): MYB4193.D
carbon tetrachloride CCl_3^+ $CHCl_2^+$

m/z	abund.	m/z	abund.	m/z	abund.	m/z	abund.
97.50	41	110.35	26	124.35	27	135.50	21
98.10	22	112.50	29	125.55	23	136.20	32
98.90	27	113.30	23	126.65	23	136.95	23
99.70	43	113.70	25	126.95	23	137.25	36
101.50	39	116.60	171776	127.25	22	137.45	33
102.10	22	118.60	179264	127.75	21	141.55	30
106.25	24	119.60	2015	128.55	24	142.15	34
106.95	28	120.55	52704	129.20	20	143.55	24
107.25	24	121.55	524	130.90	22	145.20	21
107.95	29	122.55	5096	131.40	31	145.70	35
109.15	39	123.55	90	134.00	33	146.70	21

$CHCl_2O^+$

Scan 46 (1.031 min): MYB4193.D
carbon tetrachloride $CHCl_3^+$

m/z	abund.	m/z	abund.	m/z	abund.	m/z	abund.
148.90	35	167.60	20	184.70	21	233.20	30
155.05	21	168.95	23	187.35	21	233.95	25
156.25	32	170.25	22	195.60	26		
156.85	21	170.45	21	199.10	31		
158.45	26	172.35	21	199.80	20		
160.15	23	174.45	20	201.35	23		
160.35	26	174.95	33	205.85	67		
160.75	21	177.80	32	214.10	25		
160.90	25	179.50	22	215.90	30		
162.10	22	183.20	25	219.75	21		
163.80	27	183.40	29	226.70	24		

Appendix G1: Fragments obtained before illumination of UV light for carbon tetrachloride using Zn^{2+} co-doped Fe^{3+}/TiO_2 as catalyst.

59 (1.036 min): MYB4200.D
carbon tetrachloride

m/z	abund.	m/z	abund.	m/z	abund.	m/z	abund.
10.15	75	21.40	65	36.40	2816	49.30	25840
10.45	64	22.60	104	37.40	7848	50.30	802
10.75	81	23.30	87	38.40	890	51.20	4686
10.95	79	24.35	64	40.35	38440	52.30	91
12.75	4224	25.05	112	41.35	1258	52.90	48
14.75	142144	28.55	883776	42.35	1061	53.20	56
16.70	43416	29.55	20160	43.35	457	54.30	38
17.70	19440	30.55	618	44.35	6046	54.60	38
18.70	85000	32.50	556864	45.45	119	55.50	36
19.60	463	34.50	2656	47.35	42736	55.90	34
20.60	3888	35.40	24592	48.30	2066	56.05	34

CH_2Cl^+

OCl^+

Scan 59 (1.036 min): MYB4200.D
carbon tetrachloride

CCl_2^+

m/z	abund.	m/z	abund.	m/z	abund.	m/z	abund.
56.45	47	66.00	32	77.05	38	87.90	959
56.65	43	66.50	26	77.45	29	88.55	27
57.35	62	67.50	20	78.95	30	91.25	27
58.65	3135	68.60	39	79.75	30	92.55	22
59.65	3322	70.10	1657	79.95	26	93.95	23
60.65	904	71.00	34	81.90	37736	94.95	30
61.55	110	72.10	1088	82.90	2458	96.25	24
62.25	52	73.95	168	83.90	33840	96.70	21
63.15	362	74.75	28	84.90	1714	97.60	37
64.20	31	75.55	47	85.90	9877	98.30	20
65.20	116	76.05	21	87.00	325	99.40	35

Scan 59 (1.036 min): MYB4200.D
carbon tetrachloride

CCl_3^+

$CHCl_2^+$

$CHCl_2O^+$

m/z	abund.	m/z	abund.	m/z	abund.	m/z	abund.
100.00	25	112.15	22	123.55	88	141.85	25
102.00	31	112.40	25	124.35	36	143.45	22
102.60	31	112.60	23	125.95	21	144.45	21
103.60	32	113.40	30	127.25	24	145.30	29
104.10	25	114.20	49	129.60	26	145.90	22
104.85	22	116.60	173184	131.00	22	148.20	23
105.05	21	118.60	168000	134.20	34	150.10	27
105.75	27	119.60	1985	135.60	25	151.20	22
106.65	21	120.55	51200	135.90	20	151.40	23
107.75	28	121.55	628	136.10	22	154.15	22
108.45	26	122.55	4902	138.55	25	156.75	33

Scan 59 (1.036 min): MYB4200.D
carbon tetrachloride

$CHCl_3^+$

m/z	abund.	m/z	abund.	m/z	abund.	m/z	abund.
158.15	23	230.90	21				
163.10	24	232.70	22				
185.25	20	233.45	28				
195.50	23	234.35	21				
196.10	23	247.20	22				
201.45	29						
202.15	28						
205.75	47						
217.35	29						
224.15	24						
227.00	21						

Appendix G2: Fragments obtained after illumination of UV light for carbon tetrachloride using Zn^{2+} co-doped Fe^{3+}/TiO_2 as catalyst.

Scan 59 (1.036 min): MYB4182.D
carbon tetrachloride

m/z	abund.	m/z	abund.	m/z	abund.	m/z	abund.
10.65	77	23.95	75	37.40	8630	50.30	855
12.75	5301	25.05	139	38.40	812	51.20	4562
14.75	145408	25.35	126	40.35	40200	52.10	86
16.60	44240	28.55	853632	41.35	1435	53.10	39
17.70	19120	29.55	20704	42.35	1031	53.80	33
18.70	84488	30.55	669	43.25	324	54.50	58
19.60	425	32.40	598464	44.35	5896	55.20	44
20.60	3723	33.40	768	45.45	142	56.15	43
22.00	53	34.50	2656	47.35	43248	56.65	27
22.80	113	35.40	26936	48.30	2019	57.15	41
23.60	78	36.40	2610	49.30	27336	58.65	3015

OCl^+

Scan 59 (1.036 min): MYB4182.D
carbon tetrachloride

CH_2Cl^+ CCl_2^+

m/z	abund.	m/z	abund.	m/z	abund.	m/z	abund.
59.65	2913	68.20	45	77.65	43	88.85	27
60.65	997	68.90	33	78.75	45	91.25	34
61.55	142	70.10	1697	79.35	32	92.55	34
62.15	49	72.00	1047	79.85	31	93.05	46
63.15	356	74.05	197	81.90	41232	93.85	52
64.20	24	74.65	30	82.90	2161	95.05	28
65.10	117	74.95	21	83.90	34584	95.65	27
65.90	58	75.45	26	84.90	1523	96.50	29
66.20	42	76.25	38	85.90	10275	97.10	25
67.10	54	76.65	25	86.90	329	97.70	45
67.40	46	77.15	57	87.90	956	98.30	24

Scan 59 (1.036 min): MYB4182.D
carbon tetrachloride

CCl_3^+ $CHCl_2^+$

$COCl_2^+$

$CHCl_2O^+$

m/z	abund.	m/z	abund.	m/z	abund.	m/z	abund.
98.60	34	105.25	22	113.00	26	128.05	21
98.80	30	105.95	28	114.50	61	128.80	38
99.50	31	106.75	24	116.60	177856	129.40	35
99.80	27	108.15	25	118.60	178176	130.90	27
100.10	25	108.85	26	119.60	2081	133.40	34
100.40	31	109.05	24	120.55	50664	135.80	27
101.70	20	110.05	29	121.55	631	138.65	21
102.10	20	110.55	22	122.55	5502	144.55	26
102.70	40	110.85	21	123.45	74	147.40	27
103.20	41	111.75	34	126.65	21	147.80	23
104.65	31	112.25	20	126.85	22	148.80	29

Scan 59 (1.036 min): MYB4182.D
carbon tetrachloride

$CHCl_3^+$

m/z	abund.	m/z	abund.	m/z	abund.	m/z	abund.
149.50	27	185.65	21	227.00	23		
159.35	27	186.95	27	233.30	24		
161.00	24	187.15	28				
161.90	34	196.30	23				
164.70	29	201.15	22				
169.75	20	202.75	21				
170.25	21	205.75	80				
171.65	22	206.85	49				
172.65	29	209.80	30				
174.75	24	215.60	32				
177.70	25	215.80	32				

Appendix G3: Fragments obtained before illumination of UV light for carbon tetrachloride using Zn^{2+} co-doped Fe^{3+}/TiO_2 as catalyst.

Scan 45 (1.014 min): MYB4208.D
carbon tetrachloride

m/z	abund.	m/z	abund.	m/z	abund.	m/z	abund.
10.15	90	22.50	93	33.40	799	45.45	97
11.15	116	23.40	53	34.50	2563	45.85	110
11.75	126	23.70	57	35.40	18640	47.35	30928
12.75	4039	23.95	55	36.40	1674	48.30	1602
14.75	144704	24.15	45	37.40	6578	49.30	21552 → CH_2Cl^+
16.70	44648	24.65	69	38.40	619	50.30	615
17.70	27160	25.55	203	40.35	37632	51.30	3533 → OCl^+
18.70	109536	28.55	875456	41.35	973	52.30	93
19.60	479	29.55	19504	42.35	904	53.20	36
20.60	3780	30.55	569	43.35	347	54.40	54
21.80	40	32.50	587328	44.35	6104	55.40	57

Scan 45 (1.014 min): MYB4208.D
carbon tetrachloride CCl_2^+

m/z	abund.	m/z	abund.	m/z	abund.	m/z	abund.
55.90	31	66.00	34	76.25	30	86.90	327
56.35	50	66.40	27	76.55	26	87.90	771
56.75	29	67.10	48	77.15	55	88.95	45
58.65	2111	67.90	62	78.25	27	89.95	33
59.65	2536	68.30	48	78.95	33	91.05	50
60.65	755	70.10	1429	80.05	47	91.95	23
61.65	125	70.70	33	81.90	31184	93.05	32
62.35	56	71.30	64	83.00	2150	93.85	24
63.25	249	72.00	728	83.90	26480	94.05	22
63.95	42	72.95	20	84.90	1375	94.65	25
65.10	115	74.05	158	85.90	7569	94.85	22

Scan 45 (1.014 min): MYB4208.D
carbon tetrachloride CCl_3^+ $CHCl_2^+$

m/z	abund.	m/z	abund.	m/z	abund.	m/z	abund.
95.25	31	101.40	32	111.75	30	125.75	48
96.40	36	102.10	46	111.95	29	126.75	23
96.70	30	103.10	22	112.35	27	127.55	25
96.90	33	104.00	30	113.70	38	127.75	24
97.30	29	105.65	20	116.60	129192	128.55	27
97.60	31	106.85	24	118.60	130224	131.20	22
97.80	34	107.25	20	119.60	1580	132.50	20
98.60	28	108.95	22	120.55	37672	133.50	26
99.70	23	109.75	22	121.55	454	134.40	24
100.20	28	109.95	23	122.55	4102	134.90	21
100.70	41	111.35	22	123.55	79	135.70	23

$COCl_2^+$

$CHCl_2O^+$

Scan 45 (1.014 min): MYB4208.D
carbon tetrachloride $CHCl_3^+$

m/z	abund.	m/z	abund.	m/z	abund.	m/z	abund.
140.45	28	167.20	37	195.40	31		
141.55	38	175.75	23	199.10	28		
143.25	22	177.60	26	205.75	31		
144.65	35	178.30	23	206.05	33		
145.20	31	184.40	29	209.70	22		
146.20	26	185.35	27	210.00	21		
153.55	26	186.95	22	225.25	24		
156.35	23	188.55	30				
156.75	20	189.85	27				
156.95	25	193.40	24				
164.70	20	194.80	20				

Appendix G4: Fragments obtained after illumination of UV light for carbon tetrachloride using Mn^{2+}-doped TiO_2 as catalyst.

Appendix H: Tauc's Plot for Indirect Band Gap

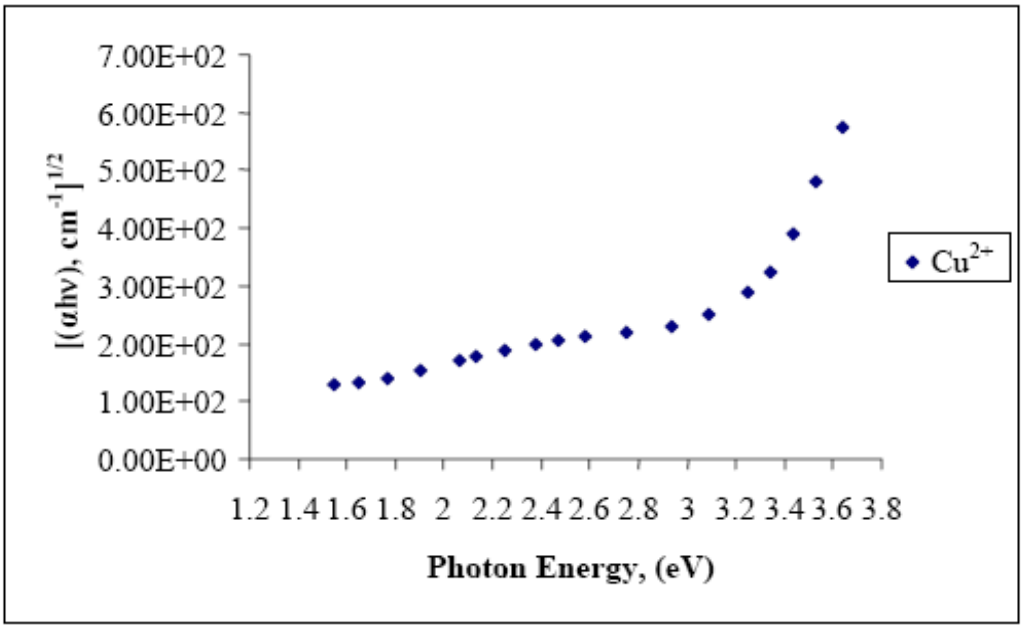

Appendix H1: Tauc's plot for indirect band gap of Cu^{2+}-doped TiO_2.

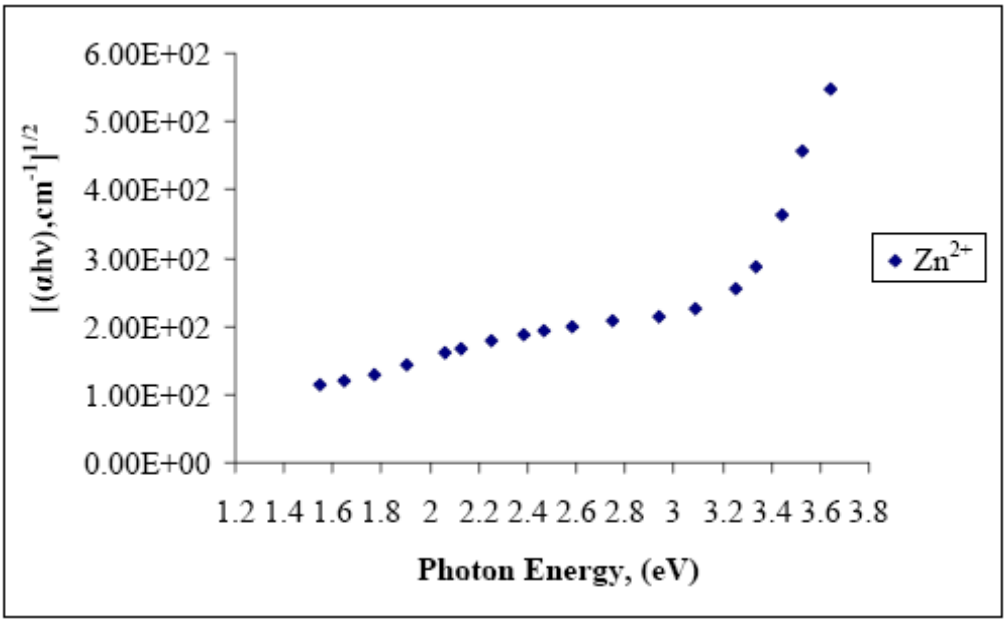

Appendix H2: Tauc's plot for indirect band gap of Zn^{2+}-doped TiO_2.

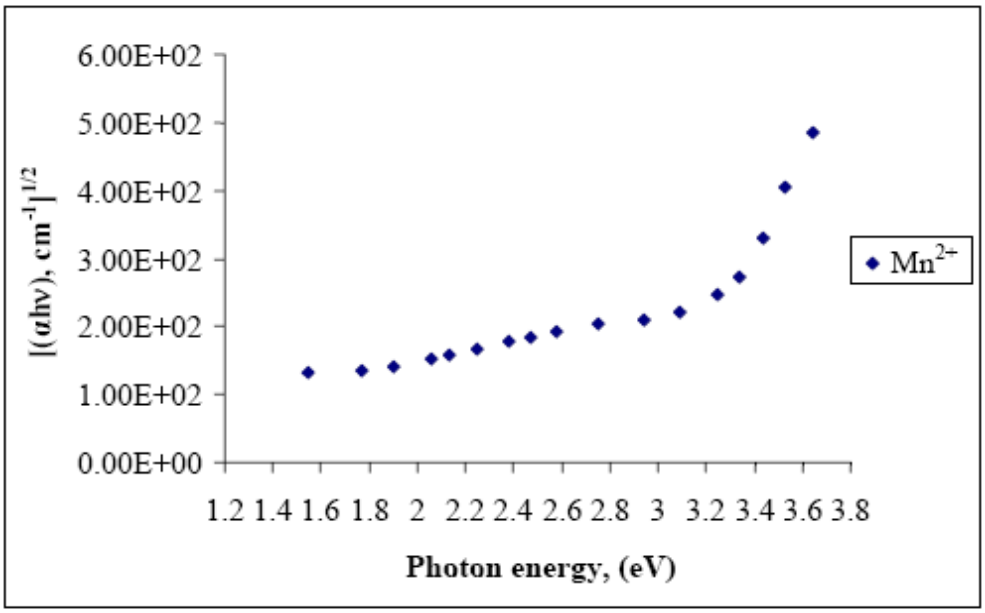

Appendix H3: Tauc's plot for indirect band gap of Mn^{2+}-doped TiO_2.

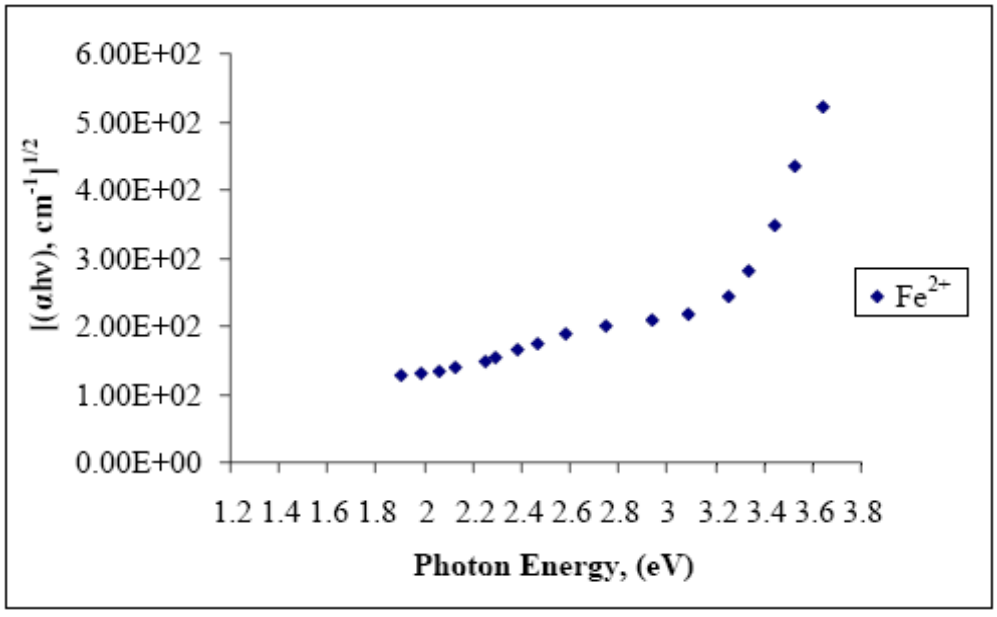

Appendix H4: Tauc's plot for indirect band gap of Fe^{2+}-doped TiO_2.

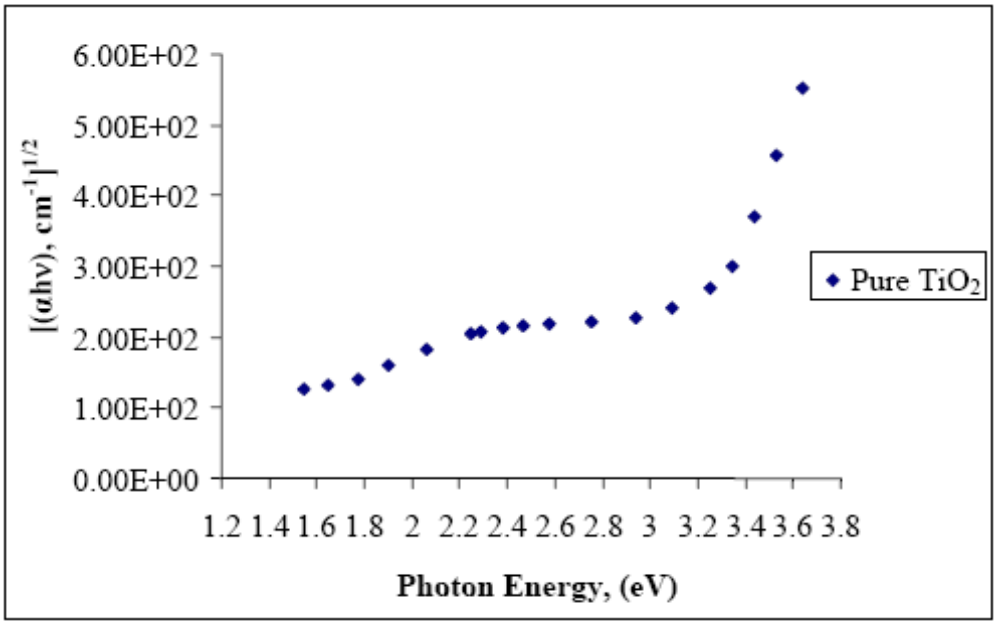

Appendix H5: Tauc's plot for indirect band gap of pure TiO_2.